OBSERVATIONAL AND THEORETICAL COSMOLOGY WITH NOVEL STATISTICAL METHODS

by

Kyle Leaf

A Dissertation Submitted to the Faculty of the

DEPARTMENT OF PHYSICS

In Partial Fulfillment of the Requirements

For the Degree of

DOCTOR OF PHILOSOPHY

In the Graduate College

THE UNIVERSITY OF ARIZONA

2019

2

THE UNIVERSITY OF ARIZONA
GRADUATE COLLEGE

As members of the Dissertation Committee, we certify that we have read the dissertation prepared by Kyle Leaf, titled Observational and Theoretical Cosmology with Novel Statistical Methods and recommend that it be accepted as fulfilling the dissertation requirement for the Degree of Doctor of Philosophy.

Fulvio Melia — Date: April 12th, 2019

Arvinder Sandhu — Date: April 12th, 2019

Shufang Su — Date: April 12th, 2019

Johann Rafelski — Date: April 12th, 2019

Sean Fleming — Date: April 12th, 2019

Final approval and acceptance of this dissertation is contingent upon the candidate's submission of the final copies of the dissertation to the Graduate College.

I hereby certify that I have read this dissertation prepared under my direction and recommend that it be accepted as fulfilling the dissertation requirement.

Date: June 10th, 2019

Dissertation Director: Fulvio Melia

DEDICATION

To Kelsey, my best friend and love of my life.

ACKNOWLEDGEMENTS

I would like to offer many thanks to my advisor Fulvio Melia for his continued patience with me and sound advice over the past few years. I must also thank my parents, Kevan and Julie, for their constant support through my entire academic career. To the rest of my family as well, Kierstan, Katherine, and Kelsey, thank you. Thank you also David, Adriana, and Mick for all of their support during my undergraduate studies. To everyone at Lutheran Church of the Risen Savior and Green Valley Concert Band, thank you for being so welcoming to two young people in Green Valley.

Finally, I would like to thank Bruce for sitting through a trial run of my presentation, you have been more helpful than you realize.

TABLE OF CONTENTS

LIST OF FIGURES

LIST OF TABLES

Abstract

The standard ΛCDM model of the universe has been shown to be consistent with a wide range of astronomical observations, including many properties of the cosmic microwave background (CMB). However, the model has significant tension with an increasing set of measurements, ranging from determinations of the Hubble Constant to the angular correlation function of the CMB. This motivates revisions to ΛCDM, or the consideration of alternative models (or even entirely new physics). The $R_h=ct$ universe is an alternative FLRW cosmology that has thus far performed very well in describing a wide range of astronomical observations. In this dissertation, I present a sequence of tests of cosmology. These tests are designed to determine whether the $R_h=ct$ universe performs better than the standard model in accounting for the considered data. First, I show the development of a two-point diagnostic to compare a model's predictions with observations. This diagnostic is applied to passively evolving elliptical galaxies (cosmic chronometers) and the Hubble diagram as constructed using HII galaxies. Second, I make use of relative likelihoods with strongly-lensed galaxies to constrain standard ΛCDM and an alternative dark matter parameterization (wCDM). These model fits are then compared with the $R_h=ct$ universe by means of several information criteria. Each of the direct comparisons using existing data favor the $R_h=ct$ universe over standard ΛCDM to different degrees, warranting further research to determine whether it accurately describes the Universe. Finally, I present a theoretical prediction of the number of $z>6$ blazars that will be detectable by upcoming surveys by the Square Kilometer Array (SKA). This prediction is entirely phenomenological, based on spectral energy distribution

(SED) measurements of known blazars. The predictions for the number of blazars detectable by SKA between these models are incompatible, such that either the $R_h{=}ct$ universe or ΛCDM will be strongly preferred by the surveys.

Introduction

Motivation

The standard model of modern cosmology is Λ-Cold Dark Matter (ΛCDM), where Λ refers to a cosmological constant. In general, the several free parameters in ΛCDM are similar whether constrained by high-redshift (such as the Cosmic Microwave Background (CMB) (Planck Collaboration 2018) or lower redshift data (Chapters 2 and 3). However, astronomical observations continue to reveal data that are difficult to reconcile with a ΛCDM model.

In 2009, Copi et al (2009) presented an analysis of the angular 2-point correlation function of temperature in the CMB based on WMAP data. Specifically, they found that on the largest angular scales, the CMB was highly inconsistent with ΛCDM, such that only 0.1% of their model realizations (with random alignment of the Milky Way, and randomizing the pattern of cosmological fluctuations) could produce an angular 2-point correlation function consistent with WMAP observations. There also exists the 'cosmological constant problem', or the disparity between treating the cosmological constant as vacuum energy and comparing it with QFT's zero-point energy (see Weinberg 1989, and Padilla 2015). Perhaps most famous at present is the fact that the most precise determinations of the Hubble constant based on measurements by *Planck* and the Hubble space telescope (Planck Collaboration 2018, Riess et al. 2019) continue to be incompatible with one another. These (and others) motivate careful consideration of modifications or alternatives to the standard model.

Over the past decade, the $R_{\rm h}=ct$ universe has been directly compared to ΛCDM by means of a large number of tests using model-independent data. When considering the aforementioned angular correlation function of the CMB,

$R_h=ct$ fits very well (Melia, & López-Corredoira 2018), (Melia, 2014). When making cosmology-independent observations of the angular-diameter or luminosity distances as a function of redshift, $R_h=ct$ is found to perform very well at all redshifts with observations thus far. The angular-diameter distance has a maximum at some redshift (z_{max}) based on choice of cosmology. Melia & Yennapureddy (2018) used observations of quasar cores and showed that $R_h=ct$'s z_{max} is more consistent with observations than ΛCDM. In addition, Wei, Wu, & Melia (2015) used the angular diameter distance in the context of galaxy cluster sizes and found that based on several information criteria, $R_h=ct$ is preferred over ΛCDM by roughly 4-to-1.

The cosmic timeline is also highly dependent on the underlying cosmology. Cosmic chronometers (Jimenez & Loeb 2002) are galaxies within which the stars are believed to have formed simultaneously, and all galaxies of similar appearance formed within a relatively short epoch of the universe. Therefore, these galaxies may be effectively considered to be clocks displaying the age of their stellar population. These ages constitute a measurement of the Hubble constant as a function of redshift (see also Chapter 1 of this dissertation). Melia & Maier (2013) demonstrated that the inferred evolution of the Hubble constant again prefers $R_h=ct$ over ΛCDM by the use of information criteria. $R_h=ct$, having performed as well as it has with respect to a wide range of astronomical data prompts further analyses of additional observations, and repeated analyses as new data becomes available, or new techniques devised.

Therefore, the work I detail in this dissertation is my analyses of several model-independent data sets. Each advances the comparative tests between cosmologies. In chapters 1&2, I develop and improve statistical analysis techniques applied to astrophysical data (Ch 1 & 2). In chapters 3, I make use of

a larger catalogs of recent observations than any prior analysis of cosmology using similar data (Ch 3), and in chapter 4, I use the diverging properties of R_h=ct and ΛCDM at z>6 in order to predict the most distant active galaxies that may be detected by an upcoming observatory.

Introduction to the primary considered cosmological models.

All of modern cosmology is based on the Friedmann- Lemaître -Robertson-Walker (FLRW) metric [see, for example, Robertson's series of papers (1935, 1936a, 1936b)].

$$ds^2 = c^2 dt^2 - a^2(t)\left[dr^2 \left(1 - kr^2\right)^{-1} + r^2 \left(d\theta^2 + \sin^2 \theta d\phi^2\right)\right] \quad (1)$$

The FLRW metric describes a spatially homogenous and isotropic three-dimensional space. Here, t is the cosmic time, measured by a comoving observer, and is the same everywhere. $a(t)$ is the expansion factor (defined as '1' for the present epoch in a flat universe), a function of time alone, and r is the radial coordinate in this comoving frame. The constant k is +1 for a closed universe, 0 for a flat universe, and -1 for and open universe.

When Einstein's field equations are applied to the FLRW metric, the result is the following differential equations of motion. The Friedmann equation,

$$H^2 \equiv \left(\frac{\dot{a}}{a}\right)^2 = \frac{8\pi G}{3c^2}\rho - \frac{kc^2}{a^2} \quad (2)$$

and the 'acceleration' equation,

$$\left(\frac{\ddot{a}}{a}\right)=\frac{-4\pi G}{3c^2}\left(\rho+3p\right) \tag{3}$$

H is the Hubble constant as a function of t, G is Newton's constant of gravitation. ρ is the energy density of the universe, and p is the pressure. Overdots are derivatives with respect to t.

Differentiating (2) with respect to t gives:

$$2\frac{\dot{a}}{a}\left(\left(\frac{\ddot{a}}{a}\right)-\left(\frac{\dot{a}}{a}\right)^2\right)=\frac{8\pi G}{3c^2}\dot{\rho}-\frac{2kc^2\dot{a}}{a^3} \tag{4}$$

Which leads to

$$2H\left(\left(\frac{-4\pi G}{3c^2}\left(\rho+3p\right)\right)-H^2\right)=\frac{8\pi G}{3c^2}\dot{\rho}-\frac{2kc^2}{a^2}H \tag{5}$$

And finally

$$\dot{\rho}=-3H\left(\rho+p\right) \tag{6}$$

A light ray follows a null geodesic, such that $ds^2=0$.

If we consider motion entirely along the r coordinate, in a flat universe,

$$0=c^2dt^2-a^2\left(t\right)dr^2, \tag{7}$$

or

$$c=a\left(t\right)\frac{dr}{dt}. \tag{8}$$

This representation demonstrates the distinction between comoving and physical distances is cosmology. c is a proper speed which is measured identically in any reference frame. While the scale factor may have been smaller at earlier times (thus making the interval dr cover more *comoving* distance), light still, physically, moves at the usual speed of c.

This dissertation concerns the physical observables that follow from the prior equations. I first consider the $R_h=ct$ universe (Melia 2019), so named for the fact that the gravitational horizon grows with the speed of light as a function of cosmic time. The gravitational horizon in a flat ($k=0$) universe is the surface which defines the surface beyond which all null geodesics recede from the observer (Melia 2018). This surface is found at the proper distance where

$$R_{\rm h}=\frac{2GM}{c^2}. \tag{9}$$

Such that the proper mass within this proper radius is

$$M\equiv\frac{4\pi}{3}R_{\rm h}^3\frac{\rho}{c^2}. \tag{10}$$

Therefore, here

$$R_{\rm h}^2=\frac{3c^4}{8\pi G\rho}. \tag{11}$$

In any flat universe ($k=0$, which is consistent with observations), it is quickly shown that combining (11) with (2) gives

$$R_{\rm h}^2=\frac{3c^4}{8\pi G\left(\frac{3c^2}{8\pi G}\left(\frac{\dot a}{a}\right)^2\right)}=c^2\left(\frac{a}{\dot a}\right)^2, \tag{12}$$

or

$$R_{\rm h}=\frac{ca}{\ddot a}=\frac{c}{H}. \tag{13}$$

It is interesting to point out that in the standard model with the usual parameters, the Hubble time H_0^{-1} is nearly identical to the age of the universe (36). The present epoch would be the only time in the history of the universe where these values coincide. Using the HST-determined $H_0=74.03\pm1.42$(km/s)/Mpc (Riess et al. 2019), and $\Omega_m=0.3$ in flat ΛCDM, the age of the universe is 12.73 ± 0.25Gyr, while the Hubble time $\left(1/H_0\right)$ is 13.21 ± 0.25Gyr.

Imposing the condition $\rho + 3p = 0$ on a flat universe necessitates that $R_h = ct$. A quick inspection of (3) with this constraint shows that, $\ddot{a} = 0$, meaning $a = \alpha t + \beta$, where α and β are constants. We eliminate β by associating the scale factor at t=0 with 0.

Going back to the Friedmann equation, in this universe we have

$$H^2 = \left(\frac{\alpha}{\alpha t}\right)^2, \tag{14}$$

and by considering only positive times:

$$H = \frac{1}{t}. \tag{15}$$

Which, when applied to (13) immediately results in

$$R_h = ct. \tag{16}$$

Several other properties of this universe may then be quickly derived. By convention, we set $a(t)$ to be equal to '1' at the present epoch. $H\left(t_{now}\right) = H_0$, the Hubble constant determined by observations. With the age of the universe at the present thus defined as the Hubble Time, we have:

$$a = \alpha t = H_0 t. \tag{17}$$

In addition, we have

$$-3H\left(\frac{2}{3}\rho\right) = \dot{\rho}, \tag{18}$$

or

$$-2\frac{\rho}{t} = \dot{\rho}. \tag{19}$$

This differential equation has solutions of the form

$$\rho = \frac{C}{t^2}, \tag{20}$$

where C is some constant.

Looking once again at the Friedmann equation (2),

$$\frac{1}{t^2} = \frac{8\pi G}{3c^2}\frac{C}{t^2} \tag{21}$$

leads to

$$C = \frac{3c^2}{8\pi G}. \tag{22}$$

Therefore,

$$\rho = \frac{3c^2}{8\pi G t^2}. \tag{23}$$

Furthermore, the full line element of the $R_h = ct$ universe is:

$$ds^2 = c^2 dt^2 - H_0^2 t^2 \left[dr^2 + r^2 \left(d\theta^2 + \sin^2 \theta d\phi^2 \right) \right]. \tag{24}$$

As a brief digression, the gravitational radius R_h was included in the original coordinate system of the metric by de Sitter (1917), but was overshadowed by the comoving coordinate system used by Friedmann (1922).

Next, we link this theory to observations.

First, the redshift z is related to the scale factor of any FRW model by

$$1 + z = \frac{1}{a(t)}. \tag{25}$$

Such that for $R_h = ct$, z is related to cosmic time by

$$1 + z = \frac{1}{H_0 t}. \tag{26}$$

Finally, we can construct the several distance measures useful in cosmology. Hogg (1999) presents a solid 'cheat sheet' of these distances. For any given cosmology we can define a function $H(z) = H_0 E(z)$, dependent on the components of the energy and pressure of the universe. In standard flat ΛCDM, the cosmic fluid consists of matter, radiation, and a cosmological constant (dark energy). Here,

$$E_{\Lambda CDM} = \sqrt{\Omega_m (1+z)^3 + \Omega_r (1+z^4) + \Omega_\Lambda}, \tag{27}$$

where subscripts *m, r,* and Λ are the proportion of the total energy density at the present epoch for matter, radiation, and dark energy, respectively. Flatness imposes the constraint of $\Omega_m + \Omega_r + \Omega_\Lambda = 1$.

In $R_h = ct$,

$$E_{R_h=ct}(z) = 1+z. \tag{28}$$

This function may then be used to determine the comoving distance between an observer and some object by

$$D_C = \frac{c}{H_0} \int_0^z \frac{dz'}{E(z')}, \tag{29}$$

which, in the context of $R_h = ct$ is

$$D_{C(R_h=ct)} \frac{c}{H_0} \int_0^z \frac{dz'}{1+z'} = \frac{c}{H_0} \ln(1+z). \tag{30}$$

In ΛCDM, the integral must be evaluated numerically.

First noted in Tolman (1929), and named the Etherington reciprocity theorem (also known as the distance-duality relation) following the publication by Etherington (1933), the relationship between this comoving distance and the angular diameter and luminosity distances is

$$D_C = (1+z) D_A = \frac{D_L}{1+z}. \tag{31}$$

Where luminosity distance is the distance inferred by comparing the bolometric (full spectrum) luminosity of some object (inferred by theory) with the observed full-spectrum flux

$$F = \frac{L}{4\pi D_L^2} = \frac{L}{4\pi (1+z)^2 D_C^2}. \tag{32}$$

And the angular diameter distance is defined as $D_A = d/\theta$,

where d is the physical diameter of the object, and θ is that angle (when small). Note that in Euclidean geometry, these distance measures are fully consistent with one another.

Finally, the age of the universe in a given cosmology is given by

$$t(z) = \frac{1}{H_0} \int_z^\infty \frac{dz'}{(1+z')E(z')}. \tag{33}$$

Each chapter that follows makes use of the differences between these distances for different cosmological models in order to determine which is most consistent with observations.

REFERENCES

Copi C. J., Huterer D., Schwarz D. J., Starkman G. D., 2009, MNRAS, 399, 295
Das S., et al., 2011, PRL, 107, 021301
Etherington I. M. H., 1933, Philosophical Magazine, 15
Friedmann A., 1922, Zeitschrift fur Physik, 10, 377
Hand N., et al., 2012, PRL, 109, 041101
Hogg D. W., 1999, arXiv Astrophysics e-prints,
Jimenez R., Loeb A., 2002, ApJ, 573, 37
Melia F., 2014, A&A, 561, A80
Melia F., 2018, American Journal of Physics, 86, 585
Melia F., 2019, arXiv e-prints, p. arXiv:1904.11365
Melia F., López-Corredoira M., 2018, A&A, 610, A87
Melia F., Maier R. S., 2013, MNRAS, 432, 2669
Melia F., Yennapureddy M. K., 2018, MNRAS, 480, 2144
Misner C. W., Sharp D. H., 1964, Physical Review, 136, 571
Padilla A., 2015, arXiv e-prints, p. arXiv:1502.05296
Planck Collaboration et al., 2018, arXiv e-prints, p. arXiv:1807.06209
Riess A. G., Casertano S., Yuan W., Macri L. M., Scolnic D., 2019, arXiv e-prints, p. arXiv:1903.07603
Robertson H. P., 1935, ApJ, 82, 284
Robertson H. P., 1936a, ApJ, 83, 187
Robertson H. P., 1936b, ApJ, 83, 257
Steinhardt P. J., 2011, Scientific American, 304, 36
Tolman R. C., 1929, ApJ, 69, 245
Wei J.-J., Wu X.-F., Melia F., 2015, MNRAS, 447, 479
Weinberg S., 1972, Gravitation and Cosmology: Principles and Applications of the General Theory of Relativity
Weinberg S., 1989, Reviews of Modern Physics, 61, 1
de Sitter W., 1917, Koninklijke Nederlandse Akademie van Wetenschappen Proceedings Series B Physical Sciences, 19, 1217

Chapter 1: Analysing H(z) data using two-point diagnostics

Chapter Summarized from MNRAS **470**, 2320-2327 (2017). Full article can be found in Appendix A.

The *Om* diagnostic was introduced by Sahni, Shafieloo, and Starobinsky (2008) as a method of testing cosmology. The *Om* diagnostic is intended to probe whether dark energy is a cosmological constant. When it is, $Om(z)=\Omega_{0m}$. The authors determined the value of *Om* at differing redshifts, and defined a two-point diagnostic $Om(z_1,z_2)\equiv Om(z_1)-Om(z_2)$. The $Om(z_1,z_2)$ diagnostic is a comparison of the inferred Ω_m behavior as a function of cosmic time. If observations are consistent with standard ΛCDM, $Om(z_1,z_2)$ would be zero, as the determination of *Om* would be independent of *z*.

Zheng et al. (2016) presented a further analysis of the two-point *Om* diagnostic. They made use of model-independent determinations of the Hubble constant as a function of redshift[$H(z)$], specifically by the use of the so-called cosmic chronometers. Cosmic chronometers (Moresco et al. 2016b) are passively-evolving elliptical galaxies that are thought to have had their stellar populations formed within a relatively short period of cosmic history. With the assumption that all stars within these galaxies formed nearly simultaneously, age of their stellar populations can be determined and the redshift-time derivative (dz/dt) may be inferred, immediately followed with

$$H(z)=-\frac{1}{1+z}\frac{dz}{dt}\approx-\frac{1}{1+z}\frac{\Delta z}{\Delta t}. \tag{34}$$

Zheng et al. converted the $H(z)$ measurements into the two-point *Om* diagnostic, and presented their results as they related to the several models considered.

In Leaf & Melia MNRAS 470, 2320-2327 (2017) we introduce a new $\Delta h\left(z_i, z_j\right)$ diagnostic, which may be applied to any cosmological model, including one that does not explicitly include Ω_m in its relevant calculations. (For example, $R_h = ct$, while certainly containing matter within its ρ term, does not make an a priori description of the relative evolution of Ω_m, Ω_r, and Ω_Λ.) Specifically, this diagnostic compares the measured Hubble constant at a given redshift with the Hubble constant predicted by a given cosmological model. It then compares observations at two separate redshifts. An average $\Delta h\left(z_i, z_j\right)$ value of '0' means that determinations of $H(z)$ across the redshift range of observations are consistent with the model (or may be consistently above or below the model by a some similar amount throughout the redshift range). The diagnostic is always ordered such that $z_i > z_j$. In contrast, a nonzero average (positive, for example), means that, generally, low-redshift determinations of $H(z)$ are less the model predictions, while high-redshift values are greater than it. This diagnostic thus tests how the *shape* of the model fit compares with the data, different in principle from a χ^2 analysis that only gives the average distance (squared) of data points from predictions. With 30 known cosmic chronometers, we consider a suite of 435 unique pairs of observations.

Of utmost importance to my analysis is the realization that the propagated errors determined by Zheng et al. in light of both weighted mean statistics (based on observer-reported measurement errors) and median statistics (see Gott et al. 2001 for the complete treatment) failed to take into account the significant systematic issues that always exist when constructing a mean or median from such a two-point diagnostic. A larger sample of data results in greater underestimates of the propagated errors when performed improperly. As

such, I first noticed the statistical issue with the larger amount of data considered in Chapter 2. I develop the proper method of applying weighted mean statistics to a two-point diagnostic, and propose a Monte-Carlo method of applying median statistics. While Zheng et al. showed that the several models considered gave diagnostics statistically incompatible with zero (thus appearing to be some evidence against the considered ΛCDM and other dark energy parameterizations), the correct application of statistics shows that those errors were significantly underestimated, alleviating most of the presumed tension. The $\Delta h\left(z_i, z_j\right)$ diagnostic applied to cosmic chronometer data strongly rules out the Einstein-de Sitter universe, while the other models are statistically consistent with the data. In addition, we show that $R_h = ct$ performs somewhat better than the other models.

Chapter 2: A two-point diagnostic for the HII galaxy Hubble diagram

Chapter summarized from MNRAS **474**, 4507-4513 (2018). Full article can be found in Appendix B.

HII galaxies and HII regions are locations in space wherein starbursts dominate the total luminosity. Melnick et al. (2000) and Siegel et al (2005) detail the potential for these sources to be used as standard candles. In Leaf & Melia MNRAS 474, 4507-4513 (2018), we present a new 2-point diagnostic comparing the expected distance modulus as a function of redshift from a given cosmological model with the distance modulus determined by the inferred luminosity distance to HII objects. This 2-point diagnostic is applied to the $R_h = ct$ universe, and two different ΛCDM parameterizations. First, we apply it to the most recent *Planck* data (Planck Collaboration 2016), and second to the best-fit Ω_m determined from the HII data set (this analysis is independent from the Hubble Constant H_0). In each case, two parameters linking the observed velocity dispersion to intrinsic luminosity are fitted, for two total free parameters in $R_h = ct$ and *Planck* ΛCDM, and three free parameters for a generic ΛCDM (the best fit-Ω_m value which was found to be consistent with *Planck*).

This analysis includes a suite of 156 sources (the same used in Terlevich et al. 2015). After the removal of several anomalous data points, we were left with 138 sources. With 138 sources, one has 9,453 pairs with which to determine a 2-point diagnostic. The issue with weighted mean and median statistics performed incorrectly is greatly compounded with a greater number of measurements, making the proper application of error propagation of utmost importance here. I also develop a different method of applying median statistics, with the goal of eliminating some systematic issues that may have existed in chapter 1. This analysis shows is $R_h = ct$ is more consistent with observations in light of this 2-point diagnostic than either of its competitors, although not to a level sufficient to draw a final conclusion.

Chapter 3: Model selection with strong-lensing systems

Chapter summarized from MNRAS **478**, 5104-5111 (2018). Full article can be found in Appendix C.

The prior chapters concerned generally lower-redshift observations. The highest-redshift cosmic chronometer considered is at z=1.965, while HII galaxies have been observed nearly to z=3. Strongly lensed galaxies are consistently being discovered at greater redshifts. The catalog of confirmed strongly-lensed galaxies is continuing to grow rapidly (Diehl et al. 2017). In Leaf & Melia MNRAS 478, 5104-5111 (2018), we compile the largest ever catalog of 158 confirmed galaxy-galaxy strong lens systems, and use the inferred angular diameter distances between the lensing and source galaxies to constrain and compare cosmological models. The most distant confirmed lens in our sample is at z=3.6, with 9 lenses at z>3. Prior analyses by Melia, Wei, & Wu (2015) and Cao et al. (2015) utilized significantly smaller catalogs.

The standard approach to determine the angular diameter distance between two galaxies is to use a simple singular isothermal ellipsoid mass profile for the intervening (lensing) galaxy. Both of the aforementioned analyses found that an even simpler singular isothermal sphere model (SIE with zero ellipticity) was consistent with the data. However, Cao et al. (2015) pointed out an interesting apparent systematic effect in the data. In our analysis in this chapter, we attempt to mitigate this effect by the use of an artificial error term. Specifically, we determine the additional percent error term that is applied to the angular diameter distance that results in a reduced χ^2 value of 1 (which would be consistent with Gaussian random errors) in a fitted ΛCDM model. This best-fit ΛCDM model remains consistent with the latest *Planck* parameters, and the

additional additive percent error found is 12.2%. Then, with this error term determined, we completed a fit to wCDM as well, and perform a direct relative likelihood comparison between the models (the empty Milne and matter-dominated Einstein-de Sitter models are also included) In order to do this, we make use of the Bayesian Information Criterion (BIC) which allows for models of differing numbers of free parameters to be compared. We show that the Milne and EdS models are strongly rejected, while $R_h = ct$ is nearly three times more likely to be the correct model than the fitted ΛCDM. In addition, we find that the 40 additional lenses from the SLAC survey (Citation) added to the catalog since Cao et al. (2015) only continued the same systematic effect they found. We conclude that either errors on the measured galaxy velocity dispersions are underestimated, or that the SIS mass model is too simplified to give accurate results for any observed velocity dispersion.

Chapter 4: Cosmological test using the high-redshift detection rate of FSRQs with the Square Kilometer Array

Chapter summarized from MNRAS **487**, 2030-2037 (2019). Full article can be found in Appendix D.

The first three chapters concerned the use of existing astronomical measurements to infer a cosmographic parameter, which was then used by some statistical method to constrain and compare several models. This final chapter is instead entirely a prediction of what the Square Kilometer Array (SKA) will be able to detect at high redshift in some given cosmology.

The objects in the universe with the greatest luminosities are active galactic nuclei. Active galactic nuclei consist of an incredibly compact, high mass central object (generally considered to be a black hole). The standard model of these highly luminous galaxies includes the possibility of a powerful relativistic jet of particles emitted along the black hole's axis of rotation. These jets, when they serendipitously point directly at us, appear to have the highest luminosities of any active galaxies (and are dubbed 'blazars'). These objects, being so luminous, I suggest are among the most distant individual objects that may be observed by any observatory. Relativistic jets are observed strongly in the radio band (citation), and as such the SKA has the potential to detect them at greater distance than any radio observatory before it.

Blazars exist in two classes, BL-Lacertae objects (BL Lacs) and Flat Spectrum Radio Galaxies (FSRQs). The current picture of these objects has BL Lacs containing extremely massive central black holes and are accreting at sub-Eddington rates. FSRQs may be (but are not required to be) of smaller mass and generally have high inferred accretion rates. BL Lacs have not been detected at

high (z>4) redshifts, while FSRQs are. Furthermore, analyses of the blazar sequence (Ghisellini et al. 2017) demonstrate that FSRQs have highly consistent broad-band spectral energy distributions across luminosity ranges.

Therefore, in chapter 4, we present a phenomenological method of characterizing FSRQ radio emission as a function of mass alone (assuming a high accretion rate and duty cycles near 1, consistent with the observation of AGNs at $z > 6$). To do this, we use a sample of high-luminosity Fermi blazars with a high accretion rate, and augment this sample with gamma-ray Seyfert 1 galaxies (which recent observations have suggested can be described as lower-mass FSRQs) to build an association of mass with radio luminosity.

The quasar mass function at $z = 6$ (Willott et al. 2010) is extrapolated to higher redshift by the assumption of Eddington-limited accretion, and the aforementioned luminosities are used to determine the smallest blazar that phase 1 of the SKA may be expected to observe. The final number of detectable blazars as a function of redshift is strongly dependent on cosmology, specifically of luminosity distance, comoving distance, and cosmic time. Our results show that in the redshift range where this analysis is most valid, the SKA1 surveys should find 40 times more blazars in ΛCDM than in $R_h = ct$. We conclude that due to the existence of a surprisingly high-mass active galaxy at $z \sim 7.5$, (Bañados et al. 2018), excluded by our simple lockstep growth model in both cosmologies, that our analysis is a lower limit on the number of anticipated galaxies in either model. Some quasars may have already passed their active phase by $z = 6$, and thus not be included in the quasar mass function at $z = 6$. In spite of this, these lower limits should allow these SKA surveys to strongly prefer one cosmology over the other. Finally, I expect that the SKA's high-redshift observations will allow for a better-constrained $z > 6$ radio-loud quasar fraction than is known at present, which will reduce the errors on this prediction considerably.

Conclusion

Throughout the completion of this research, the primary goal has been to perform unbiased comparisons between cosmological models using entirely model-independent data by the use of new or improved sta

stistical methods, new observations, and the prospect of new observations. In chapters 1, 2, and 3, I found that $R_h = ct$ performs at least as well as ΛCDM by all metrics considered. In the final chapter, I presented predictions for observables at higher redshift than the observations used in prior chapters, exemplifying the great differences between these models in the early universe.

The purpose of the first project, involving applying a 2-point diagnostic to cosmic chronometers, was to use model-independent measurements of H(z) to do a comparative analysis of cosmological models with a 2-point diagnostic. The existing $Om(z_1, z_2)$ diagnostic used by Zheng et al (2016) cannot be applied to a model without an a priori description of matter evolution. As such, I devised a new diagnostic that may be applied to any model that describes the evolution of $H(z)$. In addition, I demonstrated the proper method of performing statistical analyses of any such 2-point diagnostic. In this analysis, I found $R_h = ct$ to be preferred to ΛCDM, but not sufficient to make a definitive selection between the two.

Following the publication of chapter 1, Melia & Yennapureddy (2018) performed an additional analysis of cosmic chronometers using Gaussian processes, coming to a similar conclusion that $R_\mathrm{h} = ct$ is preferred by the data. However, a recent analysis has suggested that chronometers may not be as accurate as previously supposed, due to the potential of young stars existing in these galaxies (López-Corredoira & Vazdekis 2018). If this turns out to be a

significant effect, then it would weaken (but not invalidate) the conclusions drawn by analyses based on them. Finally, in response to my treatment of the errors of two-point diagnostics, Zheng et al (2018) acknowledged the 'more rigorous' treatment of the statistics that I developed.

The successful application of a 2-point diagnostic to cosmic chronometers influenced the decision to apply a similar diagnostic to observations of HII galaxies and regions. Here again, the 2-point diagnostic showed that $R_h = ct$ was the most consistent with the data across the entire considered redshift range as compared with ΛCDM, although we inferred some unaccounted-for random or systematic error resulting in each model being more than 1-sigma inconsistent with a diagnostic of '0'.

Observations of strongly lensed galaxies observations are experiencing rapid growth, making their analysis in a cosmological context highly desirable. The catalog used in chapter 3 is the largest of galaxy-galaxy lenses compiled as of its publication, and allowed for measurements of the angular diameter distance across a very wide redshift range. While there appears to be some issue with the singular isothermal ellipsoid model, the inferred angular diameter distances remain consistent with the $R_h = ct$ universe, despite the artificial error term used being tuned to a fitted ΛCDM model. With the understanding that the method used needs improvement, we found $R_h = ct$ to be preferred over ΛCDM. In addition, this analysis strongly excluded the Milne and Einstein-de-Sitter universes.

Looking ahead, even higher-redshift strongly lensed galaxies have been observed than those analyzed in Chapter 3. Fan et al. 2019 recently presented a strongly lensed source galaxy at z=6.51. Furthermore, the Dark Energy Survey

continues to observe new lenses (Jacobs et al. 2019) with many lens galaxies at z>0.8 (significantly higher than those in chapter 3's catalog). As spectroscopic follow-ups confirm the redshifts of these more distant lenses, I anticipate these being even more powerful probes of cosmology. A hypothetical strongly lensed galaxy with lens at z=1.3 and source at z=6 would have the angular diameter distances between them predicted by $R_h = ct$ and ΛCDM differ by 10%. This would mean that even the results of an analysis with the SIS model may be accurate enough to discriminate between models (recalling that the estimated systematic effect was ~12%). The difference in angular diameter distances predicted by each model for the sample of 158 galaxies we used was only on average 2.31%. Strong lenses have the potential to be even more powerful tools for model comparison in the very near future.

Finally, in chapter 4 we presented theoretical predictions for astronomical observations at greater redshift than any considered in the prior chapters. We proposed a phenomenological approach for determining the radio emission of high-z FSRQs as a function of their central black hole mass. This emission model was applied to a simple black hole growth method to determine the amount of AGN detectable by the upcoming Square Kilometer Array. We found drastically different predictions between $R_h = ct$ and ΛCDM, such that the former predicts far fewer observed FSRQs at z>7 than the latter. This prediction constitutes a lower limit on the number of objects to be expected by SKA. We expect the extreme difference between the two models will make the detections by SKA definitively select between $R_h = ct$ and ΛCDM.

The phenomenological approach of describing high-redshift blazar emission should be applicable to other wavebands, with the caveat that the Fermi blazar

sequence (Ghisellini et al. 2017) does not include thermal emission (either from a disk or hot corona) in its overall spectral energy distribution. The method should therefore be applicable to gamma-ray observations of high-redshift FSRQs, allowing predictions to be made for potential future gamma-ray observatories like *e-ASTROGAM* (De Angelis et al. 2017) in the 2030s, ideally with new measurements of the BH mass function in the range $6.5<z<7$ or higher.

In each of the three investigations of existing measurements detailed in this dissertation, I have demonstrated that the $R_h = ct$ universe performs at least as well as a ΛCDM model. The wide range of measurements considered here (and in other works) are evidence that the $R_h = ct$ universe ought to be taken seriously by the astronomical community at large as a viable description of many observable properties of the Universe. We are experiencing an unprecedented rate of new measurements of astrophysical phenomena at high redshifts. For example, the catalog of high-redshift AGNs maintained by Perger et al. (2017) showed that of the ~ 170 known AGNs at $z>6$ as of January 2019, 80 were discovered in 2018. This rapidly growing suite of observations will allow for a definitive conclusion in the near future regarding whether ΛCDM or $R_h = ct$ better describes our Universe, or if some new physics may be required to truly understand cosmology.

REFERENCES

De Angelis A., et al., 2017, Experimental Astronomy, 44, 25
Fan X., et al., 2019, ApJ, 870, L11
Ghisellini G., Righi C., Costamante L., Tavecchio F., 2017, MNRAS, 469, 255
Jacobs C., et al., 2019, MNRAS, 484, 5330
López-Corredoira M., Vazdekis A., 2018, A&A, 614, A127
Melia F., Yennapureddy M. K., 2018, J. Cosmology Astropart. Phys., 2, 034
Perger K., Frey S., Gabányi K. É., Tóth L. V., 2017, Frontiers in Astronomy and Space Sciences, 4, 9
Zheng X., Ding X., Biesiada M., Cao S., Zhu Z.-H., 2016, ApJ, 825, 17
Zheng X., Biesiada M., Ding X., Cao S., Zhang S., Zhu Z.-H., 2018, arXiv e-prints,

COMPLETE DISSERTATION REFERENCES

Abazajian K. N., et al., 2009, ApJS, 182, 543
Acero F., et al., 2015, ApJS, 218, 23
Ackermann M., et al., 2015, VizieR Online Data Catalog, p. J/ApJ/810/14
Alcaniz J. S., Lima J. A. S., 1999, ApJ, 521, L87
An H., Romani R. W., 2018, ApJ, 856, 105
Antonucci R., 1993, ARA&A, 31, 473
Auger M. W., Treu T., Bolton A. S., Gavazzi R., Koopmans L. V. E., Marshall P. J., Bundy K., Moustakas L. A., 2009, ApJ, 705, 1099
Bañados E., et al., 2015, ApJ, 804, 118
Bañados E., et al., 2018, Nat, 553, 473
Beckmann V., Shrader C. R., 2012, Active Galactic Nuclei
Bergeron J., 1977, ApJ, 211, 62
Betoule M., et al., 2014, A&A, 568, A22
Blake C., et al., 2012, MNRAS, 425, 405
Bolton A. S., Burles S., Koopmans L. V. E., Treu T., Gavazzi R., Moustakas L. A., Wayth R., Schlegel D. J., 2008, ApJ, 682, 964
Bordalo V., Telles E., 2011, ApJ, 735, 52
Bosch G., Terlevich E., Terlevich R., 2002, MNRAS, 329, 481
Brownstein J. R., et al., 2012, ApJ, 744, 41
Bull P., et al., 2018, arXiv e-prints, p. arXiv:1810.02680
Cao S., Pan Y., Biesiada M., Godlowski W., Zhu Z.-H., 2012, J. Cosmology Astropart. Phys., 2012, 016
Cao S., Biesiada M., Gavazzi R., Piórkowska A., Zhu Z.-H., 2015, ApJ, 806, 185
Chávez R., Terlevich E., Terlevich R., Plionis M., Bresolin F., Basilakos S., Melnick J., 2012, MNRAS, 425, L56
Chávez R., Terlevich R., Terlevich E., Bresolin F., Melnick J., Plionis M., Basilakos S., 2014, MNRAS, 442, 3565
Chávez R., Plionis M., Basilakos S., Terlevich R., Terlevich E., Melnick J., Bresolin F., González-Morán A. L., 2016, MNRAS, 462, 2431
Chevallier M., Polarski D., 2001, International Journal of Modern Physics D, 10, 213
Copi C. J., Huterer D., Schwarz D. J., Starkman G. D., 2009, MNRAS, 399, 295
Coppejans R., et al., 2016, MNRAS, 463, 3260
Dai Z. G., Liang E. W., Xu D., 2004, ApJ, 612, L101
Das S., et al., 2011, PRL, 107, 021301
De Angelis A., et al., 2017, Experimental Astronomy, 44, 25
Diehl H. T., et al., 2017, ApJS, 232, 15
Ding X., Biesiada M., Cao S., Li Z., Zhu Z.-H., 2015, ApJ, 803, L22
Einstein A., 1936, Science, 84, 506
Enea Romano A., 2016, arXiv e-prints, p. arXiv:1609.04081
Erb D. K., Steidel C. C., Shapley A. E., Pettini M., Reddy N. A., Adelberger K. L., 2006a, ApJ, 646, 107
Erb D. K., Steidel C. C., Shapley A. E., Pettini M., Reddy N. A., Adelberger K. L., 2006b, ApJ, 647, 128
Etherington I. M. H., 1933, Philosophical Magazine, 15
Fabian A. C., Walker S. A., Celotti A., Ghisellini G., Mocz P., Blundell K. M., McMahon R. G., 2014, MNRAS, 442, L81
Fan X., et al., 2001, AJ, 122, 2833
Fan X., et al., 2019, ApJ, 870, L11
Fatuzzo M., Melia F., 2017, ApJ, 846, 129
Friedmann A., 1922, Zeitschrift fur Physik, 10, 377
Fuentes-Masip O., Muñoz-Tuñón C., Castañeda H. O., Tenorio-Tagle G., 2000, AJ, 120, 752
Gavazzi R., Marshall P. J., Treu T., Sonnenfeld A., 2014, ApJ, 785, 144
Gaztañaga E., Cabré A., Hui L., 2009, MNRAS, 399, 1663
Ghirlanda G., Ghisellini G., Lazzati D., Firmani C., 2004, ApJ, 613, L13
Ghisellini G., Sbarrato T., 2016, MNRAS, 461, L21
Ghisellini G., Maraschi L., Tavecchio F., 2009a, MNRAS, 396, L105
Ghisellini G., Foschini L., Volonteri M., Ghirlanda G., Haardt F., Burlon D., Tavecchio F., 2009b, MNRAS, 399, L24
Ghisellini G., Tavecchio F., Foschini L., Ghirlanda G., Maraschi L., Celotti A., 2010, MNRAS, 402, 497
Ghisellini G., Righi C., Costamante L., Tavecchio F., 2017, MNRAS, 469, 255
Gopal Vishwakarma R., 2013, Phys. Scr., 87, 055901
Gott J. Richard I., Vogeley M. S., Podariu S., Ratra B., 2001, ApJ, 549, 1
Grillo C., Lombardi M., Bertin G., 2008, A&A, 477, 397
Hand N., et al., 2012, PRL, 109, 041101
Hanson D., et al., 2013, PRL, 111, 141301
Hogg D. W., 1999, arXiv Astrophysics e-prints,

Hovatta T., Valtaoja E., Tornikoski M., Lähteenmäki A., 2009, A&A, 494, 527
Hoyos C., Koo D. C., Phillips A. C., Willmer C. N. A., Guhathakurta P., 2005, ApJ, 635, L21
Inserra C., Smartt S. J., 2014, ApJ, 796, 87
Jacobs C., et al., 2019, MNRAS, 484, 5330
Jie A., Bao-Rong C., Li-Xin X., 2016, Chinese Physics Letters, 33, 079801
Jimenez R., Loeb A., 2002, ApJ, 573, 37
Jimenez R., Verde L., Treu T., Stern D., 2003, ApJ, 593, 622
Jorgensen I., Franx M., Kjaergaard P., 1995a, MNRAS, 273, 1097
Jorgensen I., Franx M., Kjaergaard P., 1995b, MNRAS, 276, 1341
Kauffmann G., Haehnelt M., 2000, MNRAS, 311, 576
Keenan R. C., Barger A. J., Cowie L. L., 2013, ApJ, 775, 62
King L. J., et al., 1998, MNRAS, 295, L41
Kochanek C. S., et al., 2000, ApJ, 543, 131
Koopmans L. V. E., Treu T., 2003, ApJ, 583, 606
Krolik J. H., Begelman M. C., 1986, ApJ, 308, L55
Kunth D., Östlin G., 2000, A&ARv, 10, 1
Leaf K., Melia F., 2017, MNRAS, 470, 2320
Leaf K., Melia F., 2018a, MNRAS, 474, 4507
Leaf K., Melia F., 2018b, MNRAS, 478, 5104
Leaf K., Melia F., 2019, MNRAS, 487, 2030
Lima J. A. S., Alcaniz J. S., 2000, MNRAS, 317, 893
Linder E. V., 2003, PRL, 90, 091301
López-Corredoira M., Vazdekis A., 2018, A&A, 614, A127
Lusso E., Risaliti G., 2016, ApJ, 819, 154
Mania D., Ratra B., 2012, Physics Letters B, 715, 9
Maseda M. V., et al., 2014, ApJ, 791, 17
Masters D., et al., 2014, ApJ, 785, 153
Melia F., 2003, The Edge of Infinity
Melia F., 2007, MNRAS, 382, 1917
Melia F., 2012, AJ, 144, 110
Melia F., 2013a, A&A, 553, A76
Melia F., 2013b, ApJ, 764, 72
Melia F., 2014a, A&A, 561, A80
Melia F., 2014b, J. Cosmology Astropart. Phys., 2014, 027
Melia F., 2016, Frontiers of Physics, 11, 119801
Melia F., 2017a, Frontiers of Physics, 12, 129802
Melia F., 2017b, MNRAS, 464, 1966
Melia F., 2018a, American Journal of Physics, 86, 585
Melia F., 2018b, MNRAS, 481, 4855
Melia F., Abdelqader M., 2009, International Journal of Modern Physics D, 18, 1889
Melia F., Koenigl A., 1989, in Hunt J., Battrick B., eds, ESA Special Publication Vol. 296, Two Topics in X-Ray Astronomy, Volume 1: X Ray
Binaries. Volume 2: AGN and the X Ray Background. pp 995–1000
Melia F., López-Corredoira M., 2017, International Journal of Modern Physics D, 26, 1750055
Melia F., López-Corredoira M., 2018, A&A, 610, A87
Melia F., Maier R. S., 2013, MNRAS, 432, 2669
Melia F., McClintock T. M., 2015a, AJ, 150, 119
Melia F., McClintock T. M., 2015b, Proceedings of the Royal Society of London Series A, 471, 20150449
Melia F., Shevchuk A. S. H., 2012, MNRAS, 419, 2579
Melia F., Yennapureddy M. K., 2018a, J. Cosmology Astropart. Phys., 2, 034
Melia F., Yennapureddy M. K., 2018b, MNRAS, 480, 2144
Melia F., Wei J.-J., Wu X.-F., 2015, AJ, 149, 2
Melnick J., Moles M., Terlevich R., Garcia-Pelayo J.-M., 1987, MNRAS, 226, 849
Melnick J., Terlevich R., Moles M., 1988, MNRAS, 235, 297
Melnick J., Terlevich R., Terlevich E., 2000, MNRAS, 311, 629
Misner C. W., Sharp D. H., 1964, Physical Review, 136, 571
Moresco M., 2015, MNRAS, 450, L16
Moresco M., et al., 2012, J. Cosmology Astropart. Phys., 2012, 006
Moresco M., Jimenez R., Verde L., Cimatti A., Pozzetti L., Maraston C., Thomas D., 2016, J. Cosmology Astropart. Phys., 2016, 039
Padilla A., 2015, arXiv e-prints, p. arXiv:1502.05296
Paliya V. S., Stalin C. S., Shukla A., Sahayanathan S., 2013, ApJ, 768, 52

Paliya V. S., Ajello M., Rakshit S., Mand al A. K., Stalin C. S., Kaur A., Hartmann D., 2018, ApJ, 853, L2
Paliya V. S., Parker M. L., Jiang J., Fabian A. C., Brenneman L., Ajello M., Hartmann D., 2019, ApJ, 872, 169
Perger K., Frey S., Gabányi K. É., Tóth L. V., 2017, Frontiers in Astronomy and Space Sciences, 4, 9
Perlmutter S., et al., 1998, Nat, 391, 51
Planck Collaboration et al., 2014, A&A, 571, A23
Planck Collaboration et al., 2016, A&A, 594, A11
Planck Collaboration et al., 2018, arXiv e-prints, p. arXiv:1807.06209
Plionis M., Terlevich R., Basilakos S., Bresolin F., Terlevich E., Melnick J., Chavez R., 2011, MNRAS, 416, 2981
Ratnatunga K. U., Griffiths R. E., Ostrand er E. J., 1999, AJ, 117, 2010
Riess A. G., et al., 1998, AJ, 116, 1009
Riess A. G., et al., 2018, ApJ, 861, 126
Riess A. G., Casertano S., Yuan W., Macri L. M., Scolnic D., 2019, arXiv e-prints, p. arXiv:1903.07603
Robertson H. P., 1935, ApJ, 82, 284
Robertson H. P., 1936a, ApJ, 83, 187
Robertson H. P., 1936b, ApJ, 83, 257
Sahni V., Shafieloo A., Starobinsky A. A., 2014, ApJ, 793, L40
Schmidt B. P., et al., 1998, ApJ, 507, 46
Searle L., Sargent W. L. W., 1972, ApJ, 173, 25
Shafieloo A., Sahni V., Starobinsky A. A., 2012, Phys. Rev. D, 86, 103527
Shakura N. I., 1973, Soviet Ast., 16, 756
Shi X., 1997, ApJ, 486, 32
Shu Y., et al., 2017, ApJ, 851, 48
Siegel E. R., Guzmán R., Gallego J. P., Orduña López M., Rodríguez Hidalgo P., 2005, MNRAS, 356, 1117
Sikora M., Madejski G., 2001, in Aharonian F. A., Völk H. J., eds, American Institute of Physics Conference Series Vol. 558, American Institute of
Physics Conference Series. pp 275–288 (*arXiv:astro-ph/0101382*), doi:10.1063/1.1370797
Simon J., Verde L., Jimenez R., 2005, Phys. Rev. D, 71, 123001
Smith K. M., Zahn O., Doré O., 2007, Phys. Rev. D, 76, 043510
Sonnenfeld A., Gavazzi R., Suyu S. H., Treu T., Marshall P. J., 2013a, ApJ, 777, 97
Sonnenfeld A., Treu T., Gavazzi R., Suyu S. H., Marshall P. J., Auger M. W., Nipoti C., 2013b, ApJ, 777, 98
Square Kilometre Array Cosmology Science Working Group et al., 2018, arXiv e-prints,
Steinhardt P. J., 2011, Scientific American, 304, 36
Stern D., Jimenez R., Verde L., Stanford S. A., Kamionkowski M., 2010, ApJS, 188, 280
Telles E., 2003, in Perez E., Gonzalez Delgado R. M., Tenorio-Tagle G., eds, Astronomical Society of the Pacific Conference Series Vol. 297, Star
Formation Through Time. p. 143
Terlevich R., Melnick J., 1981, MNRAS, 195, 839
Terlevich R., Terlevich E., Melnick J., Chávez R., Plionis M., Bresolin F., Basilakos S., 2015, MNRAS, 451, 3001
Tolman R. C., 1929, ApJ, 69, 245
Treu T., Koopmans L. V. E., 2002, ApJ, 575, 87
Treu T., Koopmans L. V. E., 2004, ApJ, 611, 739
Treu T., et al., 2005, ApJ, 633, 174
Treu T., Koopmans L. V., Bolton A. S., Burles S., Moustakas L. A., 2006, ApJ, 640, 662
Urry C. M., Padovani P., 1995, PASP, 107, 803
Volonteri M., Haardt F., Ghisellini G., Della Ceca R., 2011, MNRAS, 416, 216
Wang F., et al., 2018, arXiv e-prints, p. arXiv:1810.11926
Wei J.-J., Wu X.-F., Melia F., 2013, ApJ, 772, 43
Wei J.-J., Wu X.-F., Melia F., Maier R. S., 2015a, AJ, 149, 102
Wei J.-J., Wu X.-F., Melia F., 2015b, AJ, 149, 165
Wei J.-J., Wu X.-F., Melia F., Wang F.-Y., Yu H., 2015c, AJ, 150, 35
Wei J.-J., Wu X.-F., Melia F., 2015d, MNRAS, 447, 479
Wei J.-J., Wu X.-F., Melia F., 2016, MNRAS, 463, 1144
Wei J.-J., Melia F., Wu X.-F., 2017, ApJ, 835, 270
Weigel A. K., Schawinski K., Treister E., Urry C. M., Koss M., Trakhtenbrot B., 2015, MNRAS, 448, 3167
Weinberg S., 1972, Gravitation and Cosmology: Principles and Applications of the General Theory of Relativity
Weinberg S., 1989, Reviews of Modern Physics, 61, 1
Willott C. J., et al., 2010, AJ, 140, 546
Wu J., Ghisellini G., Hodges-Kluck E., Gallo E., Ciardi B., Haardt F., Sbarrato T., Tavecchio F., 2017, MNRAS, 468, 109
Wyithe J. S. B., Loeb A., 2003, ApJ, 595, 614
Yennapureddy M. K., Melia F., 2018, European Physical Journal C, 78, 258
Zhang C., Zhang H., Yuan S., Liu S., Zhang T.-J., Sun Y.-C., 2014, Research in Astronomy and Astrophysics, 14, 1221

Zheng X., Ding X., Biesiada M., Cao S., Zhu Z.-H., 2016, ApJ, 825, 17
Zheng X., Biesiada M., Ding X., Cao S., Zhang S., Zhu Z.-H., 2018, arXiv e-prints,
de Sitter W., 1917, Koninklijke Nederlandse Akademie van Wetenschappen Proceedings Series B Physical Sciences, 19, 1217

Monthly Notices of the ROYAL ASTRONOMICAL SOCIETY

MNRAS **470,** 2320–2327 (2017)
Advance Access publication 2017 June 9

doi:10.1093/mnras/stx1437

Analysing $H(z)$ data using two-point diagnostics

Kyle Leaf[1]★ and Fulvio Melia[2]★†

[1]*Department of Physics, The University of Arizona, AZ 85721, USA*
[2]*Department of Physics, The Applied Math Program, and Department of Astronomy, The University of Arizona, AZ 85721, USA*

Accepted 2017 June 7. Received 2017 June 7; in original form 2017 April 20

ABSTRACT

Measurements of the Hubble constant $H(z)$ are increasingly being used to test the expansion rate predicted by various cosmological models. But the recent application of two-point diagnostics, such as $Om(z_i, z_j)$ and $Omh^2(z_i, z_j)$, has produced considerable tension between ΛCDM's predictions and several observations, with other models faring even worse. Part of this problem is attributable to the continued mixing of truly model-independent measurements using the cosmic-chronometer approach, and model-dependent data extracted from baryon acoustic oscillations. In this paper, we advance the use of two-point diagnostics beyond their current status, and introduce new variations, which we call $\Delta h(z_i, z_j)$, that are more useful for model comparisons. But we restrict our analysis exclusively to cosmic-chronometer data, which are truly model independent. Even for these measurements, however, we confirm the conclusions drawn by earlier workers that the data have strongly non-Gaussian uncertainties, requiring the use of both 'median' and 'mean' statistical approaches. Our results reveal that previous analyses using two-point diagnostics greatly underestimated the errors, thereby misinterpreting the level of tension between theoretical predictions and $H(z)$ data. Instead, we demonstrate that as of today, only Einstein–de Sitter is ruled out by the two-point diagnostics at a level of significance exceeding $\sim 3\sigma$. The $R_h = ct$ universe is slightly favoured over the remaining models, including Lambda cold dark matter and Chevalier–Polarski–Linder, though all of them (other than Einstein–de Sitter) are consistent to within 1σ with the measured mean of the $\Delta h(z_i, z_j)$ diagnostics.

Key words: galaxies: distances and redshifts – galaxies: evolution – large-scale structure of Universe – cosmology: observations – cosmology: theory.

1 INTRODUCTION

Lambda cold dark matter (ΛCDM) has done reasonably well accounting for a broad range of data and is therefore correctly viewed as the current standard model of cosmology (see, e.g. Planck Collaboration XXIII 2014). But recent analyses of the two-point correlation function of the cosmic microwave background (Melia 2014; Copi et al. 2015), as well as the $Om(z_i, z_j)$ and $Omh^2(z_i, z_j)$ diagnostics applied to measurements of the Hubble expansion rate $H(z)$ (Shafieloo, Sahni & Starobinsky 2012; Sahni, Shafieloo & Starobinsky 2014), appear to have revealed significant tension between its predictions and recent measurements (see, e.g. Zheng et al. 2016).

In this paper, we directly address the problems highlighted by the various analyses carried out with the $H(z)$ data, which apparently do not confirm the anticipated transition from early deceleration to more recent acceleration in the cosmic expansion rate (Jimenez & Loeb 2002; Moresco et al. 2016a). With this type of work, one typically compiles a unified sample of $H(z)$ versus redshift measurements based on various approaches, including the determination of differential ages using cosmic chronometers (Moresco et al. 2016b) and the inference of a characteristic distance scale revealed in baryon acoustic oscillations (BAOs; see, e.g. Blake et al. 2012).

However, it is inadvisable to make combined use of BAO measurements with other data. The BAO approach results in certain systematic effects that are difficult to quantify, certainly without the pre-assumption of a particular model. A BAO determination of $H(z)$ relies on both determining the actual baryon acoustic peak of a cluster, and the degree of contamination from the Alcock–Paczýnski effect (see, e.g. Melia & López-Corredoira 2017).

To disentangle these effects, one must choose a cosmological model in order to determine the overall comoving acoustic scale, rendering the determination of $H(z)$ using BAO data unique to each model. BAO therefore provide useful data for analysing a specific model, but a comparative analysis of multiple cosmologies requires a careful recalibration of the acoustic scale for each individual

★ E-mail: kyleaf@email.arizona.edu (KL); melia@physics.arizona.edu (FM)
† John Woodruff Simpson Fellow.

case. In contrast, the differential age method is fundamentally much simpler. It has some systematic error based on using the Extended Press-Schechter approximation (Moresco et al. 2016a), but is heavily based on directly observable galaxy properties. Zheng et al. (2016) demonstrated via the analysis of several cosmological models that the merger of differential-age and BAO data resulted in statistically significant discrepancies when compared to the use of either data set on its own.

In this paper, we therefore restrict our attention to the sample of thirty model-independent cosmic chronometer measurements of $H(z)$ (Jimenez et al. 2003; Simon, Verde & Jimenez 2005; Stern et al. 2010; Moresco et al. 2012; Zhang et al. 2014; Moresco 2015; Moresco et al. 2016a) to carry out a comparative test of several cosmological models, using variants of the previously introduced two-point correlation functions that may be applied to any cosmology, not solely those framed in the context of ΛCDM. The previously defined $Om(z_i, z_j)$ and $Omh^2(z_i, z_j)$ diagnostics are based on the presence of an $\Omega_{\rm m}$ parameter in the formulation of the expansion rate $H(z)$, which restricts their use primarily to ΛCDM and its variations (Sahni et al. 2014). Throughout this paper, we define $\Omega_{\rm m} \equiv \rho_{\rm m}/\rho_c$ to be the matter energy density $\rho_{\rm m}$ today as a fraction of the critical density $\rho_c \equiv 3c^2H_0^2/8\pi G$.

We will be comparing the observations with the predicted expansion rate in five models, including ΛCDM, wCDM, $R_{\rm h} = ct$ (Melia 2007; Melia & Abdelqader 2009; Melia & Shevchuk 2012; Melia 2016a, 2017), Chevalier–Polarski–Linder (Chevalier & Polarski 2001; Linder 2003) and Einstein–de Sitter. Each of these cosmologies has a distinct relationship between $H(z)$ and z, and some have a parametrization that allows a best-fitting model to be identified via the optimization of certain free parameters. In previous studies, such a parametric fitting of the Hubble constant has been used with the $H(z)$ data to identify the ideal model parameters in ΛCDM, and, in a few cases, a direct comparison has also been made between ΛCDM and $R_{\rm h} = ct$, though the latter has no free parameters for this purpose, so one must necessarily rely on information criteria to calculate relative likelihoods (Melia & Maier 2013; Melia & McClintock 2015; Wei, Melia & Wu 2017).

The two-point diagnostics differ from this parametric fitting approach in several distinct ways, extending the model comparison in new and statistically meaningful directions. Previously, Ding et al. (2015) and Zheng et al. (2016) employed two two-point diagnostics (i.e. $Om[z_i, z_j]$ and $Omh^2[z_i, z_j]$), involving $\Omega_{\rm m}$ and $\Omega_{\rm m}^2$, applicable to several cosmological models. In these analyses, the two-point diagnostic was calculated based on the $\Omega_{\rm m}$ parameter in ΛCDM, such that it should be consistent with zero if ΛCDM were the correct model. Then, the expectation value of that diagnostic was determined for all the models being considered, and the one most consistent with it was judged to be favoured over the others. Their results, however, were rather inconclusive. Zheng et al. (2016) found that, while ΛCDM was the model most favoured by the data among the tested sample, it was still nonetheless significantly inconsistent with the measurements, especially on the basis of 'median statistics' (see, e.g. Gott et al. 2001). Other dark-matter parameterizations, such as wCDM and CPL (Chevalier & Polarski 2001; Linder 2003) performed even worse.

But one must be aware of the fact that in their diagnostic, a value of H_0 must be chosen a priori, even though there is still no consensus on what its true value is, given that high-redshift measurements (e.g. Planck Collaboration XXIII 2014) are in tension with H_0 measured locally (e.g. using Type Ia SNe; see Wei et al 2017, and references cited therein). In addition, we shall demonstrate in this paper that the statistics of two-point diagnostics has been used improperly in earlier applications, including those of Ding et al. (2015) and Zheng et al. (2016). Specifically, we shall show that previous applications of two-point diagnostics have overestimated the confidence level of their results, thereby overstating the tension between, for example, the measured $H(z)$ values and predictions by ΛCDM. We will introduce new two-point diagnostics similar in spirit to the previously defined $Om(z_i, z_j)$ and $Omh^2(z_i, z_j)$, which, however, are appropriate for a broader range of models, including $R_{\rm h} = ct$, that was not included in Zheng et al.'s (2016) study. In spite of these improvements to the analysis of two-point diagnostics, however, we will confirm the results first demonstrated by Ding et al. (2015) and Zheng et al. (2016), that the errors reported in conjunction with the cosmic chronometer data are at least partially non-Gaussian.

Our goals in this paper are threefold. First, we extend the previous work with two-point diagnostics to a more comprehensive comparison of various models. As noted, our approach allows the inclusion of cosmologies whose parametrization is not based on $\Omega_{\rm m}$. Secondly, we restrict our analysis to the 30 cosmic chronometer measurements to ensure that the data are as free as possible of model biases. Thirdly, we present a more in-depth analysis of the statistics used with two-point diagnostics and demonstrate that one must modify the weighted-mean and median statistics when using quantities such as $Om(z_i, z_j)$ and $Omh^2(z_i, z_j)$. In Section 2, we reintroduce these previously defined diagnostics, and then define a similar diagnostic that is applicable to a broader range of models. We summarize the data used in this paper in Section 3, and then carry out the model comparisons using the new two-point diagnostic in Section 4. We end with our conclusions in Section 5.

2 TWO-POINT DIAGNOSTICS

Two-point diagnostics are statistical tools that allow one to comparatively analyse measurements in a pairwise fashion. Specifically, they allow one to employ n measurements of a particular variable to construct $n(n-1)/2$ comparisons between each pair of data. With the 30 cosmic chronometer determinations of $H(z)$ included in this study, we therefore have 435 comparisons. With this method, one can test both how well each pair of points fits a given cosmological model, and also determine how closely the stated error bars actually fit a normal distribution. Previous work by Zheng et al. (2016) concluded that the stated errors in the cosmic-chronometer data are strongly non-Gaussian, based on the application of the $Om(z_i, z_j)$ and $Omh^2(z_i, z_j)$ diagnostics. The method employed by Zheng et al., however, was based on the definition of a single diagnostic (for which the expectation value is zero in ΛCDM), then to compare that single diagnostic with its expectation value for each model being tested. In this work, we have devized separate, but completely analogous diagnostics for each cosmology.

The apparent non-Gaussianity of the data motivates the use of a second approach, pioneered by Gott et al. (2001), based on 'median statistics', which does not rely on error propagation. In Gott et al.'s (2001) method, one takes advantage of the fact that for any single measurement taken from some truly random distribution function, one has a 50 per cent chance of that measurement being above the true median of the underlying distribution, with no assumption concerning its form. Therefore, if N measurements are taken and ranked by their value, the probability that the true median lies between measurements i and $i+1$ is given by the binomial distribution, such that

$$P_i = \frac{2^{-N}N!}{i!(N-i)!}\,. \tag{1}$$

Table 1. Parameter values adopted from the joint analysis of Betoule et al. (2014), including *Planck*+WP+BAO+JLA.

Model	$\Omega_{\rm m}$	$w_{\rm de}$	w_0	w_a
$R_{\rm h}=ct$	–	–	–	–
ΛCDM	0.305 ± 0.010	–	–	–
wCDM	0.303 ± 0.012	-1.027 ± 0.055	–	–
CPL	0.304 ± 0.012	–	-0.957 ± 0.124	-0.336 ± 0.552
Einstein–de Sitter	1.0	–	–	–

Therefore, one finds the number of measurements away from the median one needs to take in order to find the 68 per cent confidence region of the median. We shall demonstrate, however, that this approach is not strictly valid for two-point diagnostics, prompting the use of Monte Carlo simulations with mock data in order to determine the correct number of steps one ought to take away from the median to compute the actual confidence range. As detailed below, the expectation value for the two-point diagnostic introduced here is zero for the true cosmology. Based on (the modified) median statistics, the confidence with which each cosmology's median is consistent with zero will therefore determine which cosmological model is favoured by the data.

Zheng et al. (2016) found for the $Om(z_i, z_j)$ diagnostic that each cosmology they tested, i.e. ΛCDM, wCDM and CPL, had a median inconsistent with zero at more than a 68 per cent confidence level. But we will show that this blanket negative outcome is due to an improper use of median statistics. Furthermore, while useful, the $Om(z_i, z_j)$ diagnostic is suitable only for a cosmology with an $\Omega_{\rm m}$ term. Some cosmologies, such as $R_{\rm h}=ct$ and EdS, lack a parameter analogous to $\Omega_{\rm m}$, so the $Om(z_i, z_j)$ and $Omh^2(z_i, z_j)$ diagnostics cannot be used, in general, for model selection. The $R_{\rm h}=ct$ model and Einstein–de Sitter have only one independent parameter, the Hubble constant H_0 today. Therefore, we will employ a comparable two-point diagnostic, valid for each cosmology, defined as

$$\Delta h(z_i, z_j) \equiv \frac{1}{H_0}\left(\frac{H(z_i)}{E(z_i)} - \frac{H(z_j)}{E(z_j)}\right) , \tag{2}$$

where the function $E(z)$ is cosmology-dependent. We stress that the actual value of H_0 does not affect the statistical comparison between the various models, and is used solely to provide a uniform scale for the diagnostic $\Delta h(z_i, z_j)$. As such, the measured variance of the Hubble constant is also irrelevant to the statistical outcome of the $\Delta h(z_i, z_j)$ analysis. So the Hubble constant may be chosen arbitrarily without affecting the confidence of the final result, and it is not necessary to use individually optimized values in each case. For simplicity, we use the value $H_0 = 70\,{\rm km\,s^{-1}\,Mpc^{-1}}$ in all the figures and reported distributions. In each case, the $\Delta h(z_i, z_j)$ diagnostic should be zero if the cosmology being tested is a good match to the data. The models we will compare are as follows:

(i) The $R_{\rm h}=ct$ universe (a Friedmann–Robertson–Walker cosmology with zero active mass; Melia 2016a, 2017). This model is based on the total equation of state $\rho + 3p = 0$, where ρ and p are the total energy density and pressure of the cosmic fluid (Melia 2007; Melia & Abdelqader 2009; Melia & Shevchuk 2012). In this cosmology, there are no free parameters once the Hubble constant H_0 is used to scale $\Delta h(z_i, z_j)$:

$$E^{R_{\rm h}=ct}(z) = (1+z) . \tag{3}$$

(ii) Flat ΛCDM model, with matter and dark-energy densities fixed by the condition $\Omega_\Lambda = 1 - \Omega_{\rm m}$ (when radiation is insignificant). In addition to H_0, which is used to scale $\Delta h(z_i, z_j)$, this model has the parameter $\Omega_{\rm m}$, for which we use the prior value listed in Table 1. For this model,

$$E^{\Lambda{\rm CDM}}(z) = \left[\Omega_{\rm m}(1+z)^3 + \Omega_\Lambda\right]^{1/2} . \tag{4}$$

(iii) Flat wCDM model, with matter and dark-energy densities fixed by the condition $\Omega_{\rm de} = 1 - \Omega_{\rm m}$ (again, when radiation is insignificant). In this case, the dark-energy equation of state, $w_{\rm de} \equiv p_{\rm de}/\rho_{\rm de}$, in terms of the dark-energy pressure $p_{\rm de}$, is unconstrained. This model has two parameters, $\Omega_{\rm m}$ and $w_{\rm de}$, for which we use the prior values listed in Table 1. Here,

$$E^{w{\rm CDM}}(z) = \left[\Omega_{\rm m}(1+z)^3 + \Omega_{\rm de}(1+z)^{3(1+w_{\rm de})}\right]^{1/2} . \tag{5}$$

(iv) The Chevalier–Polarski–Linder model (Chevalier & Polarski 2001; Linder 2003), with

$$E^{\rm CPL}(z) = \Big[\Omega_{\rm m}(1+z)^3 + (1-\Omega_{\rm m})(1+z)^{3(1+w_o+w_a)} \times \exp(-3w_a z/[1+z])\Big]^{1/2} . \tag{6}$$

Again, we use the prior values for the parameters indicated in Table 1.

(v) Einstein–de Sitter space, which contains only one matter. This model has no additional parameters once H_0 is used to scale $\Delta h(z_i, z_j)$. In this case,

$$E^{\rm EdS}(z) = (1+z)^{3/2} . \tag{7}$$

3 OBSERVATIONS

Parametrized cosmological models, such as those considered in this work, can be optimized to fit $H(z)$ measurements, of which there exist several types. In addition to optimizing the parameters of the standard model, they have been used to comparatively analyse the predictions of ΛCDM with those of other cosmologies. However, among these $H(z)$ measurements exist those which are model dependent. If a measurement of $H(z)$ is model dependent, it cannot be used to adequately compare multiple models. As of today, the cosmic chronometer approach is the only model-independent method of determining $H(z)$, and is therefore the method used exclusively in this work.

The cosmic chronometer approach used to determine the data used here constitutes a differential age method. By comparing the redshift-time derivative (dz/dt) of galaxies undergoing passive evolution (that is, evolution on time-scales much longer than the age difference between the galaxies), one can infer the expansion rate $H(z)$ as a function of redshift. The galaxies used are elliptical and highly massive ($\gtrsim 10^{11}\,{\rm M}_\odot$). They formed most ($\sim$90 per cent) of their stellar mass in the redshift range of $2 < z < 3$, over a short time-frame of $\sim$0.1–0.3 Gyr. At any given redshift, objects in this morphological class are thus the oldest objects in the Universe (Treu et al. 2005), and due to having nearly identical evolution history,

Table 2. Hubble Parameter $H(z)$ measured at 30 different redshifts.

Redshift	$H(z)$ (km s^{-1} Mpc^{-1})	$\sigma_{\rm H}$ (km s^{-1} Mpc^{-1})	Reference
0.07	69	19.6	Zhang et al. (2014)
0.09	69	12	Jimenez et al. (2003)
0.12	68.6	26.2	Zhang et al. (2014)
0.17	83	8	Simon et al. (2005)
0.1791	75	5	Moresco et al. (2012)
0.1993	75	5	Moresco et al. (2012)
0.2	72.9	29.6	Zhang et al. (2014)
0.27	77	14	Simon et al. (2005)
0.28	88.8	36.6	Zhang et al. (2014)
0.3519	83	14	Moresco et al. (2012)
0.3802	83	13.5	Moresco et al. (2012)
0.4	95	17	Simon et al. (2005)
0.4004	77	10.2	Moresco et al. (2016a)
0.4247	87.1	11.2	Moresco et al. (2016a)
0.4497	92.8	12.9	Moresco et al. (2016a)
0.4783	80.9	9	Moresco et al. (2016a)
0.48	97	62	Stern et al. (2010)
0.5929	104	13	Moresco et al. (2012)
0.6797	92	8	Moresco et al. (2012)
0.7812	105	12	Moresco et al. (2012)
0.8754	125	17	Moresco et al. (2012)
0.88	90	40	Stern et al. (2010)
0.9	117	23	Simon et al. (2005)
1.037	154	20	Moresco et al. (2012)
1.3	168	17	Simon et al. (2005)
1.363	160	33.6	Moresco (2015)
1.43	177	18	Simon et al. (2005)
1.53	140	14	Simon et al. (2005)
1.75	202	40	Simon et al. (2005)
1.965	186.5	50.4	Moresco (2015)

the ages of stars found in them can be combined with the measured redshifts to determine $H(z)$. Specifically, these measurements are based on the observation of the 4000 Å break in the measured galaxy spectra. Metal absorption causes a discontinuity in the spectral continuum, such that the amplitude of the break increases linearly with stellar metallicity and stellar age (Moresco et al. 2016a). If the metal abundance is known, the age difference Δt between two nearby galaxies can be determined by comparing their 4000 Å amplitudes. With Δt and Δz known, one can then find the expansion rate according to

$$H(z) = -\frac{1}{(1+z)}\frac{{\rm d}z}{{\rm d}t} \approx -\frac{1}{(1+z)}\frac{\Delta z}{\Delta t}\,. \tag{8}$$

The data used in this study are listed in Table 2. These are the same as those employed by Zheng et al. (2016), with the exception that their BAO measurements are here omitted.

4 MODEL COMPARISONS

Fig. 1 shows the complete two-point diagnostic for all 435 pairs of data for $R_h = ct$. The analogous figures for the other models are very similar to this and are not shown. Note that $\Delta z = z_i - z_j$ is always positive, so that $z_i > z_j$ in each evaluation of $\Delta h(z_i, z_j)$. The error bars are calculated using standard error propagation, assuming the provided errors are consistent with a normal distribution. The variance of each $\Delta h(z_i, z_j)$ diagnostic for each model is thus given as

$$\sigma^2_{\Delta h_{ij}} = \frac{{\sigma_i}^2}{{H_0}^2[E(z_i)]^2} + \sum_x \left[\frac{\rm d}{{\rm d}x}\left(\frac{H(z_i)}{H_0[E(z_i)]}\right)\sigma_x\right]^2 + \frac{{\sigma_j}^2}{{H_0}^2[E(z_j)]^2} + \sum_x \left[\frac{\rm d}{{\rm d}x}\left(\frac{H(z_j)}{H_0[E(z_i)]}\right)\sigma_x\right]^2\,, \tag{9}$$

where $E(z_i)$ is the appropriate function for the chosen cosmology and the summation over x refers to each fitted parameter, such as $\Omega_{\rm m}$ and w in $w$cdm. There are no such terms for $R_{\rm h} = ct$ or EdS. Each σ_x value is reported in Table 1 and H_0 is taken to have the uniform value 70 km s^{-1} Mpc^{-1} in all cases, as previously noted. The choice of H_0 is just for normalization purposes and does not affect the statistical outcome in any way. The unweighted distribution of $\Delta h(z_i, z_j)$ values is shown in Fig. 2. A careful inspection reveals some departures from a pure Gaussian shape, for example, with tails in Figs 2(b)–(d) and, as we shall quantify below, a greater central peaking than one expects for a normal distribution.

Following our discussion above, we study the two-point diagnostic using both weighted-mean and median statistics. The weighted mean formula for the $\Delta h(z_i, z_j)$ diagnostic is just

$$\Delta h_{\rm w.m.} = \frac{\Sigma_{i=1}^{n-1}\Sigma_{j=i+1}^{n}\Delta h(z_i, z_j)/\sigma^2_{\Delta h_{ij}}}{\Sigma_{i=1}^{n-1}\Sigma_{j=i+1}^{n}1/\sigma^2_{\Delta h_{ij}}}\,, \tag{10}$$

and its variance would naively appear to follow as

$$\sigma^2_{\Delta h_{\rm w.m.}} = \left(\Sigma_{i=1}^{n-1}\Sigma_{j=i+1}^{n}1/\sigma^2_{\Delta h_{ij}}\right)^{-1}\,, \tag{11}$$

the approach used by Ding et al. (2015) and Zheng et al. (2016) in their analyses. This determination of the error is inaccurate, however, and significantly underestimates the true error in the mean of the two-point diagnostic. We therefore propose the following approach which, as we shall see, will by construction alleviate much of the tension in the results of the previous works.

To illustrate this point, let us suppose that a measured parameter has a mean μ and standard deviation σ. Now pull three random measurements from this distribution, each with its own reported error σ_i, at increasing redshifts z_1, z_2, and z_3. Then, if we construct the two-point diagnostics consistent with the method outlined by Ding et al. (2105) and Zheng et al. (2016), and also followed in this paper, we find three values of the diagnostic for which the lower redshift is subtracted from a higher one, that is, $z_3 - z_2$, $z_3 - z_1$ and $z_2 - z_1$. If we proceed to calculate the unweighted mean of these three diagnostic values, we find the following: $\mu_{\text{2-point}} = (2z_3 - 2z_1)/3$. Through normal error propagation, this quantity has a standard deviation $\sigma = \sqrt{4{\sigma_3}^2 + 4{\sigma_1}^2}/3$, which is very different from the more naive standard deviation given in equation (11), and in fact does not even depend on the middle measurement at all. This happens because taking the mean of a two-point diagnostic incurs a heavy contribution from the highest and lowest redshifts, but far less from the middle redshifts in the sample, as they are sometimes added and sometimes subtracted when evaluating the two-point function. Equation (11) ignores this eventuality. Therefore, the true method for determining the standard deviation of the two-point diagnostic must involve a careful application of standard error propagation to the weighted mean formula.

The actual calculation of the error in the mean becomes more complex when using weighted data. The weighted mean is calculated as in equation (10), though one must pay attention to the multiplicative terms that affect each of the original n data points.

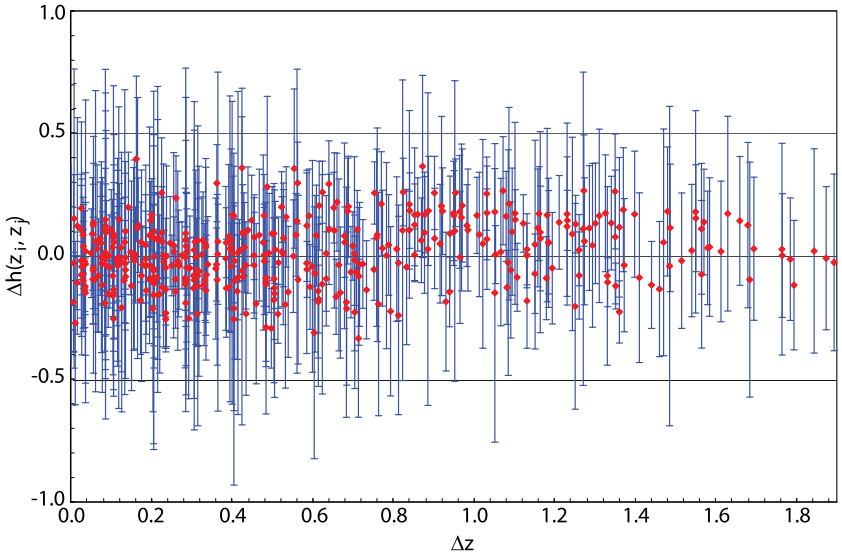

Figure 1. The $\Delta h(z_i, z_j)$ two-point diagnostic calculated for the sample of 30 cosmic-chronometer measurements of $H(z)$ in the $R_h = ct$ cosmology. Red dots denote the calculated central values and the blue bars correspond to the uncertainties. If the cosmological model is correct, $\Delta h(z_i, z_j)$ should be zero for all values of Δz. The equivalent figures for the other cosmologies tested appear very similar, and are therefore omitted.

One finds that the weighted mean (equation 10) can be rearranged into the form

$$\Delta h_{\rm w.m.} = \frac{\Sigma_{i=1}^{n} \alpha_i H(z_i)}{\Sigma_{i=1}^{n-1} \Sigma_{j=i+1}^{n} 1/\sigma^2_{\Delta h_{ij}}} \ , \tag{12}$$

with

$$\alpha_i = \Sigma_{j=1}^{i-1} \frac{1}{\sigma^2_{\Delta h_{i,j}}} - \Sigma_{k=1+i}^{N} \frac{1}{\sigma^2_{\Delta h_{i,j}}} \ , \tag{13}$$

in which each α is the sum of every term in the numerator of the weighted mean that multiplied $H(z_i)$. Note that as with the constant-dispersion case noted above, this tends to weight the measurements of $H(z)$ preferentially at the high and low redshifts, while underrepresenting the intermediate values. The true variance of the mean is therefore

$$\Delta {\sigma^2}_{\rm w.m.} = \frac{\Sigma_{i=1}^{n} \alpha_i^2 \sigma^2(z_i)}{(\Sigma_{i=1}^{n-1} \Sigma_{j=i+1}^{n} 1/\sigma^2_{\Delta h_{ij}})^2} \ , \tag{14}$$

which turns out to be always greater than the variance naively expected from equation (11).

Unlike the weighted mean, which assumes that all errors are Gaussian, median statistics makes no a priori assumption concerning the underlying distribution of a measurement compared with its true value. The probability that a given observation is above the 'true' median (i.e. the median of a very large number of measurements) is simply calculated by the binomial distribution given in equation (1), where N is the total number of measurements, and n is the value's position in the distribution. The smallest value has $n = 1$, while the largest is $n = N$. However, despite making no assumptions about the error distribution, Gott et al.'s (2001) method does assume that all measurements are completely uncorrelated, which cannot be the case in a two-point measurement, where each of the N data points affects the rest of the $N - 1$ two-point values. As such, if the binomial distribution predicts that the true median lies within a certain number of measurements of the median of the two-point distribution, the actual 68 per cent confidence region is significantly greater.

To demonstrate this, we have generated mock data sets consisting of 30 determinations of $H(z)$, using the measured $H(z)$ values in Table 2 with their reported $\sigma_{\rm H}$ standard deviations, sampling them assuming a normal distribution. These mock $H(z)$ measurements were then used to determine a mock two-point set of 435 diagnostics for each of the models. We produced 1 million such mock data samples, recorded their medians, and then determined the 68 per cent confidence region of the median. Finally, we checked to see how many steps one must take away from the median of each mock data set in order to reach that 68 per cent region. Following this approach, we have found that the two-point diagnostic for all the models has a 68 per cent chance of lying between the 192nd and 244th measurement (when ranked by value). The 218th measurement is the reported median of each set. This is a much larger range than that simply estimated using equation (1), for the simple reason that the two-point diagnostics are correlated. The proper use of median statistics in such cases is therefore not to calculate the confidence region based on a pure binomial distribution but, rather, to mitigate the impact of correlations by using a Monte Carlo approach. In this paper, we report the error above and below the median of each two-point diagnostic as the difference between the 218th and 192nd/244th ranked measurements.

Based on the weighted mean approach, using the corrected error estimation in equation (14), we find that the $\Delta h_{\rm w.m.}$ two-point diagnostic applied to $R_h = ct$, ΛCDM, wCDM and CPL is consistent with zero to within 1σ in every case (see Table 3). Einstein–de Sitter, however, is ruled out at better than $\sim 5\sigma$. Furthermore, the value of the weighted mean for EdS is negative, implying that measurements taken at greater redshift point to smaller H_0 values than observations at low redshifts. The outcomes listed in Table 1 favour $R_h = ct$ slightly over the other cosmologies, though no strong preference can be inferred from the two-point statistic used here. These results therefore weakly confirm earlier conclusions that $R_h = ct$ is strongly preferred over ΛCDM based on the use of information criteria to assess the quality of the fits to the $H(z)$ data (Melia & Maier 2013; Melia & McClintock 2015; Wei et al. 2017). More importantly, in contrast to earlier reports (e.g. Zheng et al. 2016),

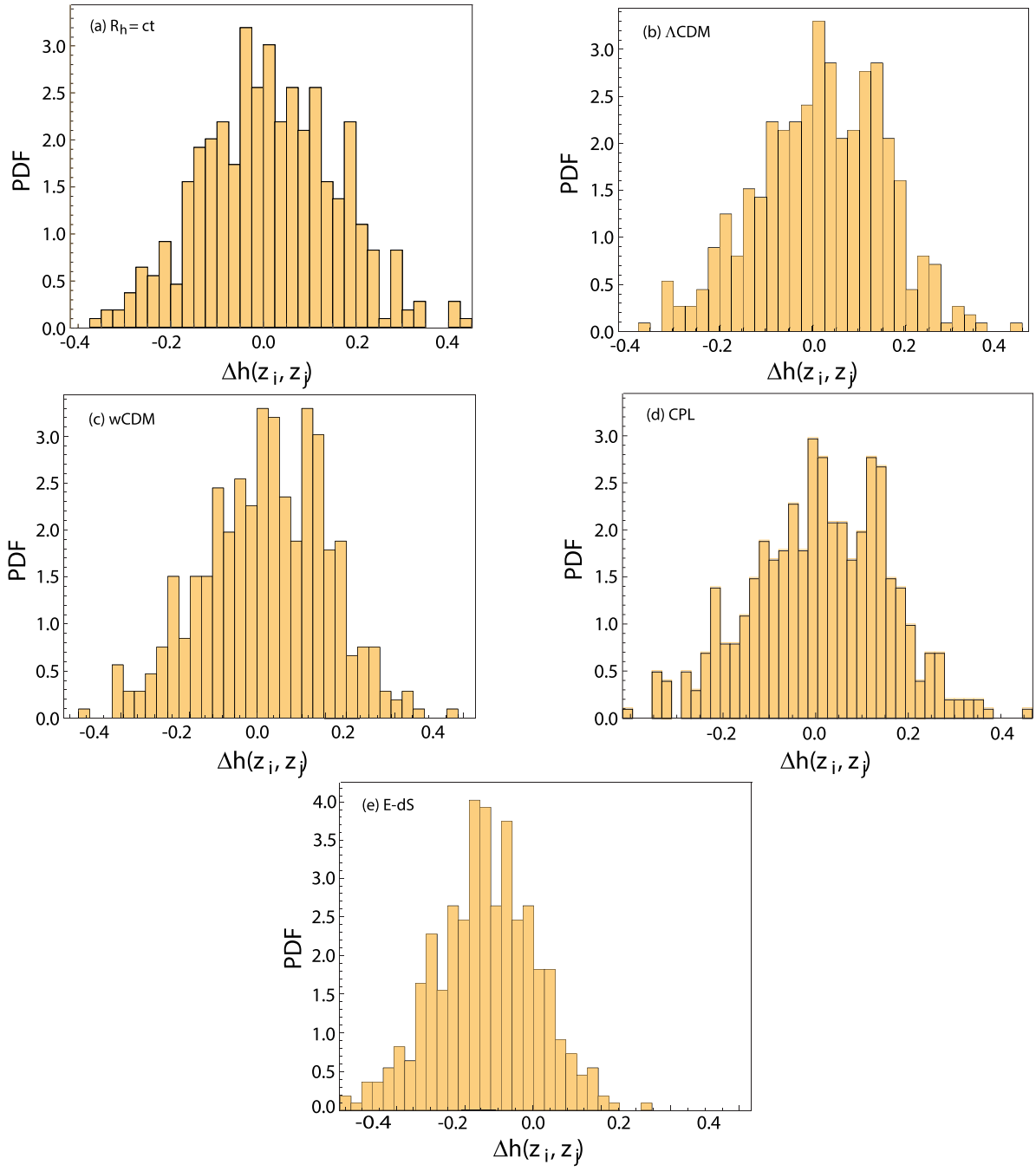

Figure 2. Histogram of the $\Delta h(z_i, z_j)$ two-point diagnostic calculated for the sample of 30 cosmic-chronometer measurements of $H(z)$, assuming (a) the $R_h = ct$ cosmology; (b) ΛCDM; (c) wCDM; (d) CPL; and (e) Einstein–de Sitter.

Table 3. Statistical Outcomes.

Model	$\Delta h_{\rm w.m.}$	Offset from zero (w.m.)	$\lvert N_\sigma \rvert < 1$	$\Delta h_{\rm m.s.}$	68 per cent range (m.s.)
$R_h = ct$	0.007 47 ± 0.027 86	0.27σ	87.36 per cent	0.00879	(−0.012 37, +0.02194)
ΛCDM	0.012 09 ± 0.030 82	0.39σ	90.11 per cent	0.02126	(−0.014 69, +0.02183)
wCDM	0.013 60 ± 0.031 22	0.4355σ	90.34 per cent	0.02528	(−0.017 80, +0.02118)
CPL	0.013 41 ± 0.039 42	0.3402σ	97.47 per cent	0.02654	(−0.015 80, +0.02362)
EdS	−0.108 51 ± 0.021 46	5.06σ	85.06 per cent	−0.10802	(−0.017 56, +0.01248)

we find a much reduced tension between theoretical predictions and the actual measurements. As we have already noted, this difference is entirely due to our more careful handling of the weighted-mean statistics.

Note also that column 4 in Table 3 indicates a deviation from true Gaussian errors, confirming the pioneering analysis by Zheng et al. (2016) in this regard, who used the $Om(z_i, z_j)$ diagnostic. For all the models we examine here, the percentage of pairs N_σ with a $\Delta h(z_i, z_j)$ within 1σ of the weighted mean is greater than the expected 68 per cent if the errors associated with the measured $H(z)$ values (Table 2) are truly Gaussian. The fact that more measurements of $\Delta h(z_i, z_j)$ lie within 1σ than predicted by Gaussianity (see also Fig. 2) suggests that the published error bars are generally larger than their actual values, or that there exists some generic systematic error that results in most measurements being offset from their true value in a similar manner.

One may already infer this for about half of the measurements in Table 2, for which both the statistical $\sigma_{\rm stat}$ and systematic $\sigma_{\rm sys}$ contributions to σ_i have been reported (Gaztanaga, Cabré & Hui 2009; Moresco et al. 2012, 2016a). In some cases, $\sigma_{\rm sys} \sim \sigma_{\rm stat}$, so even if only a portion of $\sigma_{\rm sys}$ is correlated, the overall σ_i calculated in quadrature overestimates the true Gaussian error. Unfortunately, this breakdown in statistical versus systematic errors is only known for a portion of the sample in Table 2. And even for those measurements where both $\sigma_{\rm stat}$ and $\sigma_{\rm sys}$ are available, one does not know which fraction of the latter is correlated. For the study reported in this paper, we have therefore settled on the simplest approach, which is to use all of the data in Table 2, with the caveat that the published errors are almost certainly overestimated. At least this approach ensures consistency across the entire sample, though the results do confirm that the errors are not perfectly Gaussian.

Of course, this also implies that the actual error in the weighted mean $\Delta h_{\rm w.m.}$ is probably smaller than what we find here, so the cosmologies we test are likely somewhat less consistent with $\Delta h_{\rm w.m.} = 0$ than is reported in Table 3. Clearly, this study will need to be updated once a better handle is available on the nature of $\sigma_{\rm sys}$ for $H(z)$ measurements using cosmic chronometers.

Median statistics generally provides a picture consistent with this perspective. For Einstein–de Sitter, the result is similar to that of the weighted-mean approach, in that the true median in this model is entirely inconsistent with zero. The $R_h = ct$ universe is the only model for which a diagnostic value of zero lies within the 68 per cent confidence interval. All other models are inconsistent with zero to some degree, although ΛCDM is preferred over wCDM and CPL. Notice also the apparent existence of a double peak in the ΛCDM, wCDM and CPL histograms (Fig. 2b–d). As noted earlier, the use of median statistics avoids the problem of the weighted mean, in not assuming how the data are randomly distributed. As such, results based on median statistics may be stronger than those derived from the weighted mean. Both reject EdS, however, and prefer $R_h = ct$ over other models compared here. Going forward, we suggest that our method of estimating the error in the median using Monte Carlo to construct mock samples is the proper way of finding the error associated with two-point diagnostics, rather than the binomial distribution used by Zheng et al. (2016) and others, given that the latter significantly underestimates the errors.

5 CONCLUSION

The previously introduced two-point diagnostics, such as $Om(z_i, z_j)$, have been used successfully to test the viability of various cosmologies based on the measurement of $H(z)$. Here, we have extended this work by introducing a new two-point diagnostic, $\Delta h(z_i, z_j)$, which is more generally applicable to a wider range of models, including those whose formulation does not include the normalized matter density $\Omega_{\rm m}$. It allows for the analysis of $n(n-1)/2$ pairs of data, offering different statistics than is available solely with methods that rely on just n measurements.

This approach, however, also introduces some combinatorial effects that must be properly accounted for in order to draw accurate conclusions. The diagnostic we have introduced here allows for a fair test to determine whether the errors associated with the data are being estimated correctly. Earlier uses of $H(z)$ measurements included some model-dependent data, namely those based on BAO peaks in the galaxy distribution. But most of these measurements must preassume a cosmology in order to disentangle the BAO peak position from redshift-space distortions (RSD) due to internal galaxy motions. As such, BAO data tend to be incompatible with all models other than the one used to remove the RSD, and are therefore not useful when comparing different cosmologies for model selection, unless each model was carefully considered separately from the beginning, which has not been the case with existing data. In this paper, we have avoided all such biases, relying instead on cosmic chronometer observations, which tend to be independent of any model.

Using standard weighted-mean statistics, we have found that the $\Delta h(z_i, z_j)$ diagnostic is consistent with zero to within 1σ for all the tested models, except for Einstein–de Sitter, which is ruled out at over 5σ. The caveat with this result is that our analysis has also demonstrated that the errors reported for $H(z)$ are not purely Gaussian. The true errors are almost certainly smaller than those published, or have a correlated systematic effect that would result in cosmologies having a diagnostic $\Delta h_{\rm w.m.}$ somewhat less consistent with zero than what we are reporting here.

Median statistics, based on the use of Monte Carlo methods to estimate the confidence region associated with the measured median, rather than simply using a binomial distribution that assumes uncorrelated data, has yielded a result consistent with that of the weighted mean. Einstein–de Sitter is again ruled out strongly, with $R_h = ct$ the significantly preferred model of those tested here. However, the confidence intervals of the median of these two-point diagnostics do not constitute a definitive rejection of any model other than EdS.

This result is intriguing, especially when contrasted with the analysis of the same data using the $Om(z_i, z_j)$ diagnostic (Ding et al. 2015; Zheng et al. 2016). These earlier works used an improper statistical analysis, and did not include the $R_{\rm h} = ct$ universe in their comparisons, principally because the $Om(z_i, z_j)$ diagnostic cannot be applied to it directly. Zheng et al. (2016) found that, while ΛCDM is favoured over CPL and wCDM, even ΛCDM itself has a two-point diagnostic that is strongly incompatible with zero. On the other hand, we have shown in this paper that two-point diagnostic errors reported in earlier work were severely underestimated.

The remaining issue is whether the results, we have derived here carry over to an analogous statistical analysis using the $Om(z_i, z_j)$ and $Omh^2(z_i, z_j)$ diagnostics. We have therefore repeated the work of Zheng et al. (2016) using these two-point diagnostics, both with their error methodology and our improved treatment that correctly accounts for correlations in the data. Given that $\Omega_{\rm m}$ is not a model parameter in all cosmologies, however, we have restricted this comparison to ΛCDM only. To summarize the results, we have found that, while the $Om(z_i, z_j)$ diagnostic was inconsistent with its expected value of 0 at 2.8σ based on median statistics and Zheng et al.'s incorrect error assessment, it is actually inconsistent with this value at only 0.96σ when the errors are estimated correctly using our

approach. With the use of weighted-mean statistics, this diagnostic was found by Zheng et al. to be inconsistent with 0 at 0.12σ, whereas the correct error handling yields an inconsistency at only the 0.04σ level. The former comparison is more valid in this case, however, since we all agree that the reported errors are non-Gaussian. Using median statistics, Zheng et al. also found that the measured $Omh^2(z_i, z_j)$ diagnostic is inconsistent with its expected value of 0.1426 at 4.4σ, while our corrected error assessment improves this to an inconsistency of 1.5σ.

The statistical analysis of the data using our $\Delta h(z_i, z_j)$ diagnostic therefore appears to be completely consistent with the results based on the use of $Om(z_i, z_j)$ and $Omh^2(z_i, z_j)$. The advantage of the former, however, is that it can be used for all cosmologies, not only those in which $\Omega_{\rm m}$ is a free parameter. Very importantly, we have confirmed that our improved error analysis significantly modifies the conclusions regarding which models are ruled out by the cosmic chronometer data, irrespective of which two-point diagnostic is used in the model comparisons. Based solely on these diagnostics, including $\Delta h(z_i, z_j)$, only Einstein–de Sitter is ruled out strongly by these observations, though $R_{\rm h} = ct$ is slightly preferred compared to the rest.

ACKNOWLEDGEMENTS

We are grateful to Rabindra Bhattacharya for assistance in finding the proper expression for the weighted mean of the two-point function. We are also grateful to the referee, Marek Biesiada, for his very thoughtful review, which has resulted in several notable improvements to the manuscript. FM is grateful to the Instituto de Astrofísica de Canarias in Tenerife and to Purple Mountain Observatory in Nanjing, China for their hospitality while part of this research was carried out. FM is also grateful for partial support to the Chinese Academy of Sciences Visiting Professorships for Senior International Scientists under grant 2012T1J0011, and to the Chinese State Administration of Foreign Experts Affairs under grant GDJ20120491013.

REFERENCES

Betoule M. et al., 2014. A&A, 568, 22
Blake C. et al., 2012, MNRAS, 425, 405
Chevalier M., Polarski D., 2001, IJMP-D, 10, 213
Copi C., Huterer D., Schwarz D., Starkman G., 2015. MNRAS, 451, 2978
Ding X., Biesiada M., Cao S., Li Z., Zhu Z., 2015. ApJ, 803, L22
Gaztanaga E., Cabré A., Hui L., 2009. MNRAS, 399, 1663
Gott J. R., III, Vogeley M. S., Podariu S., Ratra B., 2001, Apj, 549, 1
Jimenez R., Loeb A., 2002. ApJ, 573, 37
Jimenez R., Verde L., Treu T., Stern D., 2003. ApJ, 593, 622
Linder E. V., 2003, PRL, 90, 091301
Melia F., 2007, MNRAS, 382, 1917
Melia F., 2014, A&A, 561, A80
Melia F., 2016a, Front. Phys., 11, 119801
Melia F., 2017, Front. Phys., 12, 129802
Melia F., Abdelqader M., 2009, IJMP-D, 18, 1889
Melia F., López-Corredoira M., 2017, IJMP-D, 26, 1750055
Melia F., Maier R. S., 2013, MNRAS, 432, 2669
Melia F., McClintock T. M., 2015, AJ, 150, 119
Melia F., Shevchuk A. S. H., 2012, MNRAS, 419, 2579
Moresco M., 2015, MNRAS, 450, L16
Moresco M. et al., 2012, JCAP, 8, 006
Moresco M. et al., 2016a, JCAP, 05, 014
Moresco M., Jimenez R., Verde L., Cimatti A., Pozzetti L., Maraston C., Thomas D., 2016b, JCAP, 12, 039
Planck Collaboration XXIII, 2014, A&A, 571, id.A23
Sahni V., Shafieloo A., Starobinsky A. A., 2014, ApJ, 793, L40
Shafieloo A., Sahni V., Starobinsky A. A., 2012, PhRvD, 86, 103527
Simon J., Verde L., Jimenez R., 2005, PRD, 71, 123001
Stern D., Jimenez R., Verde L., Stanford S. A., Kamionkowski M., 2010, ApJS, 188, 280
Treu T. et al., 2005. ApJ, 633, 174
Wei J.-J., Melia F., Wu X.-F., 2017. ApJ, 835, 270
Zhang C., Zhang H., Yuan S., Liu S., Zhang T.-J., Sun Y.-C., 2014. Res. Astron. Astrophys., 14, 1221
Zheng X., Ding X., Biesiada M., Cao S., Zhu Z.-H., 2016, ApJ, 825, 17

This paper has been typeset from a TEX/LATEX file prepared by the author.

Monthly Notices
of the
ROYAL ASTRONOMICAL SOCIETY

MNRAS **474,** 4507–4513 (2018)
Advance Access publication 2017 December 1

doi:10.1093/mnras/stx3109

A two-point diagnostic for the H II galaxy Hubble diagram

Kyle Leaf[1]★ and Fulvio Melia[2]★†

[1]*Department of Physics, The University of Arizona, AZ 85721, USA*
[2]*Department of Physics, The Applied Math Program and Department of Astronomy, The University of Arizona, AZ 85721, USA*

Accepted 2017 November 27. Received 2017 November 15; in original form 2017 July 6

ABSTRACT

A previous analysis of starburst-dominated H II galaxies and H II regions has demonstrated a statistically significant preference for the Friedmann–Robertson–Walker cosmology with zero active mass, known as the $R_h = ct$ universe, over Λcold dark matter (ΛCDM) and its related dark-matter parametrizations. In this paper, we employ a two-point diagnostic with these data to present a complementary statistical comparison of $R_h = ct$ with Planck ΛCDM. Our two-point diagnostic compares, in a pairwise fashion, the difference between the distance modulus measured at two redshifts with that predicted by each cosmology. Our results support the conclusion drawn by a previous comparative analysis demonstrating that $R_h = ct$ is statistically preferred over Planck ΛCDM. But we also find that the reported errors in the H II measurements may not be purely Gaussian, perhaps due to a partial contamination by non-Gaussian systematic effects. The use of H II galaxies and H II regions as standard candles may be improved even further with a better handling of the systematics in these sources.

Key words: galaxies: general – distance scale – large-scale structure of Universe – cosmology: observations – cosmology: theory.

1 INTRODUCTION

Starbursts dominate the total luminosity of massive, compact galaxies known as HIIGx. The closely related giant extragalactic H II regions (GEHRs) also undergo massive bursts of star formation, but tend to be located predominantly at the periphery of late-type galaxies. In both environments, the ionized hydrogen is characterized by physically similar conditions (Melnick et al. 1987), producing optical spectra with strong Balmer Hα and Hβ emission lines that are indistinguishable between these two groups of sources (Searle & Sargent 1972; Bergeron 1977; Terlevich & Melnick 1981; Kunth & Östlin 2000).

Since both the number of ionizing photons and the turbulent velocity of the gas in these objects increase as the starburst becomes more massive, HIIGx and GEHR have been recognized as possible standard candles, a rather exciting prospect given that the very high starburst luminosity facilitates their detection up to a redshift $z \sim 3$ or higher (e.g. Melnick, Terlevich & Terlevich 2000; Siegel et al. 2005). The exact cause of the correlation between the luminosity $L(\mathrm{H}\beta)$ in Hβ and the ionized gas velocity dispersion σ is not yet fully understood, though an explanation may be found in the fact that the gas dynamics is almost certainly dominated by the gravitational potential of the ionizing star and its surrounding environment (Terlevich & Melnick 1981). These sources may therefore function as standard candles because the scatter in the $L(\mathrm{H}\beta)$ versus σ relation appears to be small enough for HIIGx and GEHRs to probe the cosmic distance scale independently of z (Melnick et al. 1987; Melnick, Terlevich & Moles 1988; Fuentes-Masip et al. 2000; Melnick, Terlevich & Terlevich 2000; Bosch, Terlevich & Terlevich 2002; Telles 2003; Siegel et al. 2005; Bordalo & Telles 2011; Plionis et al. 2011; Mania & Ratra 2012; Chávez et al. 2012, 2014; Terlevich et al. 2015).

Over the past several decades, HIIGx and GEHRs have been used to measure the local Hubble constant H_0 (Melnick, Terlevich & Moles 1988; Chávez et al. 2012), and to sample the expansion rate at intermediate redshifts (Melnick, Terlevich & Terlevich 2000; Siegel et al. 2005). More recently, Plionis et al. (2011) and Terlevich et al. (2015) demonstrated that the $L(\mathrm{H}\beta)$–σ correlation is a viable high-z tracer, and used a compilation of 156 combined sources, including 24 GEHRs, 107 local HIIGx, and 25 high-z HIIGx, to constrain the parameters in Λcold dark matter (ΛCDM), producing results consistent with Type Ia SNe. Most recently, we (Wei et al. 2017) extended this very promising work even further by demonstrating that GEHRs and HIIGx may be utilized, not only to refine and confirm the parameters in the standard model but, perhaps more importantly, to compare and test the predictions of competing cosmologies, such as ΛCDM and the $R_h = ct$ universe (Melia 2003, 2007, 2013a, 2016, 2017a; Melia & Abdelqader 2009; Melia & Shevchuk 2012).

These two models have been examined critically using diverse sets of data, including high-z quasars (e.g. Kauffmann & Haehnelt 2000; Wyithe & Loeb 2003; Melia 2013b, 2014; Melia & McClintock 2015b), cosmic chronometers (e.g. Jimenez &

★ E-mail: kyleaf@email.arizona.edu (KL); melia@physics.arizona.edu (FM)
† John Woodruff Simpson Fellow.

Loeb 2002; Simon, Verde & Jimenez 2005; Melia & Maier 2013; Melia & McClintock 2015a), gamma-ray bursts (e.g. Dai, Liang & Xu 2004; Ghirlanda et al. 2004; Wei, Wu & Melia 2013), Type Ia supernovae (e.g. Perlmutter et al. 1998; Riess et al. 1998; Schmidt et al. 1998; Melia 2012; Wei, Wu & Melia 2015b), and Type Ic superluminous supernovae (e.g. Inserra & Smart 2014; Wei, Wu & Melia 2015a). Their predictions have also been compared using the age measurements of passively evolving galaxies (e.g. Alcaniz & Lima 1999; Lima & Alcaniz 2000; Wei, Wu & Melia 2015c). A more complete summary of these comparisons, now based on over 20 different types of observations, may be found in table 1 of Melia (2017b).

The application of HIIGx and GEHRs as standard candles has provided one of the more compelling outcomes of this comparative study involving ΛCDM and $R_h = ct$ (Wei, Wu & Melia 2016). Using the combined sample of Chávez et al. (2014) and Terlevich et al. (2015), we constructed the Hubble diagram extending to redshifts $z \sim 3$, beyond the current reach of Type Ia SNe, and confirmed that the proposed correlation between $L(\mathrm{H}\beta)$ and σ is a viable luminosity indicator in both models. This sample is already large enough to demonstrate that $R_h = ct$ is favoured over ΛCDM with a likelihood $\gtrsim$99 per cent versus only $\lesssim$1 per cent, corresponding to a confidence level approaching 3σ.

These results, however, come with two important caveats, which partially motivate the complementary approach we are taking in this paper. Not surprisingly, the cosmological parameters are most sensitive to the high-z data, so the constraints resulting from this work are heavily weighted by the high-z sample of only 25 HIIGx. Given how sensitive the results are to the sub-sample of high-z HIIGx data, one would want to increase the significance of this analysis by increasing the number of HIIGx-related measurements. Indeed, with the K-band Multi Object Spectrograph at the Very Large Telescope, a larger sample of high-z HIIGx high-quality measurements may be available soon (Terlevich et al. 2015).

The second caveat attached to the analysis of Wei et al. (2017) is that we do not yet have a full grasp of the systematic uncertainties in the $L(\mathrm{H}\beta)$–σ correlation; these, no doubt, impact the use of HIIGx as cosmological probes. They include the burst size, its age, the oxygen abundance of HIIGx, and the internal extinction correction (Chávez et al. 2016). An example of a non-ignorable systematic uncertainty arises from the fact that the $L(H\beta)$–σ relation correlates the ionizing flux from massive stars with random velocities in the potential well created by all the stars and the surrounding gas. Thus, any systematic variation in the initial mass function would alter the mass–luminosity ratio, and therefore also the zero-point and slope of the relation (Chávez et al. 2014).

In spite of the fact that the high-z sample of HIIGx is still relatively small, we can nonetheless further test the previous results by probing this compilation more deeply (than has been attempted before) using a two-point diagnostic, $\Delta\mu(z_i, z_j)$, defined in equation (9) below. Quite generally, two-point diagnostics such as this differ from parametric fitting approaches in several distinct ways. They facilitate the comparative analysis of measurements in a pairwise fashion. One may use them with n measurements of a particular variable to generate $n(n-1)/2$ comparisons for each pair of data. The benefits are twofold: (1) one can test how well each pair of data fits the models, and (2) assess how closely the published error bars fit a normal distribution, thereby providing some indication of possible contamination by correlated systematic uncertainties. Zheng et al. (2016) recently used such an approach to conclude that the stated errors in cosmic chronometer data are strongly non-Gaussian, suggesting that the quoted measurement uncertainties are almost certainly not based exclusively on statistical randomness (see also Leaf & Melia 2017).

As we shall see, the diagnostic $\Delta\mu(z_i, z_j)$ is expected to be zero if the model being tested is the correct cosmology. To allow for possible non-Gaussianity in the published errors, we shall use both weighted-mean and median statistics to determine the degree to which each model's distribution of $\Delta\mu(z_i, z_j)$ values is consistent with this null result. So while Wei, Wu & Melia (2016) optimized the overall ΛCDM and $R_h = ct$ parametric fits to the H II galaxy Hubble diagram, here we will test the consistency of each fit with individual pairs of data. We will begin with a brief description of the data in Section 2, and then define and apply the diagnostic $\Delta\mu(z_i, z_j)$ in Section 3. The outcome of our analysis will be discussed in Section 4, followed by our conclusions in Section 5.

2 OBSERVATIONAL DATA AND METHODOLOGY

We base our analysis on the methodology described in Chávez et al. (2012, 2014) and Terlevich et al. (2015), using their total sample of 156 sources, including 107 local H II galaxies, 24 GEHRs, and 25 high-z H II galaxies. The correlation between the emission-line luminosity and the ionized gas velocity dispersion may be written as (Chávez et al. 2012; Chávez et al. 2014; Terlevich et al. 2015)

$$\log L(\mathrm{H}\beta) = \alpha \log \sigma(\mathrm{H}\beta) + \kappa\,, \tag{1}$$

where α is the slope and the constant κ represents the logarithmic luminosity at $\log\sigma(\mathrm{H}\beta) = 0$. As noted, previous applications of this relation have produced a very small scatter in the correlation for $L(\mathrm{H}\beta)$, making it a viable luminosity indicator for cosmology. But one cannot completely avoid its cosmology dependence because the Hβ luminosity is calculated using the expression

$$L(\mathrm{H}\beta) = 4\pi D_L^2(z) F(\mathrm{H}\beta)\,, \tag{2}$$

where D_L is the model-dependent luminosity distance at redshift z and $F(\mathrm{H}\beta)$ is the reddening corrected Hβ flux.

From equation (1), we may then obtain the distance modulus of an H II galaxy according to

$$\mu_{\rm obs} = 2.5\left[\kappa + \alpha\log\sigma(\mathrm{H}\beta) - \log F(\mathrm{H}\beta)\right] - 100.2\,, \tag{3}$$

with an associated error

$$\sigma_{\mu_{\rm obs}} = 2.5\left[\left(\alpha\sigma_{\log\sigma}\right)^2 + \left(\sigma_{\log F}\right)^2\right]^{1/2}, \tag{4}$$

in terms of $\sigma_{\log\sigma}$ and $\sigma_{\log F}$, these being the 1σ uncertainties in $\log\sigma(\mathrm{H}\beta)$ and $\log F(\mathrm{H}\beta)$, respectively. This is to be compared with the theoretical distance modulus

$$\mu_{\rm th} \equiv 5\log\left[\frac{D_L(z)}{\rm Mpc}\right] + 25\,, \tag{5}$$

as a function of the cosmology-dependent luminosity distance D_L.

In ΛCDM, the luminosity distance may be written

$$D_L^{\Lambda\rm CDM}(z) = \frac{c}{H_0}\frac{(1+z)}{\sqrt{|\Omega_k|}}\,{\rm sinn}\left\{|\Omega_k|^{1/2} \times \int_0^z \frac{{\rm d}z}{\sqrt{\Omega_{\rm m}(1+z)^3 + \Omega_k(1+z)^2 + \Omega_{\rm de}(1+z)^{3(1+w_{\rm de})}}}\right\}, \tag{6}$$

where $p_{\rm de} = w_{\rm de}\rho_{\rm de}$ is the dark-energy equation of state; radiation is ignored in the local Universe. Also, $\Omega_i \equiv \rho_i/\rho_c$, for matter (m), radiation (r), and dark energy (de), while $\Omega_k = 1 - \Omega_{\rm m} - \Omega_{\rm de}$

Table 1. Parameters optimized via maximization of the likelihood function.

Model	α	δ	Ω_m	Ω_{de}	w_{de}
$R_h = ct$	$4.78^{+0.07}_{-0.09}$	$32.01^{+0.32}_{-0.30}$	–	–	–
Planck ΛCDM	$4.86^{+0.08}_{-0.08}$	$32.27^{+0.22}_{-0.31}$	0.3089	$1.0 - \Omega_m$	-1
ΛCDM	$4.86^{+0.09}_{-0.10}$	$32.27^{+0.34}_{-0.36}$	$0.32^{+0.09}_{-0.06}$	$1.0 - \Omega_m$	-1

incorporates the spatial curvature of the Universe, and sinn is sinh when $\Omega_k > 0$ and sin when $\Omega_k < 0$. Today's critical density is $\rho_c \equiv 3c^2 H_0^2/8\pi G$. Since we are here assuming a flat Universe, (i.e. $\Omega_k = 0$), the right side of this equation becomes $(1 + z)c/H_0$ times the integral. For the $R_h = ct$ cosmology (Melia 2003, 2007, 2013a, 2016a,b; Melia & Abdelqader 2009; Melia & Shevchuk 2012), the luminosity distance is given by the much simpler expression

$$D_L^{R_h=ct}(z) = \frac{c}{H_0}(1+z)\ln(1+z)\,. \tag{7}$$

Here, we follow Wei, Wu & Melia (2015b, 2016) approach and circumvent circularity issues by optimizing the coefficients α and κ individually for each model, via maximization of the likelihood function. With this approach, H_0 and κ are not independent of each other; one may vary either H_0 or κ, but not both. For the purpose of maximizing the likelihood function, it is therefore useful to define a combined parameter

$$\delta \equiv -2.5\kappa - 5\log H_0 + 125.2\,, \tag{8}$$

where δ is the 'H_0-free' logarithmic luminosity and the Hubble constant H_0 is in units of km s^{-1} Mpc^{-1}. The constants α and δ are statistical 'nuisance' parameters, analogous to the adjustable coefficients characterizing the light curve in Type Ia SNe. The best-fitting parameters obtained in this fashion are shown in Table 1, for three models we will compare: Planck ΛCDM (Planck Collaboration XI 2016), ΛCDM with a re-optimized matter density Ω_m, and the $R_h = ct$ universe.

A quick inspection of equations (3) and (5) shows that the two-point diagnostic

$$\Delta\mu(z_i, z_j) \equiv \frac{-\delta + 2.5\alpha\log\sigma_i - 2.5\log F_i}{5\log\left[\frac{D_L(z_i)}{1\,\mathrm{Mpc}}\right]} - \frac{-\delta + 2.5\alpha\log\sigma_j - 2.5\log F_j}{5\log\left[\frac{D_L(z_j)}{1\,\mathrm{Mpc}}\right]} \tag{9}$$

is expected to be zero for any pair of H II data at redshifts z_i and z_j if the cosmology used to calculate D_L is correct. As one can see, the value of H_0 does not affect this constraint and is absorbed into the optimized coefficient δ. For the sake of normalizing the various quantities, however, we simply use the Planck value 67.74 km s^{-1} Mpc^{-1} throughout this analysis.

Notice in passing that α and δ are similar between the different cosmologies, varying between them by $\lesssim$4 per cent, i.e. well within 1σ. Thus, since H_0 is also not a factor in $\Delta\mu(z_i, z_j)$, equation (9) represents a powerful diagnostic for comparing the viability of different models. The application of this two-point diagnostic will be described in the next section.

Finally, to improve the statistics even further, we have removed 17 points (including one GEHR source at $z = 0.000\,01$) from our complete sample whose measurement places them more than 3σ away from the best-fitting curves. We have also chosen to remove the other GEHR source at $z = 0.000\,01$. While this point is only 2σ from the best-fitting curve, it is the lowest redshift measurement in the catalogue, which, by the nature of two-point diagnostics, causes it to drastically alter the statistical results. These anomalous points are identical for all three models, so their removal does not bias either of them. The final reduced sample therefore contains 138 measurements that are used to determine the best fits reported in Table 1. The 18 eliminated sources are the two GEHRs at $z = 0.000\,01$, and J162152+151855, J132347-013252, J211527-075951, J002339-094848, J094000+203122, J142342+225728, J094252+354725, J094254+340411, J001647-104742, J002425+140410, J103509+094516, J003218+150014, J105032+153806, WISP173-205, J084000+180531, and Q2343-BM133.

3 APPLICATION OF THE TWO-POINT DIAGNOSTIC

As discussed in more detail in Leaf & Melia (2017), the use of two-point diagnostics necessitates special care when analysing the statistics they produce. First, the weighted mean of all $n(n-1)/2$ $\Delta\mu(z_i, z_j)$ values may be calculated using the expression

$$\mu = \frac{\Sigma_{i=1}^{n-1}\Sigma_{j=i+1}^{n}\Delta\mu(z_i, z_j)/\sigma^2_{\Delta\mu_{i,j}}}{\Sigma_{i=1}^{n-1}\Sigma_{j=i+1}^{n}1/\sigma^2_{\Delta\mu_{i,j}}}\,, \tag{10}$$

in which $\sigma_{\Delta\mu_{i,j}}$ is the error for a single application of equation (9), found using standard error propagation. The error in the mean, however, must be calculated by carefully considering the correlation introduced from the repeated use of individual points in different pairs. For this purpose, we rewrite the weighted mean in the equivalent form

$$\mu = \frac{\Sigma_{i=1}^{n}\beta_i M(z_i)}{\Sigma_{i=1}^{n-1}\Sigma_{j=i+1}^{n}1/\sigma^2_{\Delta\mu_{i,j}}}\,, \tag{11}$$

with each β value given by the expression

$$\beta_i = \Sigma_{j=1}^{i-1}\frac{1}{\sigma^2_{\Delta\mu_{i,j}}} - \Sigma_{k=1+i}^{N}\frac{1}{\sigma^2_{\Delta\mu_{i,k}}}\,. \tag{12}$$

In addition, we have defined the quantity

$$M(z_i) = \frac{-\delta + 2.5\alpha\log\sigma_i - 2.5\log F_i}{5\log\left[\frac{D_L(z_i)}{1\,\mathrm{Mpc}}\right]}\,. \tag{13}$$

With the values of β thus calculated, the variance then follows and is given as

$$\Delta\sigma^2{}_{\mathrm{w.m.}} = \frac{\Sigma_{i=1}^{n}\beta_i^2\sigma_M^2(z_i)}{\left(\Sigma_{i=1}^{n-1}\Sigma_{j=i+1}^{n}1/\sigma^2_{\Delta\mu_{i,j}}\right)^2}\,. \tag{14}$$

Knowing the standard deviation of the mean, we now have a measure of the consistency of the measurements with a given model. In the case of the $\Delta\mu$ diagnostic, we expect the weighted mean to be statistically consistent with zero if the applied model is the correct cosmology. Note that we do not introduce the errors in the fitted parameters in this analysis. This is due to the error affecting both halves of the two-point diagnostics in a very similar manner. That is, if the value of α is slightly too low, it would have the effect of reducing both 'single-points', the net effect of which ends up being statistically insignificant.

When non-Gaussian errors are suspected, however, such situations motivate the use of 'median statistics', pioneered by Gott et al. (2001), in which error propagation is neither required nor assumed. This approach takes advantage of the fact that for any measurement based on some distribution function, there is a 50 per cent chance of

Table 2. Statistical analysis of the two-point diagnostic $\Delta\mu(z_i, z_j)$.

Model	Weighted mean	1σ error	|Mean| / σ	$\|N_\sigma\| < 1$	Median	Std. Dev. of the median	|Median| / Std. Dev.
$R_h = ct$	−0.00242	0.00218	1.11	51.3 per cent	−0.00425	0.00336	1.26
Planck ΛCDM	−0.00340	0.00221	1.54	52.3 per cent	−0.00483	0.00363	1.33
ΛCDM	−0.00330	0.00220	1.50	52.2 per cent	−0.00476	0.00342	1.39

it being above the true median of the underlying distribution, without any need to know its form. Thus, for N ranked measurements, the true median has a probability

$$P_i = \frac{2^{-N} N!}{i!(N-i)!} \tag{15}$$

(i.e. the binomial distribution) of being found between measurements i and $i+1$. One can use this to construct confidence regions about the median of the data, analogous to a standard deviation in Gaussian statistics, and assign to them a formal probability of finding the true median of the underlying distribution. However, it would be incorrect to apply this to, say all $n(n-1)/2$ diagnostics at once, for the same reasons noted in Leaf & Melia (2017). The fact that each measurement contributes to $N-1$ diagnostics means that the data are correlated; as a result, a single measurement can move the median farther than in the case where the two-point values are truly randomly distributed.

We propose a remedy that takes advantage of the binomial properties of the median, but instead of considering all the diagnostics simultaneously, we construct a random sub-sample, in which each realization of the diagnostic is used exactly once, except for the one that was omitted. Therefore, none of the diagnostic values is used more than once, completely avoiding any possible correlation. Following this, we record the median of the diagnostics of this uncorrelated sample, as well as the standard deviation of the realization. Next, we generate a large number (here, one million) of these realizations, and report the overall median of all the individual medians in Table 2.

In Table 2, we also report the standard deviation of the median. This value is different from the overall standard deviation of the set of all one million medians. It is fundamentally related to the error in the mean of any set of data, in that it is some distinct factor smaller than the standard deviation of the data, dependent on the size of the data set. However, the exact relationship that exists between the standard deviation of the medians and the number of sources used to determine the median of all the realizations is not empirically known.

In order to address this deficiency, we have used the following approach, based on Monte Carlo simulations with mock data to find this relationship to reasonable accuracy. We construct a mock data set by drawing at random from some probability distribution function, with the same number (i.e. 138) of points as in the real data set. Then, we construct a random set of two-point diagnostics following the same method used with the real data. We record the median and standard deviation of the realization, repeating this process a sufficiently large number of times (say, 20 000). Then, we repeat the process with a new random set of mock data drawn from the same distribution, and repeat this 5000 times. Next, we determine the standard deviation of the set of 5000 medians, as well as the mean of the 5000 standard deviations. Finally, we compare the actual standard deviation of the median of all realizations with the mean of the standard deviations of each realization. We run this simulation with three different probability density functions: a normal distribution, a skew normal distribution with shape parameter $\alpha = 4$, and a flat distribution over an interval. In all three cases, the relationship between the standard deviation of the median and the mean standard deviation of each realization is found to be statistically consistent, and apparently dependent only on the number of sources chosen.

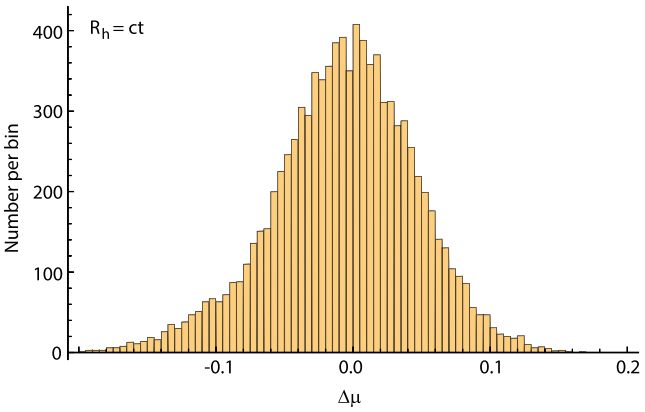

Figure 1. Unweighted histogram of all 9453 $\Delta\mu$ diagnostic values for the $R_h = ct$ universe (see equation 9). The y-axis gives the number of diagnostic values per bin.

For a sample of 138, the multiplicative factor is 1.822, always yielding a standard deviation of the medians smaller than the mean of the standard deviations by this factor. The values reported in Table 2 for the standard deviation of the median are therefore determined by taking the standard deviations of the million medians and dividing them by the corresponding factor. While this does technically include an implicit assumption that all data are sampled from a single underlying statistical distribution, we argue that by focusing on the median of these (instead of the mean), and the fact that there must certainly exist a single true cosmological model, this assumption is reasonable.

The two-point diagnostic we have introduced in equation (9) is expected to be zero for the correct cosmology. The degree by which a given model's median is consistent with zero is therefore a measure of its consistency with the observations. We discuss the results of this analysis in the next section.

4 DISCUSSION

In Table 2 and Figs 1–6, we report the results of both our weighted-mean and median statistical analyses, described in Sections 2 and 3 above. One of the principal benefits of two-point diagnostics constructed with regard to redshift ordering lies not only in determining how well a set of data fits a model, as revealed, e.g. with the use of information criteria but, also in providing insight into whether or not the low-z sources are consistent with the same model as that preferred by the higher-z sources.

Our complete sample of 138 sources constitutes the original 156 minus the 18 outliers, as detailed in Section 2. As one can see from Table 1, the optimized value of α is about 4.8 in every case,

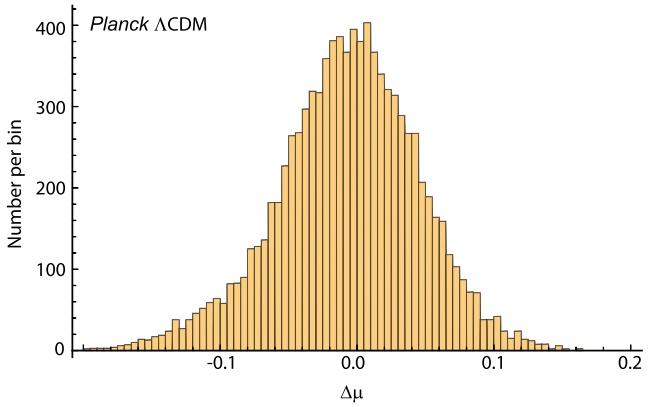

Figure 2. Same as Fig. 1, except now for Planck ΛCDM.

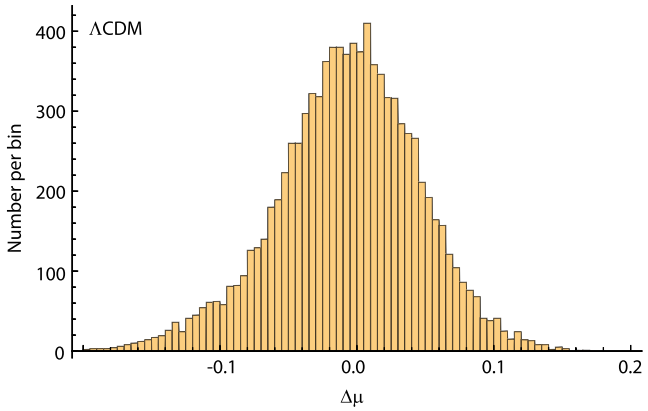

Figure 3. Same as Fig. 1, except now for ΛCDM with a re-optimized value of Ω_m (see Table 1).

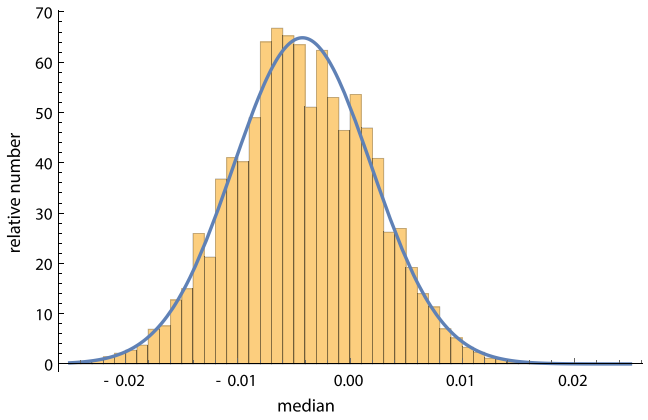

Figure 4. Histogram of the medians found in one million random realizations of the two-point diagnostic for the $R_h = ct$ universe. The y-axis denotes the number of times ($\times$1000) that the median of a realization falls within the range given on the x-axis.

statistically consistent with the results of previous analyses by Chávez et al. (2012, 2014), Terlevich et al. (2015), and Wei, Wu & Melia (2016). For these 138 measurements, we constructed for each model the 9453 unique two-point diagnostics and calculated the weighted mean and corresponding 1σ error based on the reported uncertainties (see Figs 1–3 for the complete unweighted histograms). For the $R_h = ct$ universe (Fig. 4), the weighted mean is found to be consistent with zero at about 1σ. There is mild tension

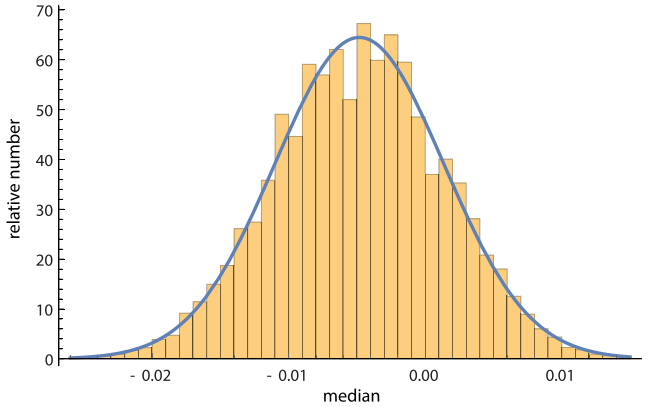

Figure 5. Same as Fig. 4, except for Planck ΛCDM.

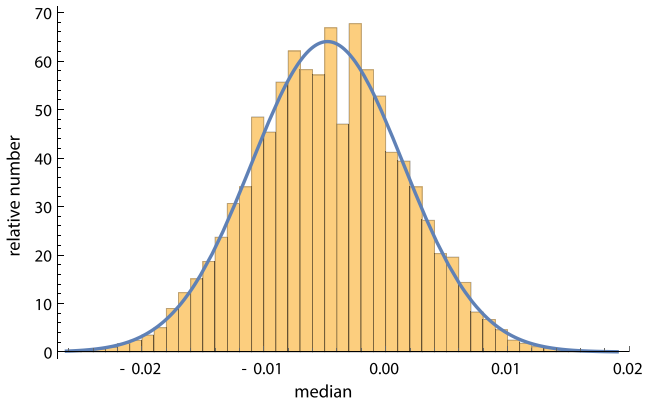

Figure 6. Same as Fig. 4, except for ΛCDM with a re-optimized Ω_m, as indicated in Table 1.

for Planck ΛCDM (Fig. 5) and the best-fitting ΛCDM cosmology (Fig. 6), however, in that the weighted mean is inconsistent with zero at about 1.5σ (compare the entries in columns 2, 3, and 4 of Table 2). Perhaps more importantly, fewer than the expected 68.3 per cent of the diagnostics lie within 1σ of the weighted mean (column 5) for all three models, implying that the reported errors are probably not purely Gaussian and that there may be an additional source of error not accounted for in this analysis.

It is therefore helpful to circumvent this possible non-Gaussianity by also analysing the two-point diagnostics using median statistics, as described above. With this approach, the three models show a similar inconsistency with a zero median (columns 5 and 6 of Table 2), with a negative value in every case, roughly 1.3σ different from zero. The fact that both the weighted mean and the median are negative for all the models suggests that the luminosity distance at low-z is generally greater than that predicted by these cosmologies, or that it is smaller than expected at high-z. The implication is that either (i) none of the models are completely correct, or (ii) there may be some systematic problems with the data at high-z or (more likely) at low-z. Thus, while a discrepancy smaller than 2σ may not be definitive, it nonetheless motivates further analysis involving a possible contamination by non-Gaussian systematic errors.

Along these lines, we point out that some authors have speculated on the possibility that a local 'Hubble bubble' (Shi 1997; Keenan, Barger & Cowie 2013; Romano 2017) might be influencing the local dynamics within a distance $\sim$300 Mpc (i.e. $z \lesssim 0.07$). If true, such a fluctuation might lead to anomalous velocities within this

region, causing the nearby expansion to deviate somewhat from a pure Hubble flow. This effect could be the reason we are seeing a slight negative bias for the weighted mean and median of the two-point diagnostic for every model, since nearby velocities would be slightly larger than Hubble, implying larger than expected luminosity distances at redshifts smaller than ∼0.07. In addition, the existence of local peculiar velocities would imply that the errors associated with low-z measurements should be bigger than quoted, increasing the number of two-point diagnostics that fall within 1σ of the expected dispersion, possibly 'filling' the distributions in Figs 1–3 sufficiently to produce entries in column 5 of Table 2 closer to the value (∼68.3 per cent) expected of a true Gaussian distribution.

5 CONCLUSIONS

The totality of the results shown in Tables 1 and 2, and illustrated in Figs 1–6, supports the use of HIIGx and GEHR sources as standard candles for cosmological testing, though the analysis based on two-point diagnostics has probed the measurement errors in greater detail than was possible solely via parametric fits to the data, the subject of our previous paper on this subject (Wei, Wu & Melia 2016).

In this paper, we have proposed a new two-point diagnostic for analysing HIIGx and GEHR data with the inclusion of median statistics, which circumvents the need for assuming Gaussian errors in the measurements. This approach may be used alongside, and compared, with the better understood weighted mean method. We have shown that these two types of analyses give generally consistent results, insofar as the H II data are concerned. Broadly speaking, one of the principal conclusions of this analysis is that employing the entire compilation of HIIGx and GEHR sources (with the exception of several outliers) produces slight tension between the cosmological parameters favoured by the data at low and high redshifts. We believe this is circumstantial evidence in support of the proposal by Shi (1997), Keenan, Barger & Cowie (2013) and Romano (2017) of a dynamical influence due to a local Hubble bubble extending out to $z \sim 0.07$, which produces local peculiar velocities comparable to those in the Hubble flow at low redshifts.

Nonetheless, probing the HIIGx and GEHR data with two-point diagnostics has not changed the essential conclusions drawn by Wei, Wu & Melia (2016), whose cosmological tests based on these sources favoured the $R_h = ct$ model over ΛCDM. Our comparison using the H II sample has shown that $R_h = ct$ is favoured over both Planck ΛCDM and ΛCDM with a variable Ω_m, at least when viewed in terms of weighted mean statistics. The caveat, however, is that an approach based on median statistics produces less differentiation between the three models.

In addition, we have found in all cases that our two-point diagnostic with the weighted mean approach yields fewer values within individual 1σ error regions than the 68.3 per cent required of a true Gaussian distribution. This may be an indication that the reported errors are not purely statistical, which may happen, e.g. when the uncertainties are contaminated by systematic effects, including at least a partially non-Gaussian component, or when there is an additional source of uncertainty, other than what we considered in this analysis.

ACKNOWLEDGEMENTS

We are very grateful to the anonymous referee for providing valuable insights and suggesting improvements to the manuscript. FM is supported by Chinese Academy of Sciences Visiting Professorships for Senior International Scientists under grant 2012T1J0011, and the Chinese State Administration of Foreign Experts Affairs under grant GDJ20120491013.

REFERENCES

Abazajian K. N. et al., 2009, ApJS, 182, 543
Alcaniz J. S., Lima J. A. S., 1999, ApJ, 521, L87
Bergeron J., 1977, ApJ, 211, 62
Bordalo V., Telles E., 2011, ApJ, 735, 52
Bosch G., Terlevich E., Terlevich R., 2002, MNRAS, 329, 481
Chávez R., Terlevich E., Terlevich R., Plionis M., Bresolin F., Basilakos S., Melnick J., 2012, MNRAS, 425, L56
Chávez R., Terlevich R., Terlevich E., Bresolin F., Melnick J., Plionis M., Basilakos S., 2014, MNRAS, 442, 3565
Chávez R., Plionis M., Basilakos S., Terlevich R., Terlevich E., Melnick J., Bresolin F., González-Morán A. L., 2016, MNRAS, 462, 2431
Dai Z. G., Liang E. W., Xu D., 2004, ApJ, 612, L101
Erb D. K., Steidel C. C., Shapley A. E., Pettini M., Reddy N. A., Adelberger K. L., 2006a, ApJ, 647, 128
Erb D. K., Steidel C. C., Shapley A. E., Pettini M., Reddy N. A., Adelberger K. L., 2006b, ApJ, 646, 107
Fuentes-Masip O., Muñoz-Tuñón C., Castañeda H. O., Tenorio-Tagle G., 2000, AJ, 120, 752
Ghirlanda G., Ghisellini G., Lazzati D., Firmani C., 2004, ApJ, 613, L13
Gott J. R., III, Vogeley M. S., Podariu S., Ratra B., 2001, ApJ, 549, 1
Hoyos C., Koo D. C., Phillips A. C., Willmer C. N. A., Guhathakurta P., 2005, ApJ, 635, L21
Inserra C., Smartt S. J., 2014, ApJ, 796, 87
Jimenez R., Loeb A., 2002, ApJ, 573, 37
Kauffmann G., Haehnelt M., 2000, MNRAS, 311, 576
Keenan R. C., Barger A. J., Cowie L. L., 2013, ApJ, 775, 62
Kunth D., Östlin G., 2000, A&AR, 10, 1
Leaf K., Melia F., 2017, MNRAS, 470, 2320
Lima J. A. S., Alcaniz J. S., 2000, MNRAS, 317, 893
Mania D., Ratra B., 2012, PhLB, 715, 9
Maseda M. V. et al., 2014, ApJ, 791, 17
Masters D. et al., 2014, ApJ, 785, 153
Melia F., Abdelqader M., 2009, IJMPD, 18, 1889
Melia F., Maier R. S., 2013, MNRAS, 432, 2669
Melia F., McClintock T. M., 2015a, AJ, 150, 119
Melia F., Shevchuk A. S. H., 2012, MNRAS, 419, 2579
Melia F., 2003, The Edge of Infinity: Supermassive Black Holes in the Universe. Cambridge Univ. Press, New York, p. 158
Melia F., 2007, MNRAS, 382, 1917
Melia F., 2012, AJ, 144, 110
Melia F., 2013a, A&A, 553, A76
Melia F., 2013b, ApJ, 764, 72
Melia F., 2014, JCAP, 1, 027
Melia F., 2016, Frontiers Phys., 11, 119801
Melia F., 2017a, Frontiers Phys., 12, 129802
Melia F., 2017b, MNRAS, 464, 1966
Melnick J., Moles M., Terlevich R., Garcia-Pelayo J.-M., 1987, MNRAS, 226, 849
Melnick J., Terlevich R., Moles M., 1988, MNRAS, 235, 297
Melnick J., Terlevich R., Terlevich E., 2000, MNRAS, 311, 629
Perlmutter S. et al., 1998, Nature, 391, 51
Planck Collaboration XI, 2016, A&A, 594, A11
Plionis M., Terlevich R., Basilakos S., Bresolin F., Terlevich E., Melnick J., Chávez R., 2011, MNRAS, 416, 2981
Riess A. G. et al., 1998, AJ, 116, 1009
Romano A. E., 2017, preprint (arXiv:1609.04081)
Schmidt B. P. et al., 1998, ApJ, 507, 46
Searle L., Sargent W. L. W., 1972, ApJ, 173, 25
Shi X., 1997, ApJ, 486, 32

Siegel E. R., Guzmán R., Gallego J. P., Orduña L. M., Rodríguez H. P., 2005, MNRAS, 356, 1117
Simon J., Verde L., Jimenez R., 2005, Ph. Rv. D, 71, 123001
Telles E., 2003, ASPC, 297, 143
Terlevich R., Melnick J., 1981, MNRAS, 195, 839
Terlevich R., Terlevich E., Melnick J., Chávez R., Plionis M., Bresolin F., Basilakos S., 2015, MNRAS, 451, 3001
Wei J.-J., Wu X.-F., Melia F., 2013, ApJ, 772, 43
Wei J.-J., Wu X.-F., Melia F., 2015a, AJ, 149, 165
Wei J.-J., Wu X.-F., Melia F., Maier R. S., 2015b, AJ, 149, 102
Wei J.-J., Wu X.-F., Melia F., Wang F.-Y., Yu H., 2015c, AJ, 150, 35
Wei J.-J., Wu X., Melia F., 2016, MNRAS, 463, 1144
Wyithe J. S. B., Loeb A., 2003, ApJ, 595, 614
Zheng X., Ding X., Biesiada M., Cao S., Zhu Z.-H., 2016, ApJ, 825, 17

This paper has been typeset from a TEX/LATEX file prepared by the author.

Monthly Notices
of the
ROYAL ASTRONOMICAL SOCIETY

MNRAS **478,** 5104–5111 (2018)
Advance Access publication 2018 May 24
doi:10.1093/mnras/sty1365

Model selection with strong-lensing systems

Kyle Leaf[1]★ and Fulvio Melia[2]★†

[1]*Department of Physics, The University of Arizona,Tucson , AZ 85721, USA*
[2]*Department of Physics, The Applied Math Program; Department of Astronomy, The University of Arizona,Tucson , AZ 85721, USA*

Accepted 2018 May 21. Received 2018 April 30; in original form 2018 January 17

ABSTRACT

In this paper, we use an unprecedentedly large sample (158) of confirmed strong lens systems for model selection, comparing five well-studied Friedmann–Robertson–Walker cosmologies: ΛCDM, *w*CDM (the standard model with a variable dark-energy equation of state), the $R_h = ct$ universe, the (empty) Milne cosmology, and the classical Einstein-de Sitter (matter-dominated) universe. We first use these sources to optimize the parameters in the standard model and show that they are consistent with *Planck*, though the quality of the best fit is not satisfactory. We demonstrate that this is likely due to underreported errors, or to errors yet to be included in this kind of analysis. We suggest that the missing dispersion may be due to scatter about a pure single isothermal sphere (SIS) model that is often assumed for the mass distribution in these lenses. We then use the Bayes information criterion, with the inclusion of a suggested SIS dispersion, to calculate the relative likelihoods and ranking of these models, showing that Milne and Einstein-de Sitter are completely ruled out, while $R_h = ct$ is preferred over ΛCDM/*w*CDM with a relative probability of ∼73 per cent versus ∼24 per cent. The recently reported sample of new strong lens candidates by the Dark Energy Survey, if confirmed, may be able to demonstrate which of these two models is favoured over the other at a level exceeding 3σ.

Key words: galaxies: general – distance scale – large-scale structure of Universe – cosmology: observations – cosmology: theory.

1 INTRODUCTION

With the continued discovery of new strong lensing systems, the gravitational bending of light is gaining importance as a diagnostic tool for the expansion of the Universe. Einstein's initial conclusion regarding the subject of gravitational lensing was that such a phenomenon would be very difficult to observe (Einstein 1936). It would take another 60 yr before the first complete Einstein Ring was discovered (King et al. 1998). Strong gravitational lenses exist as uniquely geometrical phenomena, dependent only on the mass distribution of the nearer object and the distances between observer, lens, and source. Therefore, they offer a probe of the expansion history from the time the source emitted its light to the present day.

There has been a rapid progression in the number of known strongly lensed systems since the turn of the century, starting with The Lenses Structure and Dynamics (LSD) survey (Treu & Koopmans 2002, 2004; Koopmans & Treu 2003). Its successor, The Sloan Lens ACS (Advanced Camera for Surveys; SLACS) found an additional 57 confirmed lenses (Bolton et al. 2008; Auger et al. 2009). Most recently, the SLACS survey has discovered an additional 40 lenses (Shu et al. 2017). The Baryon Oscillation Spectroscopic Survey (BOSS; Brownstein et al. 2012) produced another 25 confirmed strong galaxy–galaxy lenses, and the Strong Lensing Legacy Survey (SL2S; Sonnenfeld et al. 2013a,b; Gavazzi et al. 2014) has resulted in a catalogue of 31 confirmed lenses. Most recently, the Dark Energy Survey has compiled a catalogue of 374 candidate systems (several of which were identified in prior surveys) awaiting follow-up observations for confirmation in the near future (Diehl et al. 2017). Combined, these surveys include lenses from redshifts $z = 0.06$ to 1, and sources from $z = 0.2$ to 3.6 (9 of them beyond $z = 3$). This rapid expansion in the catalogue of available lens systems is crucial for cosmological work because the impact from the testing of cosmological models using these objects depends heavily on both the number of observations and the redshift range of the set.

In this paper, we use a catalogue of 158 confirmed, strong lens systems suitable for testing various expansion scenarios – a significantly larger compilation than that of our previous analysis (Melia, Wei & Wu 2015) and that of Cao et al. (2015). We begin by constraining the properties of dark energy within *w*CDM (i.e. the standard model with a variable dark-energy equation of state), and then proceed to use model selection tools to determine which of several

★ E-mail: kyleaf@email.arizona.edu (KL); fmelia@email.arizona.edu (FM)
† John Woodruff Simpson Fellow.

models is preferred by the strong-lens data. We consider the $R_h = ct$ universe, a Friedmann–Robertson–Walker (FRW) cosmology with zero active mass, i.e. $\rho + 3p = 0$, in terms of the total energy density ρ and pressure p (Melia 2007, 2016, 2017a; Melia & Abdelqader 2009; Melia & Shevchuk 2012), the matter only Einstein-de-Sitter universe, and the empty Milne model (see e.g. Vishwakarma 2013).

Our previous analysis (Melia, Wei, & Wu 2015) used a catalogue of 69 sources and found that ΛCDM and $R_h = ct$ both performed reasonably well, though the number of measurements was insufficient to favour one model over the other. We also constructed a much larger mock catalogue to estimate how many lensing systems would be required to carry out a definitive model selection, and concluded that a sample of several hundred lenses would suffice. The catalogue of 158 systems we use here is approaching this threshold. But note that several of the 69 sources used in our previous study are not included here. In this paper, we restrict our attention to galaxy–galaxy lens systems, while some in the (Melia, Wei, & Wu 2015) analysis are of other types. When performing a comparison between the $R_h = ct$ universe and ΛCDM, however, it is important to recognize that these models make very similar predictions at low redshifts, meaning that the most important sources in this model selection are those at the highest redshifts. Unfortunately, the most recent additions from the SLACS survey (Shu et al. 2017) constitute only sources with a measured redshift $z \lesssim 1.3$. While these lenses are indeed useful for verifying the low-redshift predictions of any model, and for constraining the parameters of *w*CDM, they do not significantly contribute to the model selection itself. The SL2S and LSD surveys include all considered sources of redshift $z \gtrsim 1.6$, and therefore have the greatest impact on a direct comparison of the models. In Section 2, we present the methods used to perform the fitting and model comparison. In Section 3, we discuss the results of these calculations, and we end with a summary and our conclusions in Section 4.

2 STRONG LENSING

Strong gravitational lensing has been used to constrain cosmological models in several recent publications, including Cao et al. (2012, 2015), Melia, Wei & Wu (2015), and An, Chang & Xu (2016). For a strongly lensed system with a single galaxy acting as the lens, the Einstein Radius depends only on three parameters: the angular diametre distances to the lens and source, and the mass distribution within the lensing galaxy. The most commonly used model for the lens galaxy's mass is a singular isothermal ellipsoid (SIE; Ratnatunga, Griffiths & Ostrander 1999). Early-type galaxies (ellipticals) contain most of the cosmic stellar mass in the universe, and are therefore more commonly found as lenses than other types; approximating these as an ellipsoid is quite reasonable (Kochanek et al. 2000). The prior analyses by Cao et al. (2015) and Melia, Wei, & Wu (2015), however, reported consistency also with the simpler singular isothermal sphere (SIS) model (i.e. an SIE with zero ellipticity). The transparency of the results and the simplicity of the methodology therefore warrant making the SIS approximation. None the less, to ensure that our results are not biased by this approach, we also consider potential random deviations from this simple model. An SIS determines the Einstein (angular) radius θ_E in terms of the 1-D velocity dispersion, σ_{SIS}, in the lensing galaxy. In terms of the ratio

$$\mathcal{D} = \frac{D_{ls}}{D_s}, \tag{1}$$

of the angular diametre distances D_{ls} and D_s between the lens and source, and source and observer, respectively, the Einstein radius is given as

$$\theta_E = 4\pi \frac{\sigma_{SIS}^2}{c^2}\,\mathcal{D}\,. \tag{2}$$

Note, however, that in place of σ_{SIS}, we follow the approach taken by Cao et al. (2015) in converting the observed velocity dispersion σ_{ap} measured within a given aperture and convert it to a velocity dispersion within a circular aperture of half the effective radius of the lens galaxy, with $\sigma_0 = \sigma_{ap}(\theta_{eff}/2\theta_{ap})^{-0.04}$, where θ_{eff} is the half-light radius of the lensing galaxy and θ_{ap} is the aperture size used to measure the velocity dispersion (Jørgensen, Franx & Kjærgaard 1995a,b). The ratio $\mathcal{D}$ therefore constitutes an observable quantity, written as

$$\mathcal{D}^{obs} = \frac{c^2\theta_E}{4\pi\,\sigma_0^2}. \tag{3}$$

The quantity $\mathcal{D}$ is well defined for any given cosmology if the redshifts of the lens and source are known. In flat *w*CDM, we have

$$D(z_1, z_2) = \frac{c}{H_0}\frac{1}{1+z_2} \times \int_{z_1}^{z_2} \frac{dz'}{\sqrt{\Omega_m(1+z')^3 + \Omega_r(1+z')^4 + \Omega_{de}(1+z')^{3(1+w_{de})}}}, \tag{4}$$

where $w_{de} \equiv p_{de}/\rho_{de}$ is the dark-energy equation of state parameter, and Ω_i is today's density of species i in terms of the critical density $\rho_c \equiv 3c^2H_0^2/8\pi G$. For our strong lens sample, Ω_r is negligible and may be ignored. For flatness, we also have $\Omega_m + \Omega_{de} = 1$, consistent with the latest *Planck* data release (Planck Collaboration 2016). This leaves only three free parameters, H_0, w_{de}, and Ω_m. When taking the ratio of two angular diametre distances, however, H_0 itself becomes irrelevant, so fitting the strong lens sample with *w*CDM reduces to an optimization based on only two free parameters.

We may use the same expression (equation 4) for the Einstein-De-Sitter universe, setting $\Omega_m = 1$, $\Omega_r = 0$, and $\Omega_{de} = 0$. For the Milne universe, the corresponding expression is

$$D(z_1, z_2) = \frac{c}{H_0}\frac{1}{1+z_2}\sinh\left(\ln\left[\frac{1+z_2}{1+z_1}\right]\right) \tag{5}$$

(e.g. Vishwakarma 2015), while for the $R_h = ct$ model it is simply

$$D(z_1, z_2) = \frac{c}{H_0}\frac{1}{1+z_2}\ln\left[\frac{1+z_2}{1+z_1}\right] \tag{6}$$

(e.g. Melia, Wei & Wu 2015). The model predictions compared to the data are based on the expected ratio $\mathcal{D}^{th}$, defined in general as

$$\mathcal{D}^{th} = \frac{D(z_1, z_2)}{D(0, z_2)}. \tag{7}$$

For example, in the $R_h = ct$ universe, it is

$$\mathcal{D}^{R_h=ct}(z_1, z_2) = 1 - \frac{\ln(1+z_1)}{\ln(1+z_2)}, \tag{8}$$

with corresponding expressions for the other cosmologies. Clearly, $\mathcal{D}$ does not depend on H_0 for any of the considered models, removing all free parameters in $R_h = ct$, Milne, and Einstein-De-Sitter, while leaving *w*CDM with the two free parameters, w_{de} and Ω_m, for the optimization process. Note also that, by definition, this ratio is restricted to the range $0 \leq \mathcal{D} \leq 1$ for all lens systems.

3 DATA AND METHODOLOGY

Previous analyses of strong lenses used a variety of approaches to constrain the model parameters and for model selection (Cao et al. 2015; Melia, Wei, & Wu 2015; An, Chang & Xu 2016). For example, Cao et al. (2015) used a subset of the data we consider in this paper and several statistical features that warrant further consideration. In this paper, we compile a catalogue of 158 confirmed sources (see Table 1), many identical to those included in Cao et al. (2015), but with the addition of 40 more discovered by SLACS (Shu et al. 2017). All redshifts are determined spectroscopically, and we use the Einstein Radii measured by the discovery teams based on fits to pixelized images of the sources. Cao et al. (2015) found that – assuming the *Planck*-optimized value for $\Omega_{\rm m}$ – the wCDM model is consistent to within 1σ with flat ΛCDM. Their fitting utilized the errors reported by the various surveys, in addition to assuming a uniform error of 5 per cent for the measured Einstein Radius $\sigma_{\theta_{\rm E}}$ (Grillo, Lombardi & Bertin, 2008). The expression for the combined error in $\mathcal{D}^{\rm obs}$ is then

$$\sigma_{\mathcal{D}} = \sqrt{4(\sigma_{\sigma_0})^2 + (\sigma_{\theta_{\rm E}})^2}, \tag{9}$$

where σ_{σ_0} is the error reported for the velocity dispersion. Note that, while σ_0 does depend on the measured effective radius $\theta_{\rm eff}$, this is also determined to be better than 5 per cent accuracy, and the low power index of 0.04 [see expression following equation (2) above] results in an insignificant error contribution compared to that from the velocity dispersion itself.

Some lensing systems have two images, while others have four, a distinction that could generate some systematic differences between the two sub-groups. The previous analysis by Melia, Wei, & Wu (2015), however, showed that there are no significant differences between two-image and four-image systems. Given (i) that the recent SLACS data are not characterized in terms of which sub-group they belong to, and (ii) that there does not appear to be any dependence of the analysis on the number of images, we do not consider the two sub-samples separately here.

Let us now describe the sequence of steps taken to minimize the overall scatter in the data. If we simply use the full set of 158 confirmed sources, without the introduction of an additional dispersion associated with the SIS and the exclusion of outliers, we find that *Planck* ΛCDM (with $\Omega_{\rm m} = 0.308$, $\Omega_{\rm de} \equiv \Omega_\Lambda = 1 - \Omega_{\rm m}$) fits the strong lenses with a reduced $\chi^2_{\rm dof}$ (χ^2 per degree of freedom) of $\backsimeq 2.7$, which is not satisfactory. A more serious issue is that most of the data – 89 out of 158 sources – are inconsistent with Planck ΛCDM at more than 1σ. By comparison, if the reported errors were truly Gaussian, we should expect $\approx$50 of the 158 measurements to deviate by more than 1σ from an accurate cosmological model. But there are clearly several mitigating circumstances. For example, in our initial analysis, we find that a single source, J0850-0347, deviates by more than 5σ from all the considered models, and we therefore exclude it as a significant outlier from all further consideration. With this single source excluded, the $\chi^2_{\rm dof}$ for *Planck* ΛCDM immediately drops to $\backsimeq 2.4$.

This improvement notwithstanding, such a poor $\chi^2_{\rm dof}$ contrasts sharply with the outcome reported in Melia, Wei & Wu (2015), but we note that an additional error term, $\sigma_{\rm f}$, was included in that earlier paper to characterize possible random deviations from the simple isothermal sphere (SIS) model. This dispersion was assumed to be 6 per cent, resulting in a 12 per cent contribution to $\sigma_{\mathcal{D}}$ based on standard error propagation. None the less, were we to include that additional scatter here, the resulting $\chi^2_{\rm dof} \backsimeq 1.5$ for the *Planck* ΛCDM best fit would still be significantly greater than the value (i.e. $\chi^2_{\rm dof} \backsimeq 1.2$) found in our previous work. The difference is entirely due to the new data we have added to the sample in this paper, at least some of which appear to deviate significantly from the *Planck* model.

We believe that contributing factors to this disparity are (i) that the reported errors are possibly underestimated, and (ii) that there is an additional unrecognized systematic effect that has yet to be included in the analysis. In addition, we carefully excluded from our previous analysis those lens systems with $\mathcal{D}^{\rm obs} > 1$, which are unphysical (see equation 8). If we follow the same steps here with the larger sample, introducing the additional SIS dispersion and excluding the 28 lenses with $\mathcal{D}^{\rm obs} > 1$, 11 of which are from the 2017 SLACS catalogue, and also exclude the aforementioned extreme outlier J0850-0347, we find that $\chi^2_{\rm dof} \approx 1.01$ for the *Planck* ΛCDM cosmology, nearly identical to our previous result. As we explain in more detail below, there are good reasons for believing that the SIS dispersion may be bigger than the value we used previously. For example, in their fitting, Cao et al. (2012) invoked possible deviations from SIS contributing a scatter of up to 20 per cent. This appears to be more in line with our preliminary finding here, so we investigate the impact of such a large dispersion on our optimization of the parameters in the wCDM cosmology.

We use maximization of the likelihood function to constrain and compare the models, including wCDM. We calculate $\mathcal{D}^{\rm obs}$ using equation (3), and $\mathcal{D}^{\rm th}$ using equation (7). For each measurement of $\mathcal{D}^{\rm obs}$ we also determine the corresponding error through standard error propagation, in which

$$\sigma_{\mathcal{D}^{\rm obs}} = \mathcal{D}^{\rm obs}\sqrt{\left(\frac{\sigma_{\theta_{\rm E}}}{\theta_{\rm E}}\right)^2 + \left(\frac{2\sigma_{\sigma_0}}{\sigma_0}\right)^2 + \sigma_X^2}, \tag{10}$$

where σ_X is a unitless composite error term comprising the scatter about the SIS average and any other source of scatter in the measurements. We iterate the value of σ_X (described below), while also systematically eliminating sources with a $\mathcal{D}^{\rm obs}$ exceeding 1, since these are clearly unphysical, and we also exclude J0850-0347, which is an extreme outlier in every model we tested.

In the method of maximum likelihood estimation (MLE; Wei at al. 2015a), the joint likelihood function for all parameters, based on a flat Bayesian prior, is

$$\mathcal{L} = \prod_i \frac{1}{\sqrt{2\pi}\,\sigma_{\mathcal{D}_i}} \exp\left[-\frac{\chi_i^2}{2}\right] \tag{11}$$

where, for each measurement,

$$\chi_i^2 \equiv \frac{\left(\mathcal{D}_i^{\rm obs} - \mathcal{D}_i^{\rm th}\right)^2}{\sigma^2_{\mathcal{D},i}}\,. \tag{12}$$

The iteration on σ_X ends when the optimization of wCDM results in a $\chi^2_{\rm dof} = 1$. Once σ_X has been identified in this way, we use the same value for all the models in order to keep the comparison as transparent as possible. Although this approach tends to favour wCDM somewhat, we will see that it does not influence the model ranking significantly. For example, the disfavoured models are rejected strongly and, clearly, changing σ_X by a few percentage points will not alter this outcome.

The resulting best-fitting values (including σ_X), calculated via the marginal probability of each parameter, are reported in Table 2 for both wCDM and ΛCDM. The latter has one fewer parameter (since $w_{\rm de} = -1$). The corresponding 1σ and 2σ confidence contours for wCDM in the $\Omega_{\rm m} - w_{\rm de}$ plane, along with the overall probability density, are shown in Fig. 1. Retaining only sources with $\mathcal{D}^{\rm obs} \leq 1$ reduces our overall sample size from 157 (excluding the extreme

Table 1. Strong-lensing systems.

Name	z_l	z_s	σ_{ap} (km s^{-1})	θ_E (arcsec)	Survey	θ_{ap} (') (arcsec)	θ_{eff} (arcsec)	σ_0 (km s^{-1})
J0151+0049	0.517	1.364	219 ± 39	0.68	BELLS	1.00	0.89	226 ± 40
J0747+4448	0.437	0.897	281 ± 52	0.61	BELLS	1.00	1.24	286 ± 53
J0747+5055	0.438	0.898	328 ± 60	0.75	BELLS	1.00	2.87	323 ± 59
J0801+4727	0.483	1.518	98 ± 24	0.49	BELLS	1.00	0.57	103 ± 25
J0830+5116	0.530	1.332	268 ± 36	1.14	BELLS	1.00	1.10	274 ± 37
J0944-0147	0.539	1.179	204 ± 34	0.72	BELLS	1.00	1.35	207 ± 35
J1159-0007	0.579	1.346	165 ± 41	0.68	BELLS	1.00	0.99	170 ± 42
J1215+0047	0.642	1.297	262 ± 45	1.37	BELLS	1.00	1.42	266 ± 46
J1221+3806	0.535	1.284	187 ± 48	0.70	BELLS	1.00	0.93	193 ± 49
J1234-0241	0.490	1.016	122 ± 31	0.53	BELLS	1.00	1.61	123 ± 31
J1318-0104	0.659	1.396	177 ± 27	0.68	BELLS	1.00	1.06	182 ± 28
J1337+3620	0.564	1.182	225 ± 35	1.39	BELLS	1.00	1.60	227 ± 35
J1349+3612	0.440	0.893	178 ± 18	0.75	BELLS	1.00	2.03	178 ± 18
J1352+3216	0.463	1.034	161 ± 21	1.82	BELLS	1.00	1.35	164 ± 21
J1522+2910	0.555	1.311	166 ± 27	0.74	BELLS	1.00	1.08	170 ± 28
J1541+1812	0.560	1.113	174 ± 24	0.64	BELLS	1.00	0.59	183 ± 25
J1542+1629	0.352	1.023	210 ± 16	1.04	BELLS	1.00	1.45	213 ± 16
J1545+2748	0.522	1.289	250 ± 37	1.21	BELLS	1.00	2.65	247 ± 37
J1601+2138	0.544	1.446	207 ± 36	0.86	BELLS	1.00	0.63	217 ± 38
J1611+1705	0.477	1.211	109 ± 23	0.58	BELLS	1.00	1.33	111 ± 23
J1631+1854	0.408	1.086	272 ± 14	1.63	BELLS	1.00	2.07	272 ± 14
J1637+1439	0.391	0.874	208 ± 30	0.65	BELLS	1.00	0.89	215 ± 31
J2122+0409	0.626	1.452	324 ± 56	1.58	BELLS	1.00	1.76	326 ± 56
J2125+0411	0.363	0.978	247 ± 17	1.20	BELLS	1.00	1.47	250 ± 17
J2303+0037	0.458	0.936	274 ± 31	1.02	BELLS	1.00	1.35	278 ± 31
CFRS03-1077	0.938	2.941	251 ± 19	1.24	LSD	1.25	1.60	256 ± 19
HST-14176	0.810	3.399	224 ± 15	1.41	LSD	1.25	1.06	232 ± 16
HST-15433	0.497	2.092	116 ± 10	0.36	LSD	1.25	0.41	125 ± 11
MG-2016	1.004	3.263	328 ± 32	1.56	LSD	0.65	0.31	347 ± 34
Q0047-2808	0.485	3.595	229 ± 15	1.34	LSD	1.25	0.82	239 ± 16
J0212-0555	0.750	2.740	273 ± 22	1.27	SL2S	0.90	1.22	277 ± 22
J0213-0743	0.717	3.480	293 ± 34	2.39	SL2S	1.00	1.97	293 ± 34
J0214-0405	0.609	1.880	287 ± 47	1.41	SL2S	1.00	1.21	293 ± 48
J0217-0513	0.646	1.847	239 ± 27	1.27	SL2S	1.50	0.73	253 ± 29
J0219-0829	0.389	2.150	289 ± 23	1.30	SL2S	1.00	0.95	298 ± 24
J0223-0534	0.499	1.440	288 ± 28	1.22	SL2S	1.00	1.31	293 ± 28
J0225-0454	0.238	1.199	234 ± 21	1.76	SL2S	1.00	2.12	233 ± 21
J0226-0420	0.494	1.232	263 ± 24	1.19	SL2S	1.00	0.84	272 ± 25
J0232-0408	0.352	2.340	281 ± 26	1.04	SL2S	1.00	1.14	287 ± 27
J0848-0351	0.682	1.550	197 ± 21	0.85	SL2S	0.90	0.45	208 ± 22
J0849-0251	0.274	2.090	276 ± 35	1.16	SL2S	0.90	1.34	279 ± 35
J0849-0412	0.722	1.540	320 ± 24	1.10	SL2S	0.90	0.46	338 ± 25
J0850-0347	0.337	3.250	290 ± 24	0.93	SL2S	0.70	0.28	309 ± 26
J0855-0147	0.365	3.390	222 ± 25	1.03	SL2S	0.70	0.69	228 ± 26
J0855-0409	0.419	2.950	281 ± 22	1.36	SL2S	0.70	1.13	283 ± 22
J0904-0059	0.611	2.360	183 ± 21	1.40	SL2S	0.90	2.00	182 ± 21
J0959+0206	0.552	3.350	188 ± 22	0.74	SL2S	0.90	0.46	199 ± 23
J1359+5535	0.783	2.770	228 ± 29	1.14	SL2S	1.00	1.13	233 ± 30
J1404+5200	0.456	1.590	342 ± 20	2.55	SL2S	1.00	2.03	342 ± 20
J1405+5243	0.526	3.010	284 ± 21	1.51	SL2S	1.00	0.83	294 ± 22
J1406+5226	0.716	1.470	253 ± 19	0.94	SL2S	1.00	0.80	262 ± 20
J1411+5651	0.322	1.420	214 ± 23	0.93	SL2S	1.00	0.85	221 ± 24
J1420+5258	0.38	0.990	246 ± 23	0.96	SL2S	1.00	1.11	252 ± 24
J1420+5630	0.483	3.120	228 ± 19	1.40	SL2S	1.00	1.62	230 ± 19
J2203+0205	0.400	2.150	213 ± 21	1.95	SL2S	1.00	0.99	219 ± 22
J2205+0147	0.476	2.530	317 ± 30	1.66	SL2S	0.90	0.66	330 ± 31
J2213-0009	0.338	3.450	165 ± 20	1.07	SL2S	1.00	0.27	179 ± 22
J2219-0017	0.289	1.020	189 ± 20	0.52	SL2S	0.70	1.01	191 ± 20
J2220+0106	0.232	1.070	127 ± 15	2.16	SL2S	1.00	0.80	132 ± 16
J2221+0115	0.325	2.350	222 ± 23	1.40	SL2S	1.00	1.12	227 ± 24
J2222+0012	0.436	1.360	221 ± 22	1.44	SL2S	1.00	1.56	223 ± 22
J0008-0004	0.440	1.192	193 ± 36	1.16	SLACS	1.50	1.71	197 ± 37
J0029-0055	0.227	0.931	229 ± 18	0.96	SLACS	1.50	2.16	232 ± 18
J0037-0942	0.196	0.632	279 ± 10	1.53	SLACS	1.50	2.19	283 ± 10

Table 1 – *continued*

Name	z_l	z_s	σ_{ap} (km s^{-1})	θ_E (arcsec)	Survey	θ_{ap} (') (arcsec)	θ_{eff} (arcsec)	σ_0 (km s^{-1})
J0044+0113	0.120	0.196	266 ± 13	0.79	SLACS	1.50	2.61	267 ± 13
J0109+1500	0.294	0.525	251 ± 19	0.69	SLACS	1.50	1.38	259 ± 20
J0157-0056	0.513	0.924	295 ± 47	0.79	SLACS	1.50	1.06	308 ± 49
J0216-0813	0.332	0.524	333 ± 23	1.16	SLACS	1.50	2.67	335 ± 23
J0252+0039	0.280	0.982	164 ± 12	1.04	SLACS	1.50	1.39	169 ± 12
J0330-0020	0.351	1.071	212 ± 21	1.10	SLACS	1.50	1.20	220 ± 22
J0405-0455	0.075	0.810	160 ± 8	0.80	SLACS	1.50	1.36	165 ± 8
J0728+3835	0.206	0.688	214 ± 11	1.25	SLACS	1.50	1.78	219 ± 11
J0737+3216	0.322	0.581	338 ± 17	1.00	SLACS	1.50	2.82	339 ± 17
J0808+4706	0.219	1.025	236 ± 11	1.23	SLACS	1.50	2.42	238 ± 11
J0822+2652	0.241	0.594	259 ± 15	1.17	SLACS	1.50	1.82	264 ± 15
J0841+3824	0.116	0.657	225 ± 11	1.41	SLACS	1.50	4.21	222 ± 11
J0903+4116	0.430	1.065	223 ± 27	1.29	SLACS	1.50	1.78	228 ± 28
J0912+0029	0.164	0.324	326 ± 12	1.63	SLACS	1.50	3.87	323 ± 12
J0935-0003	0.348	0.467	396 ± 35	0.87	SLACS	1.50	4.24	391 ± 35
J0936+0913	0.190	0.588	243 ± 12	1.09	SLACS	1.50	2.11	246 ± 12
J0946+1006	0.222	0.608	263 ± 21	1.38	SLACS	1.50	2.35	266 ± 21
J0956+5100	0.240	0.470	334 ±17	1.33	SLACS	1.50	2.19	338 ± 17
J0959+0410	0.126	0.535	197 ± 13	0.99	SLACS	1.50	1.39	203 ± 13
J1016+3859	0.168	0.439	247 ± 13	1.09	SLACS	1.50	1.46	254 ± 13
J1020+1122	0.282	0.553	282 ± 18	1.20	SLACS	1.50	1.59	289 ± 18
J1023+4230	0.191	0.696	242 ± 15	1.41	SLACS	1.50	1.77	247 ± 15
J1100+5329	0.317	0.858	187 ± 23	1.52	SLACS	1.50	2.24	189 ± 23
J1106+5228	0.096	0.407	262 ± 13	1.23	SLACS	1.50	1.68	268 ± 13
J1112+0826	0.273	0.630	320 ± 20	1.49	SLACS	1.50	1.50	329 ± 21
J1134+6027	0.153	0.474	239 ± 12	1.10	SLACS	1.50	2.02	243 ± 12
J1142+1001	0.222	0.504	221 ± 22	0.98	SLACS	1.50	1.91	225 ± 22
J1143-0144	0.106	0.402	269 ± 13	1.68	SLACS	1.50	4.80	264 ± 13
J1153+4612	0.180	0.875	226 ± 15	1.05	SLACS	1.50	1.16	235 ± 16
J1204+0358	0.164	0.631	267 ± 17	1.31	SLACS	1.50	1.47	275 ± 17
J1205+4910	0.215	0.481	281 ± 14	1.22	SLACS	1.50	2.59	283 ± 14
J1213+6708	0.123	0.640	292 ± 15	1.42	SLACS	1.50	3.23	291 ± 15
J1218+0830	0.135	0.717	219 ± 11	1.45	SLACS	1.50	3.18	218 ± 11
J1250+0523	0.232	0.795	252 ± 14	1.13	SLACS	1.50	1.81	257 ± 14
J1251-0208	0.224	0.784	233 ± 23	0.84	SLACS	1.50	2.61	234 ± 23
J1330-0148	0.081	0.712	185 ± 9	0.87	SLACS	1.50	0.89	194 ± 9
J1402+6321	0.205	0.481	267 ± 17	1.35	SLACS	1.50	2.70	268 ± 17
J1403+0006	0.189	0.473	213 ± 17	0.83	SLACS	1.50	1.46	219 ± 17
J1416+5136	0.299	0.811	240 ± 25	1.37	SLACS	1.50	1.43	247 ± 26
J1430+4105	0.285	0.575	322 ± 32	1.52	SLACS	1.50	2.55	324 ± 32
J1436-0000	0.285	0.805	224 ± 17	1.12	SLACS	1.50	2.24	227 ± 17
J1451-0239	0.125	0.520	223 ± 14	1.04	SLACS	1.50	2.48	225 ± 14
J1525+3327	0.358	0.717	264 ± 26	1.31	SLACS	1.50	2.90	264 ± 26
J1531-0105	0.160	0.744	279 ± 14	1.71	SLACS	1.50	2.50	281 ± 14
J1538+5817	0.143	0.531	189 ± 12	1.00	SLACS	1.50	1.58	194 ± 12
J1621+3931	0.245	0.602	236 ± 20	1.29	SLACS	1.50	2.14	239 ± 20
J1627-0053	0.208	0.524	290 ± 14	1.23	SLACS	1.50	1.98	295 ± 14
J1630+4520	0.248	0.793	276 ± 16	1.78	SLACS	1.50	1.96	281 ± 16
J1636+4707	0.228	0.674	231 ± 15	1.09	SLACS	1.50	1.68	236 ± 15
J2238-0754	0.137	0.713	198 ± 11	1.27	SLACS	1.50	2.33	200 ± 11
J2300+0022	0.228	0.464	279 ± 17	1.24	SLACS	1.50	1.83	285 ± 17
J2303+1422	0.155	0.517	255 ± 16	1.62	SLACS	1.50	3.28	254 ± 16
J2321-0939	0.082	0.532	249 ± 8	1.60	SLACS	1.50	4.11	246 ± 8
J2341+0000	0.186	0.807	207 ± 13	1.44	SLACS	1.50	3.15	207 ± 13
J0143-1006	0.221	1.1046	203 ± 17	1.23	SLACS2017	1.50	3.24	202 ± 17
J0159-0006	0.1584	0.7477	216 ± 18	0.92	SLACS2017	1.50	1.58	222 ± 18
J0324+0045	0.321	0.9199	183 ± 19	0.55	SLACS2017	1.50	1.67	187 ± 19
J0324-0110	0.4456	0.6239	310 ± 38	0.63	SLACS2017	1.50	2.23	314 ± 38
J0753+3416	0.1371	0.9628	208 ± 12	1.23	SLACS2017	1.50	1.89	212 ± 12
J0754+1927	0.1534	0.7401	193 ± 16	1.04	SLACS2017	1.50	1.46	199 ± 16
J0757+1956	0.1206	0.8326	206 ± 11	1.62	SLACS2017	1.50	3.67	204 ± 11
J0826+5630	0.1318	1.2907	163 ± 8	1.01	SLACS2017	1.50	1.64	167 ± 8
J0847+2348	0.1551	0.5327	199 ± 16	0.96	SLACS2017	1.50	1.54	204 ± 16
J0851+0505	0.1276	0.6371	175 ± 11	0.91	SLACS2017	1.50	1.35	181 ± 11

Table 1 – *continued*

Name	z_l	z_s	σ_{ap} (km s^{-1})	θ_E (arcsec)	Survey	θ_{ap} (') (arcsec)	θ_{eff} (arcsec)	σ_0 (km s^{-1})
J0920+3028	0.2881	0.3918	297 ± 17	0.70	SLACS2017	1.50	4.25	293 ± 17
J0955+3014	0.3214	0.4671	271 ± 33	0.54	SLACS2017	1.50	2.95	271 ± 33
J0956+5539	0.1959	0.8483	188 ± 11	1.17	SLACS2017	1.50	1.96	191 ± 11
J1010+3124	0.1668	0.4245	221 ± 11	1.14	SLACS2017	1.50	3.26	220 ± 11
J1031+3026	0.1671	0.7469	197 ± 13	0.88	SLACS2017	1.50	1.04	206 ± 14
J1040+3626	0.1225	0.2846	186 ± 10	0.59	SLACS2017	1.50	1.30	192 ± 10
J1041+0112	0.1006	0.2172	200 ± 7	0.60	SLACS2017	1.50	2.50	201 ± 7
J1048+1313	0.133	0.6679	195 ± 10	1.18	SLACS2017	1.50	1.90	199 ± 10
J1051+4439	0.1634	0.538	216 ± 16	0.99	SLACS2017	1.50	1.66	221 ± 16
J1056+4141	0.1343	0.8318	157 ± 10	0.72	SLACS2017	1.50	1.81	160 ± 10
J1101+1523	0.178	0.5169	270 ± 15	1.18	SLACS2017	1.50	0.89	283 ± 16
J1116+0729	0.1697	0.686	190 ± 11	0.82	SLACS2017	1.50	2.44	192 ± 11
J1127+2312	0.1303	0.361	230 ± 9	1.25	SLACS2017	1.50	2.69	231 ± 9
J1137+1818	0.1241	0.4627	222 ± 8	1.29	SLACS2017	1.50	1.79	227 ± 8
J1142+2509	0.164	0.6595	159 ± 10	0.79	SLACS2017	1.50	1.51	163 ± 10
J1144+0436	0.1036	0.2551	207 ± 14	0.76	SLACS2017	1.50	1.22	215 ± 15
J1213+2930	0.0906	0.5954	232 ± 7	1.35	SLACS2017	1.50	1.73	237 ± 7
J1301+0834	0.0902	0.5331	178 ± 8	1.00	SLACS2017	1.50	1.25	184 ± 8
J1330+1750	0.2074	0.3717	250 ± 12	1.01	SLACS2017	1.50	2.85	251 ± 12
J1403+3309	0.0625	0.772	190 ± 6	1.02	SLACS2017	1.50	2.00	193 ± 6
J1430+6104	0.1688	0.6537	180 ± 15	1.00	SLACS2017	1.50	2.24	182 ± 15
J1433+2835	0.0912	0.4115	230 ± 6	1.53	SLACS2017	1.50	3.23	229 ± 6
J1541+3642	0.1406	0.7389	194 ± 11	1.17	SLACS2017	1.50	1.55	199 ± 11
J1543+2202	0.2681	0.3966	285 ± 16	0.78	SLACS2017	1.50	2.32	288 ± 16
J1550+2020	0.1351	0.3501	243 ± 9	1.01	SLACS2017	1.50	1.68	249 ± 9
J1553+3004	0.1604	0.5663	194 ± 15	0.84	SLACS2017	1.50	2.15	197 ± 15
J1607+2147	0.2089	0.4865	197 ± 16	0.57	SLACS2017	1.50	2.63	198 ± 16
J1633+1441	0.1281	0.5804	231 ± 9	1.39	SLACS2017	1.50	2.39	233 ± 9
J2309-0039	0.2905	1.0048	184 ± 13	1.14	SLACS2017	1.50	2.08	187 ± 13
J2324+0105	0.1899	0.2775	245 ± 15	0.59	SLACS2017	1.50	1.10	255 ± 16

Table 2. Best-fitting parameters for the CDM models (constrained by $\mathcal{D}^{obs} \leq 1$).

Model	Ω_m	w_{de}	σ_X	χ^2_{dof}
wCDM	$0.33^{+0.13}_{-0.15}$	$-1.29^{+0.97}_{-6.09}$	12.2 per cent	0.998
ΛCDM	$0.29^{+0.12}_{-0.08}$	−1 (fixed)	12.2 per cent	0.999

outlier) to 129 lenses, but it also decreases the magnitude of σ_X compared to what it would have been for the entire sample. A quick inspection of Table 2 shows that the steps we have taken in identifying the final sample for model selection produces results that are consistent with the *Planck* measurements. Both Ω_m and w_{de} are fully consistent with the parameter values in the concordance model, particularly in the case of ΛCDM.

With the best-fitting parameters for flat wCDM thus determined, we now proceed to carry out model selection based on the Bayes information criterion (BIC; Schwarz 1978; Melia & Maier 2013; Wei et al. 2015b). The BIC is defined as

$$\mathrm{BIC} = -2\mathcal{L} + n\ln(N), \tag{13}$$

where $\mathcal{L}$ is the likelihood in equation (11), N is the number of measurements in the final reduced sample, here 129, and n is the number of free parameters. In this application, wCDM is penalized with $n = 2$, and ΛCDM with $n = 1$, while $R_h = ct$, Milne, and Einstein-de-Sitter each have $n = 0$ (no free parameters). When comparing cosmologies using the BIC, the probability that a specific

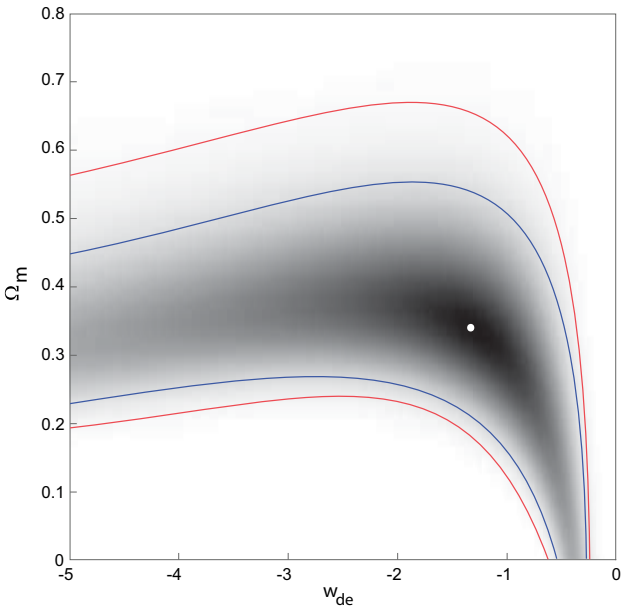

Figure 1. Probability density plot in the $\Omega_m - w_{de}$ plane for wCDM. The contours give the 1σ and 2σ (i.e. the 68 per cent and 95 per cent) confidence regions for the optimized parameters in wCDM. The white dot shows the best-fitting values.

Table 3. Model comparisons and ranking (based on 129 lenses with the constraint $\mathcal{D}^{\rm obs} \leq 1$).

Model	$\chi^2_{\rm dof}$	BIC	Relative likelihood
$R_{\rm h} = ct$	1.020	131.56	73.03 per cent
ΛCDM	0.999	133.75	24.44 per cent
wCDM	0.998	138.48	2.29 per cent
Milne	1.109	143.06	0.23 per cent
EdS	1.194	151.31	3.75×10^{-3} per cent

model $\mathcal{M}_\alpha$ is the correct one among the set being considered is

$$P(\mathcal{M}_\alpha) = \frac{\exp(-{\rm BIC}_\alpha/2)}{\sum_i \exp(-{\rm BIC}_i/2)}\,. \tag{14}$$

Table 3 summarizes the $\chi^2_{\rm dof}$, the BIC, and *relative* likelihood (calculated from equation 14) of each model in this comparison.

4 DISCUSSION

Our analysis in this paper affirms the important role played by strong lenses in helping to refine the parameters in the standard model and, perhaps more importantly going forward, providing ample confirmation, if not definitive evidence, in model selection. Previous work by Melia, Wei & Wu (2015) and Cao et al. (2015), albeit with smaller samples, suggested that – while individual lenses may deviate from an SIS model – the statistics of a large sample appears to be consistent with this simple internal structure of the lens's mass distribution. We have therefore adopted this approach to update the optimization of parameters in the standard model based on fits to the strong lens angular diametre distance dependence on redshift, and then to compare the predictions of wCDM with those of four other cosmologies. We have found, however, that ignoring individual variations from a pure SIS structure results in an unsatisfactory fit using wCDM and ΛCDM, necessitating the introduction of a dispersion to represent the scatter associated with this oversimplified lens model.

It is important to emphasize that our sample is larger than that used in any previous attempt to carry out this type of analysis, and that it includes all of the sources used by Cao et al. (2015) (with the exception of a single outlier). We have supplemented this catalogue with the 40 recently confirmed lenses uncovered with SLACS (Shu et al. 2017). Our best-fitting parameters for the standard model are consistent with those of *Planck*, but based solely on the reported errors, the reduced $\chi^2_{\rm dof}$ for the optimized model is unacceptably large, unless we include the aforementioned additional scatter in the analysis. We argue that either the errors have been underreported, or that the additional dispersion cannot be ignored with observations such as these. We have therefore sought to identify its magnitude, representing deviations from a pure homogeneous SIS model for all the lenses. Note, however, that our inferred uncertainty on the optimized value of $w_{\rm de}$ (in the case of wCDM) is larger than that obtained by Cao et al. (2015), in spite of the larger lens catalogue at our disposal.

But though the introduction of the dispersion σ_X to account for individual departures from a pure SIS lens structure has greatly reduced the scatter about the best-fitting model in wCDM/ΛCDM, the problems with using such a simple lens have not been completely eliminated, as demonstrated in Fig. 2. Cao et al. (2015) reported a significant trend in deviations from their fitted cosmological model as a function of σ_0. We find the same trend with the larger sample used in this paper, in which $\mathcal{D}^{\rm obs}$ decreases faster than

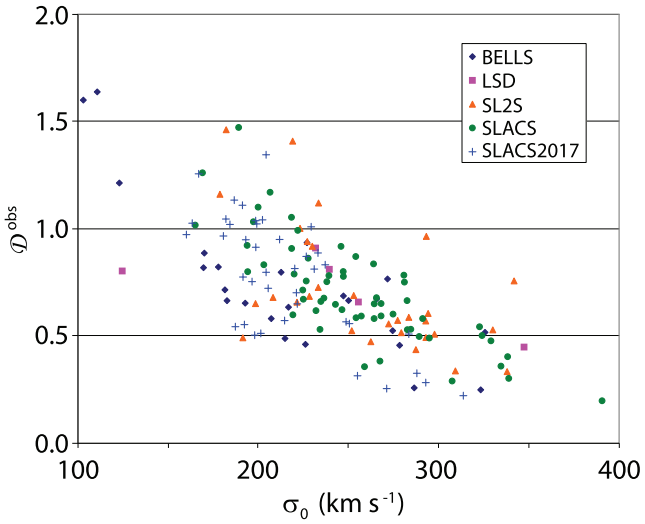

Figure 2. An apparent bias in the measured ratio $\mathcal{D}^{\rm obs}$ with increasing velocity dispersion σ_0. This trend exceeds the dependence of $\mathcal{D}^{\rm obs}$ on σ_0 expected from equation (3), in which $\theta_{\rm E}$ ought to change in concert with σ_0 to largely offset such a correlation. Two outliers, J2220+0106 and J1352+3216, lie outside this plot due to their extreme $\mathcal{D}^{\rm obs}$ values of 4.32 and 2.36, respectively.

expected from equation (3) with increasing σ_0. Certainly equation (3) predicts that for a fixed $\theta_{\rm E}$, one should see such a trend. But the Einstein radius also depends on the lens galaxy's mass distribution and the distance ratio between the lens and source objects, which should largely offset the trend seen in Fig. 2. There is no reason to expect a significant correlation between the mass distribution of the lensing object and the distance ratio between it and the source galaxy, as these are two independent parameters that produce the Einstein ring. For this reason, such a significant correlation between $\mathcal{D}^{\rm obs}$ and σ_0 can be taken as some evidence that the simple SIS galaxy mass distribution model is not robust enough to accurately account for all the individual variations seen from source to source.

In the redshift range of these data, the best-fitting wCDM, ΛCDM, and $R_{\rm h} = ct$ models predict comparable $\mathcal{D}^{\rm th}$ ratios. In each case, strongly lensed systems with $\sigma_0 \lesssim 250\,{\rm km\,s^{-1}}$ generally have $\mathcal{D}^{\rm obs} > \mathcal{D}^{\rm th}$, but this trend is reversed for $\sigma_0 \gtrsim 250\,{\rm km\,s^{-1}}$. The effect tends to get bigger as σ_0 increases or decreases away from its median value $\sim$233 km s^{-1}. In fact, all lens systems with an unphysical $\mathcal{D}^{\rm obs} > 1$ have $\sigma_0 \lesssim 233\,{\rm km\,s^{-1}}$. Working with a smaller sample of the data than we have here, Cao et al. (2015) attempted to generalize the SIS model by characterizing it as a spherically symmetric power-law mass distribution of the form $\rho \sim r^{-\gamma}$. Their optimized value of γ was consistent with -2, however, which is in fact the SIS model, but they also noticed large deviations from their fits for σ_0 very different from 250 km s^{-1}. One should therefore be cautious with the use of an SIS model in future attempts to constrain or compare cosmologies using strong lensing data. At a minimum, one should carefully study the impact of a density profile varying with changing σ_0.

A principal goal of this paper has been to significantly update the results of Melia, Wei & Wu (2015). In that analysis, with only 69 strong lenses, no significant preference was determined for either ΛCDM or $R_{\rm h} = ct$. Based on a much larger sample of mock data, however, these authors concluded that approximately 200 lenses

would be required to show that ΛCDM is preferred over $R_h = ct$ at the 99.7 per cent confidence level if the standard model is the correct description of nature. On the flip side, this earlier work also showed that about 300 lenses would be needed to demonstrate the superiority of $R_h = ct$ over ΛCDM at a comparable level of confidence if it turned out that the former was the correct model. With the 158 systems we have considered here, reduced to 129 with the exclusion of the unphysical ones, our sample has not quite reached that size yet, but we are rapidly approaching these thresholds. As Table 3 shows, the current status has the $R_h = ct$ universe as the preferred model, followed by ΛCDM, which is favoured over *w*CDM. Although *w*CDM is slightly more flexible in fitting the data than ΛCDM, the penalty incurred by the additional free parameter causes it to be favoured less than the standard model with a fixed dark-energy equation of state. At the same time, these results show that the Milne universe and Einstein-de Sitter are completely ruled out. The sample of strong lenses now available for model selection is therefore already large enough to provide results consistent with those of many other kinds of observation, all of which have thus far tended to favour $R_h = ct$ over *w*CDM/ΛCDM (see e.g. Melia 2013a,b; and especially Table 1 in Melia 2017b).

5 CONCLUSION

An important by-product of this analysis has been our assessment of the likely intrinsic scatter associated with the SIS model for the lens. If the random variation in galaxy morphology is almost Gaussian, we find that an additional error term of about 12.22 per cent is necessary to have 68 per cent of the observations lie within 1σ of the best-fitting *w*CDM model. This factor is smaller than – though consistent with – the 20 per cent scatter suggested by Cao et al. (2012). Thus, in spite of the fact that our sample here is twice as large as that used in our previous analysis (Melia, Wei & Wu 2015), our conclusion regarding the size of this scatter is virtually identical to that of our previous work, in which we found that $\sigma_X \sim 0.12$. Interestingly, this is very close to the conclusion drawn earlier by Treu et al. (2006), who also argued for the inclusion of a scatter of about 12 per cent. But this is only true when sources with $\mathcal{D}^{\rm obs} > 1$ are excluded. Were we to include all 157 sources (the complete sample of 158 minus the significant outlier J0850-0347), we would find that σ_X is closer to 18 per cent. As noted, this difference provides some evidence that the SIS lens model breaks down for the more extreme values of σ_0.

Based on our earlier work (Melia, Wei & Wu 2015) and the significant improvement we have seen using a much bigger sample in this paper, we are certain that strong lenses will play a pivotal role in model selection going forward—but preferably with an improved model for the lens mass. Already DES has released a catalogue of 348 new strong lens candidates (Diehl et al. 2017). Spectroscopic follow-up observations are anticipated over the next several years. Even if only half of these are verified lenses, with a sufficient number of sources at $z > 3$, we anticipate that the next update of our analysis may offer an even stronger answer as to whether $R_h = ct$ or ΛCDM is the correct cosmology.

ACKNOWLEDGEMENTS

We are grateful to Joel Brownstein, Raphel Gavazzi, and Tommaso Treu for their correspondence and helpful suggestions, and to the anonymous referee for a very constructive and thoughtful review. FM is supported by the Chinese Academy of Sciences Visiting Professorships for Senior International Scientists under grant 2012T1J0011, and the Chinese State Administration of Foreign Experts Affairs under grant GDJ20120491013.

REFERENCES

An J., Chang B., Xu L., 2016, Chin. Phys. Lett., 33, 079801
Auger M. W., Treu T., Bolton A. S., Gavazzi R., Koopmans L. V. E., Marshall P. J., Bundy K., Moustakas L. A., 2009, ApJ, 705, 1099
Bolton A. S., Burles S., Koopmans L. V. E., Treu T., Gavazzi R., Moustakas L. A., Wayth R., Schlegel D. J., 2008, ApJ, 682, 964
Brownstein J. R. et al., 2012, Apj, 744, 41
Cao S., Pan Y., Biesiada M., Godlowski W., Zhu Z-H., 2012, J. Cosmol. Astropart. Phys., 3, 016
Cao S., Biesiada M., Gavazzi R., Piórkowska A., Zhu Z.-H., 2015, ApJ, 806, 185
Diehl H. T. et al., 2017, ApJS, 232, 15
Einstein A., 1936, Sci, 84, 506
Gavazzi R., Marshall P. J., Treu T., Sonnenfeld A., 2014, ApJ, 785, 144
Grillo C., Lombardi M., Bertin G., 2008, A&A, 477, 397
Jørgensen I., Franx M., Kjærgaard P., 1995a, MNRAS, 273, 1097
Jørgensen I., Franx M., Kjærgaard P., 1995b, MNRAS, 276, 1341
King L. J., Jackson N., Blandford R. D., Bremer M. N., Browne I. W. A., de Bruyn A. G., 1998, MNRAS, 295, L41
Kochanek C. S. et al., 2000, ApJ, 543, 131
Koopmans L. V. E., Treu T., 2003, ApJ, 583, 137
Melia F., Shevchuk A. S. H., 2012, MNRAS, 419, 2579
Melia F., Abdelqader M., 2009, IJMP-D, 18, 1889
Melia F., Maier R. S., 2013, MNRAS, 432, 2669
Melia F., 2007, MNRAS, 382, 1917
Melia F., 2013a, A&A, 553, A76
Melia F., 2013b, ApJ, 764, 72
Melia F., 2016, Front. Phys., 11, 119801
Melia F., 2017a, Front. Phys., 12, 129802
Melia F., 2017b, MNRAS, 464, 1966
Melia F., Wei J-J., Wu X-F., 2015, AJ, 149, 2
Planck Collaboration, 2016, A&A, 594, A13
Ratnatunga K. U., Griffiths R. E., Ostrander E. J., 1999, AJ, 117, 2010
Schwarz G. E., 1978, Ann. Stat., 6, 461
Shu Y. et al., 2017, ApJ, 851, 48
Sonnenfeld A., Gavazzi R., Suyu S. H., Treu T., Marshall P. J., 2013a, ApJ, 777, 97
Sonnenfeld A., Treu T., Gavazzi R., Suyu S. H., Marshall P. J., Auger M. W., Nipoti C., 2013b, ApJ, 777, 98
Treu T., Koopmans L. V. E., 2002, ApJ, 575, 87
Treu T., Koopmans L. V. E., 2004, ApJ, 611, 739
Treu T., Koopmans L. V. E., Bolton A. S., Burles S., Moustakas L. A., 2006, ApJ, 640, 662
Vishwakarma R. G., 2013, Phys. Scr., 87, 055901
Wei J.-J., Wu X., Melia F., 2015a, AJ, 149, 165
Wei J.-J., Wu X., Melia F., Maier R. S., 2015b, AJ, 149, 102

This paper has been typeset from a TEX/LATEX file prepared by the author.

Monthly Notices of the ROYAL ASTRONOMICAL SOCIETY

MNRAS **00,** 1 (2019)
Advance Access publication 2019 May 21

doi:10.1093/mnras/stz1396

Cosmological test using the high-redshift detection rate of FSRQs with the Square Kilometre Array

Kyle Leaf[1]★ and Fulvio Melia[2]★†

[1]*Department of Physics, The University of Arizona, Tucson, AZ 85721, USA*
[2]*Department of Physics, The Applied Math Program, and Department of Astronomy, The University of Arizona, Tucson, AZ 85721, USA*

Accepted 2019 May 16. Received 2019 May 13; in original form 2019 March 29

ABSTRACT

We present a phenomenological method for predicting the number of flat-spectrum radio quasars (FSRQs) that should be detected by upcoming Square Kilometre Array (SKA) SKA1-MID Wide Band 1 and Medium-Deep Band 2 surveys. We use the *Fermi* blazar sequence and mass estimates of *Fermi* FSRQs, and γ-ray emitting narrow-line Seyfert 1 galaxies, to model the radio emission of FSRQs as a function of mass alone, assuming a near-Eddington accretion rate, which is suggested by current quasar surveys at $z \gtrsim 6$. This is used to determine the smallest visible black hole mass as a function of redshift in two competing cosmologies we compare in this paper: the standard Λ cold dark matter (ΛCDM) model and the $R_h = ct$ universe. We then apply lockstep growth to the observed black hole mass function at $z = 6$ in order to devolve that population to higher redshifts and determine the number of FSRQs detectable by the SKA surveys as a function of z. We find that at the redshifts for which this method is most valid, ΛCDM predicts $\sim$30 times more FSRQs than $R_h = ct$ for the Wide survey, and $\sim$100 times more in the Medium-Deep survey. These stark differences will allow the SKA surveys to strongly differentiate between these two models, possibly rejecting one in comparison with the other at a high level of confidence.

Key words: galaxies: general – distance scale – large-scale structure of Universe – cosmology: observations – cosmology: theory.

1 INTRODUCTION

The Square Kilometre Array (SKA) is a premier upcoming radio observatory, expected to provide a powerful probe of cosmological features (Square Kilometre Array Cosmology Science Working Group 2018, hereafter SKA CSWG 2018). Phase 1 of the SKA, constituting roughly 10 per cent of the design collecting area, is expected to be constructed from 2020 to 2025. Of principal interest for the work reported in this paper, SKA will significantly enhance our ability to detect high-redshift, radio-loud quasars. The primary goal of this analysis is to calculate the number of such sources that ought to be detectable by Phase 1 of the SKA in two competing models – standard Λ cold dark matter (ΛCDM) and the $R_h = ct$ universe – thereby providing a new test of the background cosmology.

The current standard model has been quite successful in describing many evolutionary aspects of the Universe, though we have begun to see growing tension between its predictions and several key observations. For example, the Hubble constant measured with *Planck* (Planck Collaboration VI 2018) disagrees with the locally measured value at over 4σ significance (Riess et al. 2018). A very different type of measurement, based on the angular diameter distance, shows that the peak of this integrated measure also disagrees with our expectation from ΛCDM (Melia & Yennapureddy 2018a). All in all, comparative tests between the standard model and the alternative picture we shall consider in this paper have now been completed using over 25 different kinds of data. The standard model has been disfavoured by the observations in all of these cases (see e.g. table 2 in Melia 2018). We are therefore motivated to at least consider modifications to the background cosmology, perhaps eventually even replacing it, in order to determine whether different physics may better describe the growing observational evidence.

The SKA, with its unprecedented capabilities, is poised to probe the intermediate- to high-redshift radio universe with greater sensitivity than any instrument before it. In our previous study of high-redshift active galaxies (Fatuzzo & Melia 2017), we analysed the high-redshift quasar detection rate based on their X-ray emission in order to predict the various quasar counts to be compiled by the upcoming *extended Roentgen Survey with an Imaging Telescope Array* (*eROSITA*) and *Advanced Telescope for High ENergy Astrophysics* (*ATHENA*) observatories. While $R_h = ct$ and ΛCDM

★ E-mail: kyleaf@email.arizona.edu (KL); melia@physics.arizona.edu (FM)
† John Woodruff Simpson Fellow.

are very similar in describing the local universe, their predictions diverge towards higher redshifts. Of direct relevance to this study are the differences in the two models between the comoving volume and age of the Universe as functions of redshift. In our previous work, the combination of those factors, based on the existing observations of quasars at $z \sim 6$, resulted in predictions of $\sim$0.16 X-ray emitting quasars detectable by *ATHENA* at $z \sim 7$ in $R_h = ct$, compared to $\sim$160 such objects in ΛCDM. Such a stark difference will be easily measurable by these upcoming *ATHENA* observations. In this paper, we extend this work significantly by considering the radio-loud quasar population, which will allow us to probe the Universe even more deeply with SKA. Indeed, we shall demonstrate that SKA1's Medium-Deep survey has the potential of detecting jetted active galactic nuclei (AGNs) with central black hole masses as small as $M \sim 10^6$ M$_\odot$ out to a redshift of $z = 9$.

However our chief concern here is not only to estimate how many new radio-loud quasars we can hope to see with SKA in the remote Universe; we shall argue that their detection rate will be strongly dependent on the assumed background cosmology – offering us the interesting prospect of using these counts as a powerful test of the cosmology based on techniques that are quite different from the more conventional, integrated measures, such as the luminosity distance and the Hubble parameter. We shall seek to characterize the radio emission profile of a specific class of high-redshift active galaxies and evolve the population known at $z \sim 6$ to higher redshifts, assuming standard Eddington-limited accretion, in order to predict their detection rate as a function of z for each cosmological model.

In Section 2, we shall discuss the radio emission characteristics of these high-redshift quasars, and describe the methods used to estimate their growth and evolution with redshift in each of these models in Section 3. To do this, we shall also summarize here the key differences between $R_h = ct$ and ΛCDM to the extent that these variations affect the AGN population synthesis. We shall present and discuss our results in Section 4, and finally conclude in Section 5.

2 THE RADIO EMISSION OF HIGH-z QUASARS

As of today, approximately half of the high-z (i.e. $z > 5.5$) radio-loud quasars have been identified as flat-spectrum radio quasars (FSRQs), with the remaining half showing steeper spectra similar to Faranov–Riley II (FR-II) galaxies (Coppejans et al. 2016). FSRQs are generally considered to be AGNs with powerful relativistic jets in a configuration such that the jet is aligned towards the observer, commonly referred to as a blazar (Beckmann & Shrader 2012). Blazars also include BL Lacertae objects (BL Lacs; see e.g. the review papers by Antonucci 1993; Sikora & Madejski 2001). These, however, have not been detected at high redshifts. As discussed in Ghisellini, Maraschi & Tavecchio (2009a), another distinguishing feature between BL Lacs and FSRQs is that the former have significantly lower accretion rates, while, in the high-redshift ($z > 5.5$) Universe, the central black holes of FSRQs are found to be emitting at or near the Eddington luminosity (Willott et al. 2010). Circumstantial evidence, largely based on superluminal motion (Hovatta et al. 2009), suggests that the relativistic jets of FSRQs have bulk Lorentz factors $\Gamma \sim 5$–15 (Ghisellini & Sbarrato 2016).

Assuming a random distribution of AGN orientation, the probability of seeing any given jetted (and thus radio-loud) quasar in its blazar configuration is $\sim 1/2\Gamma^2$, implying roughly a range of 1 in 50 to 1 in 450 (Volonteri et al. 2011). While this low blazar fraction is consistent with observations of AGNs at low z (i.e. $z < 3$), it stands in sharp contrast to the roughly 1 in 2 chance of a radio-loud, $z > 4.5$, AGN being an FSRQ (Coppejans et al. 2016). Several mechanisms have been proposed to help explain this observation (Fabian et al. 2014; Ghisellini & Sbarrato 2016; Wu et al. 2017), but analyses have been inconclusive. These proposals generally suggest that the fraction of jetted AGNs at high redshift that appear as FSRQs are the same as their lower redshift counterparts, but that those without the jet preferentially directed at the observer are not observed strongly in the radio band.

The total spectral energy distribution (SED) across all wavebands for an AGN depends on a large number of physical phenomena. The more commonly included components of quasar emission are as follows: a relativistic jet emitting in the radio (Urry & Padovani, 1995) and, sometimes, in X-rays and γ-rays via inverse Compton scattering (Melia & Königl 1989); a thermally radiating accretion disc emitting predominantly at ultraviolet (UV) wavelengths (Shakura 1973); a hot corona emitting primarily in X-rays (Lusso & Risalti 2016; Fatuzzo & Melia 2017), and an obscuring torus (Krolik & Begelman 1986); and any radiation from the stars in the rest of the galaxy. Roughly $8.1^{+5.0}_{-3.2}$ per cent (Bañados et al. 2015) of the AGNs at high redshift are known to emit strongly at radio frequencies. Disentangling all of the various contributions to the overall SED can be quite challenging, especially given the diversity of AGNs subsamples distinguished primarily upon the dominant contributions from these many components. Rather than constructing a model based on this comprehensive emission picture, we therefore take a more phenomenological approach, analysing one specific class of quasar that ought to be the most relevant for their detection by the upcoming SKA surveys.

Our empirical approach is geared towards modelling the appearance of high-z FSRQs in order to estimate the number of such objects that will be visible to SKA. In spite of the different population statistics referenced previously, FSRQs at high redshift appear to have very similar SEDs to those at lower redshift. For instance, the confirmed highest redshift FSRQ to date, J0906+6930 at $z = 5.47$, has an observed SED similar to lower z FSRQs (An & Romani 2018). It is therefore reasonable to suppose that the large suite of lower redshift FSRQ observations may be used to characterize the radio emission profile of such objects even at higher redshifts.

Ghisellini et al. (2017) presented the so-called blazar sequence based on the *Fermi* observations compiled in Acero et al. (2015), an attempt to characterize the average SED of blazars separated into γ-ray luminosity bins. That work included separate analyses of BL Lac objects and FSRQs. As no BL Lacs have been observed at high redshifts, we here limit ourselves to the FSRQ data, in which the blazars are grouped into five bins based on their γ-ray luminosity, L_γ. These authors included the observation that the overall SED of FSRQs does not change significantly with changing L_γ, instead generally differing only in terms of emitted power. Furthermore, all FSRQs in each bin were found to be consistent with a radio spectral index $\alpha_R \approx -0.1$, a parameter that was then held fixed in the fitting. The results presented in Ghisellini et al. (2017) are based on an assumed $0.7 = h = \Omega_\Lambda$ cosmology. Therefore, in order to extract the results relevant for $R_h = ct$, we recalibrate the inferred luminosity using the ratio $(d_L^{R_h=ct}/d_L^{\Lambda\mathrm{CDM}})^2$ to account for the differences between these models, in terms of the luminosity distance d_L. For objects in the Third *Fermi*-LAT AGN Catalog (3LAC), the inferred luminosities are $\sim$15–19 per cent smaller in $R_h = ct$ than in the fiducial ΛCDM model.

For each of the five phenomenological SEDs from Ghisellini et al. (2017), we determine the γ-ray luminosity over the *Fermi* band (0.1–100 GeV), and compare these results to the catalogue of bright *Fermi* blazars in Ghisellini et al. (2010). This sample includes 22 FSRQs with both observed γ-ray luminosities and published central black hole mass estimates. The masses are determined by associating an optical–UV bump in each object's SED with direct emission from the accretion disc. Ghisellini et al. (2009b, 2010) suggest that this method is accurate to within a factor of 2. The νF_ν peak of the disc luminosity is used to determine the maximum temperature of the accretion disc, which scales as $T_{\rm max} \propto (\lambda_{\rm Edd})^{1/4} M^{-1/4}$, where $\lambda_{\rm Edd}$ is the Eddington factor (i.e. the ratio of luminosity to its Eddington value). Furthermore, the total observed flux from the accretion disc scales as $\lambda_{\rm Edd} M / d_L^2$. Therefore, each mass determined by Ghisellini et al. (2010) must be multiplied by the factor $d_L^{R_{\rm h}=ct} / d_L^{\Lambda{\rm CDM}}$ in order to get the appropriate inferred mass for the $R_{\rm h} = ct$ universe. The inferred Eddington ratio in $R_{\rm h} = ct$ changes by the same factor.

These masses recorded in Ghisellini et al. (2010) (quoted as $\log_{10}[M/{\rm M}_\odot]$) range from 8.17 to 9.78, with luminosities ($\log_{10}[L_\gamma/{\rm erg\ s^{-1}}]$) from 45.93 to 49.10, at redshifts from $z = 0.213$ to 2.19. Using the fitted SEDs from Ghisellini et al. (2010), we estimate the average disc luminosity of these observed FSRQs as a ratio of the Eddington limit, yielding a value $\approx$0.22, providing some evidence that the accretion rates are generally high. Since the lowest γ-ray bin in the *Fermi* blazar sequence of FSRQs falls in the range 10^{44}–10^{45} erg s^{-1}, below the range of the bright *Fermi* blazars, we need an additional sample of high accretion rate active galaxies in order to associate that bin with a central black hole mass.

With high-redshift FSRQs known to have generally high accretion rates, in order to associate the lower γ-ray luminosity bins of the blazar sequence with some fiducial central black hole mass, we must select those objects among this category that themselves have a high accretion rate, but also lower luminosity. γ-ray emitting narrow-line Seyfert 1 galaxies (γ-NLSy1) are radio-loud active galaxies characterized by flat radio spectra, exhibiting a core–jet structure, high brightness temperature, and apparent superluminal motion. Indeed, the broad-band SEDs of γ-NLSy1 resemble those of FSRQs, but merely less powerful (Paliya et al. 2013). More recent analyses of these objects (Paliya et al. 2018, 2019) have further established a link between γ-NLSy1s and FSRQs. For example, attempts to fit their SEDs have shown that their jets have bulk Lorentz factors in the range $7 < \Gamma < 17$, comfortably within the usual estimated factors of FSRQs, as noted above.

For our phenomenological model construction, we therefore use the 14 known γ-NLSy1's included in Paliya et al.'s (2018) sample. We take their reported γ-ray luminosity and the mass estimates derived from optical spectroscopy recorded in Paliya et al. (2019), and citations recorded therein. In $R_{\rm h} = ct$, these mass estimates are adjusted in the same manner as FSRQs. This sample includes reported luminosities $\log_{10}(L_\gamma/{\rm erg\ s^{-1}})$ from 44.4 to 47.4, and estimated black hole masses from $10^{6.7}$ to $10^{8.85}$ M$_\odot$. Together with the highly luminous *Fermi* FSRQs from Ghisellini et al. (2010), we therefore have a sample of 36 active galaxies with observed γ-ray luminosities, mass estimates, and a generally high estimated inferred accretion rate, consistent with those $z > 5.5$ quasars observed to date. Fig. 1 shows the γ-ray luminosity plotted against the central black hole mass for this sample, as well as our best-fitting (power-law) function to describe their correlation.

This best-fitting power law is found with linear regression using the logarithms of the estimated central black hole mass and luminosity, which is taken as the independent variable. The error in

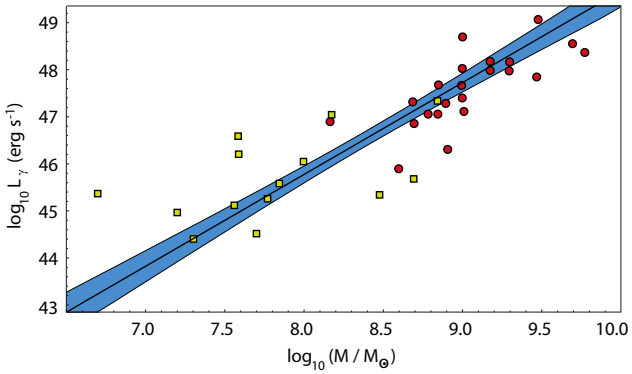

Figure 1. γ-ray luminosity $\log_{10}(L/{\rm erg\ s^{-1}})$ versus central black hole mass $\log_{10}(M/{\rm M}_\odot)$ in ΛCDM for bright *Fermi* FSRQs (red circles) (Ghisellini et al. 2009a,b), and the 14 γ-NLSy1s (yellow squares) with measured γ-ray luminosity and central black hole mass in the context of ΛCDM (Paliya et al. 2018, 2019). The line shows the best-fitting power law, along with its estimated uncertainty (blue swath) based on standard error propagation.

the mean mass is estimated according to

$$\delta\mu\,(l_\gamma) = \frac{\sigma_\mu}{\sqrt{n}} \sqrt{1 + \frac{l_\gamma - \langle l_\gamma \rangle}{\sigma^2_{l_\gamma}}}, \qquad (1)$$

where $\mu \equiv \log_{10}({\rm M/Msol})$, $l_\gamma \equiv \log_{10}(L_\gamma\ /\ {\rm erg\ s^{-1}})$, n is the number of observations, σ_μ is the square root of the reduced χ^2/dof, $\sigma^2_{l_\gamma}$ is the population variance of l_γ, and $\langle l_\gamma \rangle$ is the mean of all l_γ values. Table 1 shows the five SED bins from Ghisellini et al. (2017), the γ-ray luminosity found by integrating the SED from 0.1 to 100 GeV (we point out that integrating from 0.1 to 300 GeV instead does not change the numerical result by more than 3.7 per cent or 0.016 dex), and the mass we associate with each luminosity in both models. The errors in the masses are simply those described by equation (1) for the given L_γ.

The *Fermi* blazar sequence of Ghisellini et al. (2017) models their complete non-thermal SED in terms of two broad humps and a flat radio spectrum. Beginning at the lowest energies, the sequence starts with the flat radio segment from arbitrarily low frequencies up to some cut-off $\nu_{\rm t}$. Above this, the single power law connects with two smoothly broken power laws. The lower frequency power law is associated with the synchrotron flux, and the higher frequency is associated with inverse Compton flux. Altogether, there are 11 parameters determined by observations. The first set contains three typical frequencies: $\nu_{\rm t}$ is where the flat radio spectrum ends; $\nu_{\rm S}$ is the peak of the synchrotron spectrum; and $\nu_{\rm C}$ is the peak of the high-energy spectrum. Second, there are two cut-off frequencies at which the power laws start to exhibit exponential decay. These are $\nu_{\rm Cut,S}$ and $\nu_{\rm Cut,C}$. Third are the four power-law indices: $\alpha_{\rm R}$ for the radio band; α_1 connecting $\nu_{\rm t}$ and $\nu_{\rm S}$; α_2 giving the downward slope after both the $\nu_{\rm S}$ and $\nu_{\rm C}$ peaks; and α_3 yielding the upward slope toward the $\nu_{\rm C}$ peak. The remaining two parameters are the luminosities at the two peaks, which are included as $\nu_{\rm S} L(\nu_{\rm S})$ (the luminosity at the synchrotron peak) and ratio of the νL_ν Compton and synchrotron luminosities, known as the Compton dominance (CD).

Having associated each *Fermi* blazar sequence SED with a central black hole of some mass undergoing Eddington-limited accretion, we interpolate the parameters characterizing the five models, resulting in a phenomenological SED for FSRQs as a function of M. Following Ghisellini et al. (2017), we hold the radio spectral index constant at $\alpha_{\rm R} = -0.1$ throughout this work. For

Table 1. *Fermi* blazar sequence bins, their γ-ray luminosities, and their fitted masses.

$\log_{10} L_\gamma$ (erg s^{-1})	$\log_{10} L_\gamma^{\Lambda\mathrm{CDM}}$ (erg s^{-1})	$\log_{10} M^{\Lambda\mathrm{CDM}}$ ($\mathrm{M}_\odot$)	$\log_{10} L_\gamma^{R_\mathrm{h}=ct}$ (erg s^{-1})	$\log_{10} M^{R_\mathrm{h}=ct}$ ($\mathrm{M}_\odot$)
$48 < L$	48.27	9.28 ± 0.10	48.19	9.24 ± 0.10
$47 < L < 48$	47.43	8.84 ± 0.07	47.34	8.80 ± 0.07
$46 < L < 47$	46.54	8.39 ± 0.07	46.64	8.34 ± 0.07
$45 < L < 46$	45.59	7.90 ± 0.10	45.59	7.87 ± 0.10
$44 < L < 45$	44.59	7.39 ± 0.14	44.59	7.36 ± 0.14

this interpolation, we additionally hold $\nu_{\mathrm{cut,S}}$ and $\nu_{\mathrm{cut,C}}$ constant at 10^{16} and 10^{27} Hz, respectively, as they were inferred to be relatively constant across the sequence models and do not significantly affect the overall SED. The indices α_1 and α_2 show no significant evolution with luminosity bin, so we hold them fixed at 0.5 and 1.43, respectively, while α_3 is fitted by a linear relation in $\log M$. The frequencies ν_{t} and ν_{S} are fitted by linear functions in $\log M$ for the lower bins, and both are held at 10^{12} Hz for the brightest two bins. The frequency ν_{C} is fitted with a quadratic interpolation between the lowest three bins, and held fixed for $M > 10^{8.23}$ $\mathrm{M}_\odot$, while ν_{SL} and CD are interpolated with quartic polynomial functions of $\log M$.

The final interpolated blazar sequence may be used to estimate the emission profile of any FSRQ within any waveband, from radio to γ-rays. We use the mass-dependent SED function to find a simple relationship between an FSRQ's central black hole mass and its radio luminosity, which we then extrapolate downward to smaller masses. To do this, we switch from the full interpolated SED to a simplified relationship covering only the radio emission below $10^{7.39}$ $\mathrm{M}_\odot$ in ΛCDM, and $10^{7.36}$ $\mathrm{M}_\odot$ in $R_\mathrm{h} = ct$. We fit a power law to the three lower luminosity SEDs, and find a relationship $L_\mathrm{R} \propto M^{1.55}$ in ΛCDM, and $L_\mathrm{R} \propto M^{1.56}$ in $R_\mathrm{h} = ct$. Even at a redshift of 7, an FSRQ matching the SED in the lowest bin of the blazar sequence would have a radio flux density in the SKA1 band of 300 μJy in ΛCDM, and 269 μJy in $R_\mathrm{h} = ct$, significantly above the 22.8 μJy flux limit of the Wide Band 1 survey (SKA CSWG 2018), requiring some extrapolation to lower masses in order to estimate the detection rate of smaller – though more numerous – AGNs.

3 CALCULATIONS

Now that the blazar radio emission may be estimated as a function of black hole mass, we use the distribution from Willott et al. (2010) to establish (i.e. normalize) the mass function at a known redshift. Following Fatuzzo & Melia (2017), we begin with the observed black hole mass function at $z = 6$, and devolve the entire population in lockstep towards higher redshifts, with the assumption that all quasars at $z = 6$ are undergoing Eddington-limited accretion, with a duty cycle very close to 1. This growth with a fiducial efficiency of 10 per cent corresponds to an e-folding time of $t_{\mathrm{Edd}} \approx 45$ Myr (known as the Salpeter time; see e.g. Melia 2013). The overall growth rate of quasars at high redshifts is therefore highly dependent on the cosmology, given that the predicted timeline $t(z)$ changes considerably between models.

The two competing cosmological models we consider here are the standard flat ΛCDM model and the $R_\mathrm{h} = ct$ universe. As noted earlier, while ΛCDM continues to account reasonably well for a broad range of data, several significant tensions continue to grow. For instance, the final results of the *Planck* mission (Planck Collaboration VI 2018) suggest a Hubble constant statistically incompatible (now over 4σ) with that inferred by *Hubble Space Telescope* data (Riess et al. 2018). In addition – and a primary motivator for this work – Weigel et al. (2015) have estimated that, in the context of ΛCDM, ∼20 AGNs should have been observed at $z > 5$ in the *Chandra Deep Field*-South survey, while none were identified – strongly favouring $R_\mathrm{h} = ct$ over the standard model (Fatuzzo & Melia 2017). Though possible systematic effects may be at least partially responsible for this, at face value we estimate that this negative result constitutes a roughly $\sim 20/\sqrt{20}$ effect, i.e. another $\sim 4\sigma$ disparity between the predictions of the standard model and actual observations. And more recently, Wang et al. (2018) derived the quasar luminosity function at $z \sim 6.7$, which shows a significantly steeper reduction of the comoving quasar number density as a function of redshift than earlier estimates by Fan et al. (2001) based on ΛCDM. Of utmost importance in calculating this change in quasar number density as a function of redshift is the amount of time elapsed from one redshift to another, which is strongly dependent on the presumed cosmological model.

For example, $z = 6$ corresponds to ≈0.92 Gyr after the big bang in flat ΛCDM with parameters $\Omega_\mathrm{m} = 0.3$, $H_0 = 70$ km s^{-1} Mpc^{-1}. We adopt this parametrization for the entire analysis. By comparison, it is ≈2 Gyr in $R_\mathrm{h} = ct$ with the same Hubble constant (which is the only free parameter in this model). The $R_\mathrm{h} = ct$ universe is a Friedman–Lemaître–Robertson–Walker (FLRW) cosmology with zero active mass, $\rho + 3p = 0$ (Melia 2003, 2007, 2016, 2017, 2018; Melia & Abdelqader 2009; Melia & Shevchuk 2012). As noted in the Introduction, it has accounted for the observations better than ΛCDM in comparative tests, including such notable cases as cosmic chronometers (Melia & Maier 2013; Leaf & Melia 2017; Melia & Yennapureddy 2018b), strongly lensed galaxies (Leaf & Melia 2018; Yennapureddy & Melia 2018), and measurements of the maximum angular diameter distance (Melia 2018; Melia & Yennapureddy 2018a). The different timeline in $R_\mathrm{h} = ct$ makes it especially attractive when considering the growth rates of black hole seeds into supermassive black holes, a topic addressed in detail in Melia (2013) and Melia & McClintock (2015). In ΛCDM, the time elapsed between $z = 7$ and 6 is 167 Myr, compared with 249 Myr in $R_\mathrm{h} = ct$. With a ∼45 Myr e-folding time associated with Eddington-limited growth based on 10 per cent efficiency (see e.g. Fatuzzo & Melia 2017), black holes in the $R_\mathrm{h} = ct$ universe could grow by a factor of ∼150 in that redshift range, while they would only have had time to grow by a factor of ∼28 in ΛCDM. This choice–that all of the blazars of interest are experiencing Eddington-Limited growth–is motivated by the inferred Eddington ratio of high-z quasars (such as those in the Willott et al. 2010 sample). Thus, with the greater elapsed time, black holes at $z > 6$ are naturally expected to have been significantly smaller in $R_\mathrm{h} = ct$ (for a given redshift) than in the concordance ΛCDM model.

The extrapolation to lower masses brings its own issues with the Willott et al. (2010) black hole mass function, however. This distribution is well constrained only for masses in the range $10^8 \lesssim M \lesssim 3 \times 10^9$ $\mathrm{M}_\odot$. As we shall demonstrate below, the Willott et al. mass function, when extrapolated to lower masses,

may significantly overestimate the number of active galaxies. We begin with the black hole mass function observed at $z = 6$, then devolve objects to higher redshift by assuming all central black holes were accreting at the Eddington rate with an efficiency of 0.1. Analytically, a black hole accreting with efficiency ϵ_r, and with a bolometric luminosity of some fraction of the Eddington luminosity $\lambda_{Edd} \equiv L_{Bol}/L_{Edd}$ will have a mass-growth rate of

$$\dot{M} = \frac{(1-\varepsilon_r)}{\varepsilon_r}\frac{\lambda_{Edd} L_{Edd}}{c^2} = \frac{(1-\varepsilon_r)}{\varepsilon_r}\frac{\lambda_{Edd}}{t_{Edd}} M. \quad (2)$$

Integrating with respect to time gives the mass of the black hole as a function of time:

$$M(t_z) = M_0\, e^{\frac{(1-\varepsilon_r)}{\varepsilon_r}\frac{\lambda_{Edd}}{t_{Edd}}(t_z - t_{obs})}, \quad (3)$$

where t_{obs} is the age of the universe at the observed redshift, and t_z is the age of the universe at redshift z.

The black hole mass function may then be written as

$$\Phi_M(M, z) = \Phi_{z=6}\left[M\, e^{\frac{(1-\varepsilon_r)}{\varepsilon_r}\frac{\lambda_{Edd}}{t_{Edd}}(t_6 - t_z)}\right], \quad (4)$$

where t_6 and t_z are the ages of the Universe, respectively, at redshifts 6 and z, and $1 - \epsilon_r$ gives the fraction of infalling material accreted onto the central black hole. We follow Willott et al. (2010) by setting a fiducial $\lambda_{Edd} = 1$, $\epsilon_r = 0.1$ and adopt $t_{Edd} = 0.045$ Gyr, corresponding to the Salpeter (e-folding) time of 45 Myr.

The normalization $\Phi_{z=6}$ in this expression is the fitted Schechter mass function

$$\Phi_{z=6}(M) = \Phi_0 \left(\frac{M}{M^*}\right)^{\beta} e^{-M/M^*} \quad (5)$$

from Willott et al. (2010), with the best-fitting parameters $\Phi_0 = 1.23 \times 10^{-8}$ Mpc^{-3} dex^{-1}, $M^* = 2.24 \times 10^9$ M$_\odot$, and $\beta = -1.03$. This mass function is best constrained for the $z = 6$ quasars with $M > 10^8$ M$_\odot$. Note, however, that no formal error estimation was made in that paper. We do not attempt to estimate that error here either, but infer that it would not be significant to our final results compared with the error in the high-z radio-loud fraction and the errors in associating an FSRQ central black hole mass with a SED.

Over the frequency range (0.35–1.05) GHz, the SKA1-Wide survey will probe 20 000 deg^2 of sky (representing ∼48 per cent coverage) to a sensitivity of 22.8 μJy (SKA CSWG 2018). A 10^9 M$_\odot$ FSRQ at redshift 6 is expected to have a flux ∼0.1 Jy in this range, making it easily detectable. Likewise, the SKA1-Medium-Deep survey will probe from 0.95 to 1.75 GHz down to its sensitivity limit of 8.2 μJy over 5000 deg^2 of sky (SKA CSWG 2018). We can therefore determine the smallest (in terms of black hole mass) AGN as a function of redshift visible to the SKA1 surveys for each cosmological model. The SED is shifted out of the AGN's rest frame by the required factor of $1 + z$, such that the luminosity over SKA's observable band is

$$L_R(M) = \int_{\nu_1(z+1)}^{\nu_2(z+1)} L_{R,\nu}(M)\, d\nu. \quad (6)$$

The flux density in Jy over the observable band is then

$$F_R(M, z) = \frac{L_R(M)}{(\nu_2 - \nu_1)\, 4\pi d_L^2(z)}, \quad (7)$$

where $d_L(z)$ is given in equations (7) and (8) as a function of z, and ν_1 and ν_2 are the upper and lower frequencies of the observable band. In ΛCDM, we have

$$d_L^{\Lambda CDM} = \frac{c}{H_0}(1+z)\int_0^z \frac{du}{\sqrt{\Omega_m(1+u)^3 + \Omega_r(1+u)^4 + \Omega_\Lambda}}, \quad (8)$$

while in $R_h = ct$ it takes the simpler form

$$d_L^{R_h = ct} = \frac{c}{H_0}(1+z)\ln(1+z). \quad (9)$$

Next, we find the central black hole mass that satisfies the equality $F_{lim} = F_R(M, z)$, where F_{lim} is the flux limit of SKA. The error in these masses is the same as the error associated with each luminosity from equation (1). This error is represented by the coloured swaths in Figs 2 and 3.

Since the e-folding growth time is ∼45 Myr, a 10^8 M$_\odot$ object at $z = 6$ would have grown from a 5×10^6 M$_\odot$ black hole (the smallest estimated central black hole mass from our Seyfert sample) 135 Myr earlier, or from a 2.5×10^6 M$_\odot$ black hole (the lower limit to the estimate of smallest visible quasars by the Wide survey at $z > 6$) 166 Myr earlier. In ΛCDM, these correspond to redshifts $z = 6.78$ and 7, respectively, while in $R_h = ct$, these times are associated with $z = 6.51$ and 6.64. Our minimum detectable mass estimate for the Medium-Deep survey is roughly 1.3×10^6 M$_\odot$ in the middle of the redshift range for ΛCDM. Thus, a 10^8 M$_\odot$ black hole at $z = 6$ would have passed through this minimum at redshift $z \sim 7.22$ in ΛCDM and $z = 6.76$ in $R_h = ct$. Therefore, the predictions made

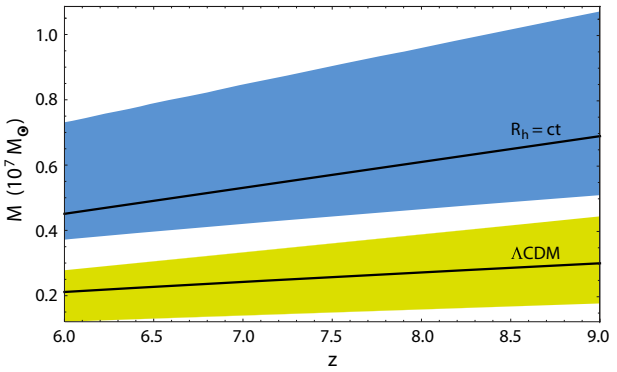

Figure 2. Smallest visible blazar in the SKA1 Wide Band 1 survey, along with our estimated errors: blue (dark) for $R_h = ct$, and yellow (light) for ΛCDM (with $\Omega_m = 0.3$). The difference is due to the different radio luminosities associated with each mass, and the difference in luminosity distance for each model. The radio luminosity from the *Fermi* blazar sequence is extrapolated to lower masses with a power law.

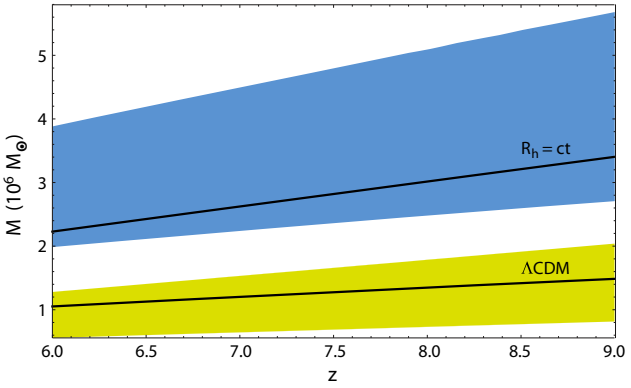

Figure 3. Same as Fig. 2, except for the SKA1 Medium-Deep Band 2 survey.

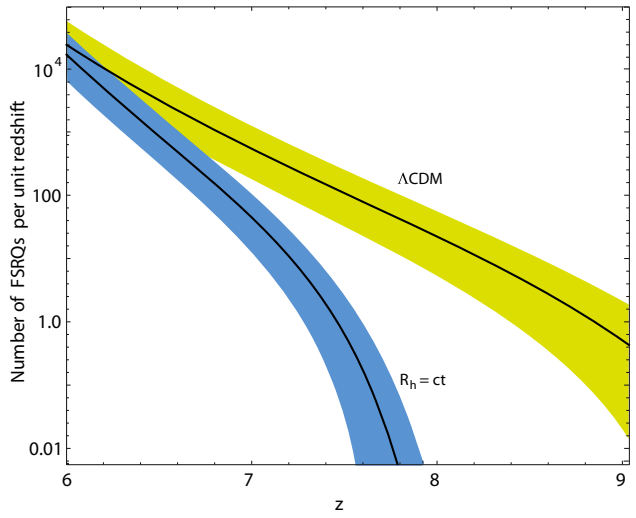

Figure 4. Estimated number of detected high-z FSRQs expected per unit redshift in the Wide survey, and our estimated error for, $R_h = ct$ (blue swath) and ΛCDM (yellow swath).

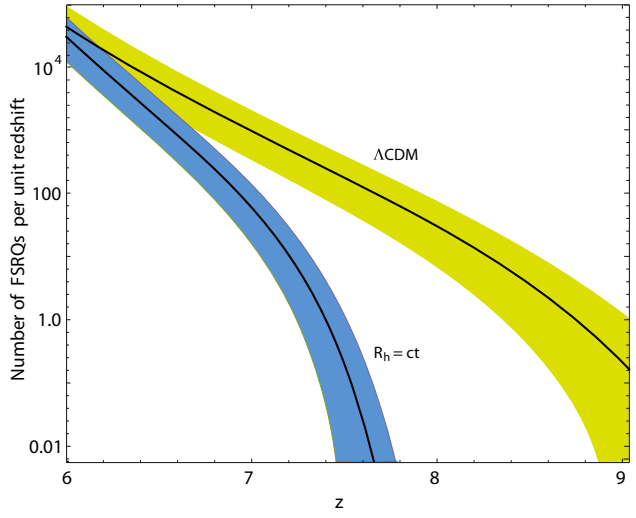

Figure 5. Estimated number of detected high-z FSRQs expected per unit redshift in the Medium-Deep survey, and our estimated error, for $R_h = ct$ (blue swath) and ΛCDM (yellow swath).

in this paper are to be relied upon most strongly for $z > 6.51$ in $R_h = ct$, and $z > 6.78$ for ΛCDM, in the case of the Wide-Field survey, and at $z > 7$ and >7.22, respectively, for the Medium-Deep survey.

From here, we estimate the number of objects that would be visible over the whole sky within some redshift bin, using the integrated number

$$N = \int_{z_{\rm low}}^{z_{\rm high}} {\rm d}z' \int_{\log_{10}[M_{\rm min}(z')]}^{\infty} \Phi(M, z')\, V_{z'}\, {\rm d}(\log_{10} M), \qquad (10)$$

where $V_z = 4\pi d_c^2\, {\rm d}/{\rm d}z(d_c)$ is the differential comoving volume, and $M_{\rm min}(z)$ is the smallest detectable black hole mass at redshift z. The function plotted in Figs 4 and 5 is

$${\rm d}N(z) = \int_{\log_{10}[M_{\rm min}(z')]}^{\infty} \Phi(M, z')\, V_{z'}\, {\rm d}(\log_{10} M). \qquad (11)$$

The comoving distance, $d_c = d_L/(1+z)$, and volume are used based on the assumption that the number, N, of active galaxies remains constant in comoving volume regardless of redshift. Finally, we multiply this number by 0.0405, based on the inferred fraction of flat-spectrum radio-loud quasars at $z > 5.5$ (Bañados et al. 2015; Coppejans et al. 2016), and then multiply it again by the fraction of sky covered by the survey (0.485 for the Wide survey and 0.121 for the Medium-Deep survey), to give a final estimate of the number of radio-loud objects expected to be visible with SKA. The results are presented in Figs 4 and 5 and Tables 2 and 3.

Included in each of these figures and tables are our estimated errors. In both cases, the Hubble constant acts as an inverse length scale that defines the comoving volume, which goes as H_0^{-3}. The primary source of uncertainty in our phenomenological model lies in the error associated with the smallest detectable black hole mass. For example, when the best estimate for a minimum mass is $10^6\,{\rm M}_\odot$, the error from equation (1) is ± 0.28 mass dex, or up to 90 per cent. Since the Schechter mass function predicts more numerous smaller black holes, these variations can drastically alter the expected object counts. As such, we use the error in the central black hole mass to adjust the lower limit of integration of equations (10) and (11) in order to determine an upper and lower limit on the expected all-sky objects. This error is

$$\delta N = \mp \int_{z_{\rm low}}^{z_{\rm high}} {\rm d}z' \int_{\log_{10}[M_{\rm min}(z')]\pm\delta\log_{10}[M_{\rm min}(z')]}^{\log_{10}[M_{\rm min}(z')]} \Phi(M, z') \times V_{z'}\, {\rm d}(\log_{10} M), \qquad (12)$$

with the choice in signs corresponding to the upper and lower errors. We also include the errors in the high-z radio-loud fraction (i.e. $8.1^{+5.0}_{-3.2}$ per cent; Bañados et al. 2015) and the blazar fraction (0.5 ± 0.1) of those radio-loud objects, based on the 26 objects in Coppejans et al. (2016). Added in quadrature, we find a final fractional error in the expected counts of

$$\sigma_N^+ \equiv \left(\frac{\delta N}{N}\right)^2 + \left(\frac{0.1}{0.5}\right)^2 + \left(\frac{0.05}{0.081}\right)^2 \qquad (13)$$

at the upper end, and an analogous expression, σ_N^- (with 0.05 replaced with 0.032), at the lower end. These errors correspond to the coloured swaths visualized in Figs 4 and 5.

4 DISCUSSION

The results of this analysis suggest that SKA will detect a highly significant difference in the number of blazars as a function of redshift for the two cosmological models we have compared in this paper. We expect to find far more quasars in ΛCDM than in $R_h = ct$. The first few columns in Tables 2 and 3 point to the deficiencies in Willott et al.'s (2010) black hole mass function at $z = 6$. These suggest that SKA would be able to find nearly 10 000 radio-loud quasars in the redshift range $6 \lesssim z \lesssim 6.5$, roughly one per 2 deg^2 in the Wide survey. But the vast majority of these are due to an extrapolation of the $z = 6$ mass function to masses far below those used to construct this distribution. With no real existing data to motivate the counts of smaller black holes at this redshift, these results have very little predictive power. Therefore, the predictions made in this paper are reliable only at $z \gtrsim 7$, as discussed in Sections 3 and 4.

The differences between the two models become more extreme with increasing redshift. At $z > 7.22$, the standard ΛCDM model predicts that SKA will detect 80 times more blazars than $R_h = ct$. The latter cosmology predicts effectively zero detection in either

Table 2. Estimated counts of objects to be detected by the SKA1 Wide Band 1 survey. Note the anomalously high expected detections for $z < 6.5$. This is due to the black hole (BH) mass function at $z = 6$ being extrapolated to lower masses. The two rightmost columns present the estimates for z above the redshifts for BHs in ΛCDM to have devolved such that a BH at $z = 6$ is smaller than the smallest known γ-ray radio-loud Seyfert 1 by $z = 6.78$, and below the inferred lower limit for detectable BHs at $z = 7$, respectively.

	Redshift range (z)							
	6–6.5	6.5–7	7–7.5	7.5–8	8–8.5	8.5–9	6.78–9	7–9
ΛCDM	9881^{+10117}_{-6193}	1492^{+1545}_{-945}	271^{+296}_{-178}	51^{+64}_{-36}	$8.0^{+13.5}_{-6.5}$	$0.80^{+2.33}_{-0.75}$	694^{+757}_{-454}	330^{+375}_{-221}
$R_h = ct$	5178^{+4785}_{-3089}	273^{+273}_{-172}	$8.1^{+12.4}_{-6.3}$	$0.01^{+0.08}_{-0.01}$	0	0	45^{+54}_{-31}	$8.1^{+12.4}_{-6.3}$

Table 3. Estimated counts of objects to be detected by the SKA1 Medium-Deep Band 2 survey. Redshift bins are the same as the Table 2, except the rightmost bin covers $z > 7.22$.

	Redshift range (z)							
	6–6.5	6.5–7	7–7.5	7.5–8	8–8.5	8.5–9	6.78–9	7.22–9
ΛCDM	5107^{+5768}_{-3341}	786^{+891}_{-517}	151^{+176}_{-101}	32^{+41}_{-23}	$6.6^{+10.3}_{-5.2}$	$1.1^{+2.5}_{-1}$	385^{+452}_{-259}	96^{+120}_{-67}
$R_h = ct$	2706^{+2741}_{-1688}	157^{+167}_{-101}	$7.2^{+10.3}_{-5.4}$	$0.05^{+0.23}_{-0.05}$	0	0	31^{+38}_{-22}	$1.2^{+2.5}_{-1.1}$

survey at $z > 7.5$. The current most-distant known quasar of any type lies at a redshift $z = 7.54$. This object has an estimated mass of $\sim 10^8$ $M_\odot$ (Bañados et al. 2018). When we begin with Willot et al.'s black hole mass function at $z = 6$ and apply lockstep evolution, objects such as J1342+0928 appear to be statistically impossible for both considered cosmologies. But evidently this object and other similar objects at $z \gtrsim 7$ exist. Therefore, it becomes immediately clear that the simple evolution of the $z = 6$ mass function does not accurately describe the full AGN population, if either of these cosmological models is to be believed. We point out, however, that the $z = 6$ mass function does not take into account black holes that have already evolved past their primary active phase. Their host galaxies would then no longer appear active, and would be missed (or classified as some other kind of object if detected) by a survey. Therefore, we suggest that the $z = 6$ mass function devolved to higher redshifts is a *lower limit* to the expected counts of existing AGNs. Our predicted numbers of FSRQs to be detected by SKA1 Wide and Medium-Deep surveys thus represent lower limits on the number of objects that would be detected in either cosmological model.

None the less, we point out that the number of objects predicted by ΛCDM at $z > 7$ in the Wide survey is more than a factor of 40 greater than the prediction by $R_h = ct$. With the lower end of the $z > 7$ estimate being 174, significantly above the $R_h = ct$ range, we expect the results of the survey to strongly prefer one model over the other. Furthermore, $R_h = ct$ predicts fewer than one detected blazar at $z > 7.5$ in both surveys, while ΛCDM still predicts ∼60 in the Wide survey, and ∼40 in the Medium-Deep survey. Likewise, in the deep survey, ΛCDM predicts roughly 100 blazars at $z > 7.22$, while only ∼1 is expected in $R_h = ct$. We do not anticipate that quasars unaccounted for in our simplified evolution picture could overcome this large difference between the two models.

5 CONCLUSION

We have presented a method for predicting the number of FSRQs based on a phenomenological approach to estimating the radio luminosity of high-redshift sources. Using the observed population of AGNs with known γ-ray luminosities and mass estimates at lower redshifts, and using the *Fermi* blazar sequence, we have constructed a broad-band SED of FSRQs as a function of mass alone. We have then used this spectrum to estimate the smallest black hole mass of a FSRQ detectable by SKA as a function of redshift. Finally, we have devolved the black hole mass function observed at $z = 6$ to higher redshifts, assuming lockstep evolution.

With the assumption that all the black holes above the limiting mass at a given redshift would be visible to a complete flux-limited survey, we have predict the number counts of FSRQs expected as a function of redshift for two competing models, ΛCDM and $R_h = ct$. Taking into account the limitations used to construct the black hole mass function at $z = 6$, we have predicted the counts of objects at $z > 7$ for the Wide-Field SKA Band 1 survey, and at $z > 7.22$ in the Medium-Deep SKA Band 2 survey. These results offer a definitive method of discriminating between these two cosmological models, in which ΛCDM predicts 30 times more blazar counts than $R_h = ct$ in the Wide survey, and 80 times more in the Medium-Deep survey.

While there appear to be other influences at work regarding the evolution of the black hole mass at high redshifts, this analysis may be viewed as providing a lower limit to the overall number of such sources expected to be seen by SKA at those redshifts. At this time, we do not anticipate any additional corrections in $R_h = ct$ that could reasonably explain the detection of ∼200 such sources by the Wide survey at $z > 7$ if this is what SKA finds. But if fewer than ∼50 detections are made by the time the survey is completed, it would correspondingly be very difficult to explain this deficit in the context of the standard model, thereby strongly favouring $R_h = ct$.

We also point out that the phenomenological approach used in this paper may be applied to any other non-thermal waveband of interest, allowing for predictions of FSRQ-type objects by different surveys in other parts of the spectrum. In addition, the SKA surveys are poised to discover AGNs with smaller black hole masses than ever observed before at $z > 6$. We expect that SKA detections at $z \sim 6$ will thereby extend the $z = 6$ black hole mass function to significantly lower masses, thus permitting us to eventually devolve this improved mass distribution towards higher redshifts. Our ultimate goal is to form a sufficiently complete picture of AGN growth in the early universe in order to convincingly rule out one or other of these two models at a very high level of confidence.

ACKNOWLEDGEMENTS

We thank Jinyi Yang, Xiaohui Fan, and Feige Wang for helpful discussions concerning recent measurements of high-redshift quasars.

REFERENCES

Acero F. et al., 2015, ApJ , 218, 23
An H., Romani R. W., 2018, ApJ, 856, 105
Antonucci R., 1993, ARA&A, 31, 473
Bañados E. et al., 2015, ApJ, 804, 118
Bañados E. et al., 2018, Nature, 553, 473
Beckmann V., Shrader C. R., 2012, Active Galactic Nuclei. Wiley-VCH, Weinheim, Germany
Coppejans R. et al., 2016, MNRAS, 463, 3260
Fabian A. C., Walker S. A., Celotti A., Ghisellini G., Mocz P., Blundell K. M., McMahon R. G., 2014, MNRAS, 442, L81
Fan X. et al., 2001, AJ, 122, 2833
Fatuzzo M., Melia F., 2017, ApJ, 846, 129
Ghisellini G., Sbarrato T., 2016, MNRAS, 461, L21
Ghisellini G., Maraschi L., Tavecchio F., 2009a, MNRAS, 396, L105
Ghisellini G., Foschini L., Volonteri M., Ghirlanda G., Haardt F., Burlon D., Tavecchio F., 2009b, MNRAS, 399, L24
Ghisellini G., Tavecchio F., Foschini L., Ghirlanda G., Maraschi L., Celotti A., 2010, MNRAS, 402, 497
Ghisellini G., Righi C., Costamante L., Tavecchio F., 2017, MNRAS, 469, 255
Hovatta T., Valtaoja E., Tornikoski M., Lähteenmäki A., 2009, A&A, 494, 527
Krolik J. H., Begelman M. C., 1986, ApJ, 308, L55
Leaf K., Melia F., 2017, MNRAS, 470, 2320
Lusso E., Risalti G., 2016, ApJ, 819, 154
Melia F., 2003, The Edge of Infinity. Cambridge Univ. Press, Cambridge
Melia F., 2007, MNRAS, 382, 1917
Melia F., 2013, ApJ, 764, 72
Melia F., 2016, Frontiers Phys., 11, 119801
Melia F., 2017, MNRAS, 464, 1966
Melia F., 2018, MNRAS, 481, 4855
Melia F., Abdelqader M., 2009, Int. J. Modern Phys. D, 18, 1889
Melia F., Königl A., 1989, in Hunt J., Battrick B., eds, ESA Special Publication Vol. 296, Two Topics in X-Ray Astronomy, Vol. 1: X Ray Binaries; Vol. 2: AGN and the X Ray Background. ESA, Noordwijk, p. 995
Melia F., McClintock T. M., 2015, Proc. R. Soc. Lond. Ser. A, 471, 20150449
Melia F., Maier R. S., 2013, MNRAS, 432, 2669
Melia F., Shevchuk A. S. H., 2012, MNRAS, 419, 2579
Melia F., Yennapureddy M. K., 2018a, MNRAS, 480, 2144
Melia F., Yennapureddy M. K., 2018b, J. Cosmol. Astropart. Phys., 02, 034
Paliya V. S., Stalin C. S., Shukla A., Sahayanathan S., 2013, ApJ, 768, 52
Paliya V. S., Ajello M., Rakshit S., Mandal A. K., Stalin C. S., Kaur A., Hartmann D., 2018, ApJ, 853, L2
Paliya V. S., Parker M. L., Jiang J., Fabian A. C., Brenneman L., Ajello M., Hartmann D., 2019, ApJ, 872, 169
Planck Collaboration VI, 2018, preprint (arXiv:1807.06209)
Riess A. G. et al., 2018, ApJ, 861, 126
Shakura N. I., 1973, SvA, 16, 756
Sikora M., Madejski G., 2001, in Aharonian F. A., Völk H. J., eds, AIP Conf. Proc. Vol. 558, High Energy Gamma-Ray Astronomy: International Symposium. Am. Inst. Phys., New York, p. 275
Square Kilometre Array Cosmology Science Working Group et al., 2018, preprint (arXiv:1811.02743)
Urry C. M., Padovani P., 1995, PASP, 107, 803
Volonteri M., Haardt F., Ghisellini G., Della Ceca R., 2011, MNRAS, 416, 216
Wang F. et al., 2018, preprint (arXiv:1810.11926)
Weigel A. K., Schawinski K., Treister E., Urry C. M., Koss M., Trakhtenbrot B., 2015, MNRAS, 448, 3167
Willott C. J. et al., 2010, AJ, 140, 546
Wu J., Ghisellini G., Hodges-Kluck E., Gallo E., Ciardi B., Haardt F., Sbarrato T., Tavecchio F., 2017, MNRAS, 468, 109
Yennapureddy M. K., Melia F., 2018, Eur. Phys. J. C, 78, 258

This paper has been typeset from a TEX/LATEX file prepared by the author.